

**DEVELOPMENT OF BOVINE HYDROXYAPATITE
COATING ON Ti6Al4V IMPLANT BY PLASMA
ELECTROLYTIC OXIDATION**

ADELEKE SAKIRU ADEKUNLE

**FACULTY OF ENGINEERING
UNIVERSITY OF MALAYA
KUALA LUMPUR**

2018

**DEVELOPMENT OF BOVINE HYDROXYAPATITE
COATING ON Ti6Al4V IMPLANT BY PLASMA
ELECTROLYTIC OXIDATION**

ADELEKE SAKIRU ADEKUNLE

**THESIS SUBMITTED IN FULFILMENT OF THE
REQUIREMENTS FOR THE DEGREE OF
DOCTOR OF PHILOSOPHY**

**FACULTY OF ENGINEERING
UNIVERSITY OF MALAYA
KUALA LUMPUR**

2018

UNIVERSITY OF MALAYA
ORIGINAL LITERARY WORK DECLARATION

Name of Candidate: **ADELEKE SAKIRU ADEKUNLE**

Matric No: **KHA150009**

Name of Degree: **DOCTOR OF PHILOSOPHY**

Title of Project Paper/Research Report/Dissertation/Thesis (“this Work”):

Development of bovine hydroxyapatite coating on Ti6Al4V implant by plasma electrolytic oxidation

Field of Study: **MATERIALS ENGINEERING**

I do solemnly and sincerely declare that:

- (1) I am the sole author/writer of this Work;
- (2) This Work is original;
- (3) Any use of any work in which copyright exists was done by way of fair dealing and for permitted purposes and any excerpt or extract from, or reference to or reproduction of any copyright work has been disclosed expressly and sufficiently and the title of the Work and its authorship have been acknowledged in this Work;
- (4) I do not have any actual knowledge nor do I ought reasonably to know that the making of this work constitutes an infringement of any copyright work;
- (5) I hereby assign all and every rights in the copyright to this Work to the University of Malaya (“UM”), who henceforth shall be owner of the copyright in this Work and that any reproduction or use in any form or by any means whatsoever is prohibited without the written consent of UM having been first had and obtained;
- (6) I am fully aware that if in the course of making this Work I have infringed any copyright whether intentionally or otherwise, I may be subject to legal action or any other action as may be determined by UM.

Candidate’s Signature

Date:

Subscribed and solemnly declared before,

Witness’s Signature

Date:

Name:

Designation:

DEVELOPMENT OF BOVINE HYDROXYAPATITE COATING ON Ti6Al4V IMPLANT BY PLASMA ELECTROLYTIC OXIDATION

ABSTRACT

Plasma electrolytic oxidation (PEO) is used to prepare bioactive hydroxyapatite ceramic coatings on light metals. The extensive literature reports on the bioactive hydroxyapatite-oxide coatings formed under a wide range of different electrical parameters and in various electrolyte concentrations. However, little work is available that investigates systematically the influence of hydroxyapatite concentration in the oxide film using a solitary sodium phosphate (NAP) electrolyte solution. In this present work, a single PEO process was used to produce film incorporating HA, and the aftermath effects of various HA concentrations in the oxide film on the Ti6Al4V alloy substrate were examined. The findings revealed that the oxide film was greatly influenced by the various hydroxyapatite particles. It was found that the amount of hydroxyapatite particles infiltrated into the coatings layer as well as the thickness and the surface roughness of the coating increased with increasing HA concentration. The porosity of the HA coatings indicated an inverse relationship with the concentration of HA particles in the NAP solution. The result also demonstrates that higher scratch adhesive strength was achieved using 1.5 g/L HA solution, producing a critical load of 2099 mN, while 0 g/L HA only produced a critical load of 1247 mN. The adhesion becomes independent of thickness when the concentration of HA exceeds 1.5 g/L. The failure of the coating was characterized by large periodic hemispherical chipping, while intermittent delamination was noticed with the coating embedded with HA particles. Due to the increasing demand to develop coatings with unique phase/elemental composition similar to hard bone tissues. The study also examined the coatings formed in a biologically friendly electrolyte containing natural bovine bone-derived HA (BHA) under a range of different voltage regimes, current density and time. The results

indicated that the combination of a various voltage regime 225-325 V, current density of 500 mAcm⁻² and deposition time of 5 mins produced a rough and porous surface coating. The surfaces of the coated layers were filled with anatase-TiO₂, cubic-MgO and hexagonal-BHA particles. The coatings formed in a newly developed bovine-bone derived-HA revealed an additional MgO phase in the coating layer. A film-to-substrate adhesion strength of 2010 mN was achieved. Moreover, the PEO-BHA coatings significantly improved the wear performance of titanium alloy. However, the coefficient of friction (COF) for the coating at 325 V is almost the same with the one produced at 300 V due to porous layer of the coating formed at 325 V. A comparative study on the in vitro corrosion and bioactive performance of commercial hydroxyapatite (CHA) and BHA coatings was also studied. The corrosion and bioactivity properties were evaluated using potentiodynamic polarization and simulated body fluid, respectively. The electrochemical tests demonstrated that the oxide coatings containing different phases possess sufficient protection efficiency. The apatite layer formed on the PEO-BHA coating was more and denser than that of PEO-CHA coating, whereas apatite structure was completely formed on the two surfaces.

Keywords: plasma electrolytic oxidation, hydroxyapatite, bovine hydroxyapatite, sodium phosphates, Ti6Al4V

**PENGHASILAN SALUTAN HIDROSIPTIT LEMBU KE ATAS TI6AL4V
IMPLAN DARIPADA OKSIDASI ELECTROLITIK PLASMA**

ABSTRAK

Oksidasi elektrolitik plasma (PEO) telah digunakan untuk menyediakan salutan seramik bioaktif hidrosipatit ke atas logam ringan. Laporan kajian literatur ke atas salutan seramik bioaktif hidrosipatit yang terhasil di bawah parameter elektrik dan konsentrasi elektrolit yang pelbagai. Walaubagaimanapun, sedikit kajian yang telah dijalankan untuk mengkaji secara sistematik, kesan konsentrasi hidrosipatit dalam filem oksida menggunakan larutan elektrolit solitari natrium fosfat (NAP). Dalam kajian ini, proses PEO tunggal digunakan untuk menghasilkan filem yang mengandungi HA, dan pelbagai kesan konsentrasi HA di dalam filem oksida ke atas Ti6Al4V aloi substrat telah diuji. Hasil menunjukkan bahawa filem oksida telah dipengaruhi oleh pelbagai partikel hidrosipatit. Ia menunjukkan, jumlah partikel hidrosipatit telah meresap ke dalam lapisan salutan, dan juga ketebalan dan kekasaran permukaan salutan akan meningkat berkadar dengan peningkatan konsentrasi HA. Keliangan salutan HA menunjukkan hubungan berkadar songsang dengan konsentrasi partikel HA di dalam larutan NAP. Hasil kajian juga menunjukkan kekuatan kecalaran yang tinggi telah dicapai menggunakan 1.5g larutan HA, menghasilkan berat kritikal 2099 mN, manakala 0 g/L HA, hanya menghasilkan berat kritikal melebihi 1.5 g/L. Kegagalan salutan dicirikan oleh penarahan hemisferal yang berkala besar. Manakala, penyingkiran sementara telah dikenal pasti dengan salutan yang dibenamkan dengan partikel HA. Oleh kerana permintaan yang tinggi untuk membangunkan salutan dengan fasa/elemen yang mempunyai komposisi unik seperti mana tisu tulang yang kuat. Kajian ini juga menganalisa salutan yang terhasil dari elektrolit yang mesra biologi yang mengandungi tulang lembu yang dihasilkan secara semulajadi di bawah voltan, kepadatan arus dan masa yang berbeza. Hasil juga menunjukkan kombinasi pelbagai voltan di bawah 225-

325 V, kepadatan arus 500 mAcm⁻² dan tempoh selama 5 minit menghasilkan permukaan salutan yang kasar dan berliang. Permukaan salutan diisi oleh partikel anatase- TiO₂ cubic-MgO dan hexagonal-BHA. Salutan ini dihasilkan oleh tulang lembu HA yang menunjukkan fasa MgO yang berlebihan di dalam lapisan salutan. Kekuatan pegangan filem-substrat sebanyak 2010 mN telah dicapai. Selain itu, salutan PEO-BHA telah memperbaiki secara signifikan prestasi koyakan aloi titanium. Walau bagaimanapun, pekali geseran (COF) untuk salutan pada 325 V adalah hampir sama dengan yang terhasil pada 300 V, di mana ia bergantung pada lapisan keliangan lapisan salutan yang terhasil pada 325 V. Satu kajian perbandingan ke atas kakisan in vitro dan prestasi bioaktif salutan CHA dan BHA telah dijalankan. Maklumat kakisan dan aktiviti bio yang dikaji menggunakan teknik “potentio dynamic polarization” dan “simulated body fluid”. Ujian elektro kimia menunjukkan salutan oksida mengandungi fasa yang mengandungi pekali perlindungan yang berbeza. Lapisan apatit yang terbentuk di atas salutan PEO-BHA adalah berlebihan dan lebih padat berbanding salutan PEO-CHA, di mana struktur apatit telah dihasilkan secara keseluruhan di atas kedua-dua permukaan.

Kata utama: Oksida elektrolitik plasma, hidrosipatif, hydrosipatif lembu, natrium fosfat, Ti6Al4V

ACKNOWLEDGEMENTS

My sincere gratitude goes to Almighty Allah for His inspiration, guidance and strength to complete my research work and this thesis.

I express my profound and sincere gratitude to Prof. Ir. Dr. Ramesh Singh under whom effective guidance the work presented in this thesis was undertaken. His effective mentoring guides and discussions have been of tremendous benefit to me. I would like to thank Prof. Iis Sopyan and Assoc. Prof. Dr. Bushroa for the assistance rendered. Similar appreciation also goes to technical staff Madam Hartini in Surface Engineering Lab for the unflinching support and kind gesture throughout my study.

Special thanks are due to my in-law, Alhaji and Alhaja Osundina for the words of encouragement throughout my study.

Finally, special thanks to my parents, Mr. and Mrs. Alasoro, and Mrs. Taibat Osundina for the patience, sacrifice and care to make my research a reality. I pray Almighty Allah grant us long life to enjoy the fruit of the sacrifice.

TABLE OF CONTENTS

Abstract	iii
Abstrak	v
Acknowledgements	vii
Table of Contents	viii
List of Figures	xiii
List of Tables	xvii
List of Symbols and Abbreviations	xix
CHAPTER 1: INTRODUCTION	1
1.1 Introduction	1
1.2 Problem statement	5
1.3 Objective of the study	6
1.4 Research scope	7
1.5 Research methodology	7
1.6 Organization of the thesis	9
CHAPTER 2: LITERATURE REVIEW	12
2.1 Introduction	12
2.2 Researches on titanium alloys	12
2.2.1 Titanium alloys	12
2.2.2 Corrosion resistance of titanium alloys	15
2.2.3 Wear characteristics of titanium materials	17
2.2.3.1 Abrasive wear	19
2.2.3.2 Adhesive wear	20
2.2.3.3 Fatigue wear	20

2.2.3.4	Tribochemical wear	21
2.2.4	Titanium alloy as an orthopaedic implant	21
2.3	Research trends in CaP coating on titanium alloy implant.....	23
2.3.1	Fabrication of bioactive CaP on titanium alloy implant.....	24
2.3.2	Surface engineering techniques of producing CaP coatings	25
2.3.2.1	Thermal spray for CaP coating.....	26
2.3.2.2	Radio frequency magnetron sputtering for CaP coating	27
2.3.2.3	Electrophoretic deposition of CaP coating.....	29
2.3.2.4	Sol-gel deposition for CaP coating.....	31
2.3.2.5	Plasma electrolytic oxidation for CaP coating	33
2.4	State of the art on the PEO coating process.....	36
2.4.1	Plasma electrolytic oxidation	36
2.4.2	Characteristics features of PEO.....	36
2.4.3	PEO coating procedure.....	38
2.4.3.1	Influence of substrate composition and property	39
2.4.3.2	Influence of electrolytes	40
2.4.3.3	Influence of deposition time.....	42
2.4.3.4	Influence of deposition voltage	43
2.5	Mechanisms of PEO coating formation.....	45
2.5.1	PEO electrical transient phenomena.....	45
2.6	Summary.....	48
 CHAPTER 3: METHODOLOGY		49
3.1	Introduction.....	49
3.2	Materials	49
3.2.1	Bovine hydroxyapatite derived from cortical bone.....	49
3.2.2	Substrate preparation	50

3.2.3	Electrolyte preparation	51
3.3	Characterization.....	52
3.3.1	PEO coating.....	53
3.3.2	Development of films by PEO treatment	55
3.4	Morphological characterization of the PEO coatings.....	56
3.4.1	FESEM microstructural/XPS examination	56
3.4.2	XRD and FTIR analysis	58
3.5	Mechanical characterization of PEO films.....	59
3.5.1	Surface roughness of the PEO films.....	59
3.5.2	Micro-scratch examination.....	60
3.5.2.1	Scratch hardness of PEO coatings.....	60
3.5.3	Wear resistance.....	61
3.5.4	In vitro corrosion resistance	62
3.5.5	In vitro bioactivity test	63
3.6	Summary.....	64
 CHAPTER 4: RESULTS AND DISCUSSIONS		65
4.1	Introduction.....	65
4.2	Influence of electrolyte concentration on PEO.....	65
4.2.1	Coating fabrication	65
4.2.2	Characteristics of PEO process	66
4.2.3	Surface morphology of PEO coated layers	68
4.2.4	Surface chemistry and phase compositions.....	69
4.2.4.1	Porosity of PEO coatings	73
4.2.5	Coating thickness	74
4.2.6	Mechanism of TiO ₂ /HA coating formation.....	76
4.2.7	Mechanical properties	77

4.2.7.1	Surface roughness	77
4.2.7.2	Adhesive strength of PEO coatings.....	78
4.2.7.3	Elemental analysis of the PEO scratches	82
4.2.7.4	Scratch hardness of PEO coatings.....	83
4.2.7.5	Failure mode of PEO coatings.....	84
4.3	Summary.....	86

CHAPTER 5: INVESTIGATION OF VOLTAGE REGIME EFFECT ON THE PEO COATINGS CONTAINING BOVINE-HA PARTICLES SOLUTION..... 88

5.1	Introduction.....	88
5.2	Influence of applied voltage on BHA film	88
5.2.1	Coating fabrication	88
5.2.2	PEO process characterization.....	89
5.2.3	Surface morphology of PEO-BHA coated layers.....	90
5.2.4	Surface chemistry and phase composition	91
5.2.5	Coating thickness of PEO-BHA films.....	97
5.2.6	Mechanical properties of PEO film.....	99
5.2.6.1	Surface roughness of PEO-BHA film	99
5.2.6.2	Adhesion strength of the PEO-BHA coating	100
5.2.6.3	Wear resistance of the PEO-BHA coatings.....	102
5.3	Summary.....	106

CHAPTER 6: INVESTIGATION OF PEO COATING PERFORMANCE IN A SOLUTION CONTAINING CHA AND BHA PARTICLES 108

6.1	Introduction.....	108
6.2	Influence of electrolyte CHA and BHA composition on PEO coatings.....	108
6.2.1	Coating fabrication	108

6.2.2	PEO voltage-time process characterization.....	109
6.2.3	Coating morphologies of PEO-CHA-BHA coated layers.....	110
6.2.4	Elemental and phase composition of the coatings.....	112
6.2.5	Surface roughness of PEO coatings	115
6.2.6	Potentiodynamic corrosion evaluation	117
6.2.7	In vitro-bioactivity of the PEO coatings.....	118
6.3	Discussion.....	125
6.4	Summary.....	131
CHAPTER 7: CONCLUSION AND RECOMMENDATION		133
7.1	Conclusions	133
7.2	Contributions to knowledge.....	136
7.3	Recommendation for future work.....	137
	References	138
	List of Publications and Papers Presented	150

LIST OF FIGURES

Figure 1.1: Schematic view of artificial hip joint (Liu et al., 2004)	1
Figure 1.2: Work flow of the research work	9
Figure 1.3: Structure of the thesis	11
Figure 2.1: Wear classified by the type of relative motion, such as sliding, impact and rolling contact (Davis, 2001).....	18
Figure 2.2: Various categories of wear based on abrasion, erosion, adhesion and surface fatigue (Davis, 2001).....	19
Figure 2.3: Example of a bone plate implant, CP titanium grade 3 (Donald et al., 2001).	22
Figure 2.4: Scanning electron micrograph of a typical as-sprayed HAp coating: (a) top surface; b) cross-section (Ntsoane et al., 2016).	27
Figure 2.5: SEM image of: acid-etched uncoated titanium surface (a), cross-section of the deposited CaP coating (b) and the surface morphology (c, d) of the CaP coating deposited on acid-etched titanium surfaces over different amounts of time. Thickness: (b,c) 170 nm, (d) 440 nm (Surmenev et al., 2014).....	29
Figure 2.6: SEM images of sintered HA coatings on TiAlV substrates (Zhitomirsky & Gal-Or, 1997).	30
Figure 2.7: Optical micrographs of (a) uncoated and HA–Alg-coated sample (0.4 mm; 1,1) before (b) and after (c) sintering (Kollath et al., 2016).....	31
Figure 2.8: FESEM images of nano-HA coatings after sintering at: (a) 500 °C for 10 min; (b) 500 °C for 30 min; (c) 600 °C for 10 min; (d) 600 °C for 30 min; (e) 700 °C for 10 min, and (f) 700 °C for 30 min (Jafari et al., 2016).....	33
Figure 2.9: (a) Typical arrangement of the equipment used for PEO treatment (1. window, 2. mixer, 3. connecting wires, 4. exhaust/ventilation system, 5. grounded case, 6. power supply unit, 7. workpiece, 8. cooling system, 9. bath, 10 insulating plate). (b) Electrolyte bath (Yerokhin et al., 1999).....	37
Figure 2.10: Roughness of the sample produced using MAO&EPD process in the NaOH electrolyte solution with different HA concentrations (Bai et al., 2011).	40
Figure 2.11: Thickness and adhesive strength of MAO coatings formed in electrolyte E ₁ and E ₂ (Pan et al., 2013).....	41

Figure 2.12: (a) Linear (Hussein et al., 2013) and (b) non-linear growth (Wang et al., 2004) of the PEO coating with different deposition time.	43
Figure 2.13: Thickness of the PEO coated layer and (b) Surface roughness as a function of the applied voltages (Li et al., 2004).	44
Figure 2.14: Voltage-time response of the PEO treated Al 6082 alloy under the current density 467 A.m ² and electrolyte concentration 1 g/L KOH. (a) Voltage-time response (Yerokhin et al., 2004) (b) identification of different PEO stages based on voltage transient (Gao, 2014).	46
Figure 3.1: XRD pattern (a) and FTIR spectrum (b) of the BHA powder.	50
Figure 3.2: Illustrative outline of the apparatus for the electrolyte formulation: (a) Weighing balance, (b) NAP dissolution, (c) NAP+BHA particle suspension, and (d) Magnetic stirrer of the particle suspension.	52
Figure 3.3: Experimental setup for the PEO process.	54
Figure 3.4: Schematic view of the operation of SEM.	57
Figure 3.5: Schematic view of XRD principle.	58
Figure 3.6: Schematic view of potentiodynamic polarization curve using Tafel plots.	63
Figure 4.1: Voltage-time plots obtained during the PEO process in different electrolyte concentration.	66
Figure 4.2: Surface plane SEM micrographs (a) 0 g/L, (b) 1 g/L, (c) 1.5 g/L, and (d) 2 g/L HA.	68
Figure 4.3: Representative EDS spectrum of the PEO coating produced at 2 g/L HA.	70
Figure 4.4: XRD patterns of the coating produced at varied concentrations: (a) 0 g/L, (b) 1 g/L, (c) 1.5 g/L, and (d) 2 g/L HA.	72
Figure 4.5: Dependence of pore size in the PEO coatings on the HA concentration.	73
Figure 4.6: Cross-sectional morphologies of PEO coatings produced at varied concentrations: (a) 0 g/L, (b) 1 g/L, (c) 1.5 g/L, and (d) 2 g/L HA.	74
Figure 4.7: Correlation between the final voltage and coating thickness of the PEO coatings produced at varied concentrations.	75
Figure 4.8: Dependence of PEO coating roughness produced on titanium at various concentrations.	78

Figure 4.9: Residual scratch tract after scratch test: (a) 0 g/L, (b) 1 g/L, (c) 1.5 g/L, and (d) 2 g/L HA.....	79
Figure 4.10: Adhesion strength of PEO coatings formed at varied concentration.....	81
Figure 4.11: Elemental constituent analysis of the left over scratches (a) 1.5 g/L spalt region (a') profile and (b) 2 g/L HA spalt region, (b') profile.....	82
Figure 4.12: Scratch hardness number of PEO coatings formed at varied concentration	84
Figure 5.1: Voltage-time behaviour during PEO process at varying voltages.....	89
Figure 5.2: Surface SEM morphologies of PEO coatings formed at different voltages (a) 225 V, (b) 250 V, (c) 275 V, (d) 300 V, and (e) 325 V	91
Figure 5.3: Representative EDS of PEO-BHA coating produced at 325 V.....	92
Figure 5.4: Elemental mappings of PEO-BHA coatings produced at 325 V.....	93
Figure 5.5: XRD patterns of the PEO coatings produced at varying voltages: (a) 225 V, (b) 250 V, (c) 275 V, (d) 300 V, and (e) 325 V	94
Figure 5.6: XPS survey spectrum of PEO-BHA coating produced at 325 V	95
Figure 5.7: XPS binding energies of the PEO coating produced at 325 V: (a) O (1s), (b) Ti (2p _{3/2}), (c) Ca (2p), (d) P (2p), and (e) Mg (2p).....	96
Figure 5.8: Cross-sectional SEM morphologies of PEO-BHA coatings produced at different voltages: (a) 225 V, (b) 250 V, (c) 275 V, (d) 300 V, and (e) 325 V.....	98
Figure 5.9: Dependence of coating roughness on the applied voltages	100
Figure 5.10: Adhesion strength of PEO-BHA coatings formed at different applied voltages	101
Figure 5.11: COF of the untreated (a) Ti6Al4V and (b) coatings at varying voltages .	102
Figure 5.12: Wear tracks of untreated Ti6Al4V alloy and the PEO-BHA coatings	104
Figure 6.1: Voltage-time response of the PEO coatings: (a) CHA and (b) BHA	109
Figure 6.2: SEM images of PEO coatings fabricated with different electrolytes: (a) CHA and (b) BHA.....	111
Figure 6.3: Cross-sectional morphologies of the PEO coatings produced at different electrolyte (a) CHA and (b) BHA	112

Figure 6.4: EDS spectra of PEO coatings produced under different hydroxyapatites: (a) CHA and (b) BHA	113
Figure 6.5: XRD patterns of PEO coatings: (a) CHA and (b) BHA (1: Titanium-Ti6Al4V, 2: Anatase-TiO ₂ , 3: Magnesium oxide-MgO, 4: Hydroxyapatite-HA, 5: Calcium titanate-CaTiO ₃ , and 6: Sodium titanium phosphate-NaTi ₂ (PO ₄) ₃	114
Figure 6.6: Surface profile graphs of: (a) untreated Ti6Al4V, and PEO layers (b) CHA, and (c) BHA	116
Figure 6.7: Potentiodynamic polarization Tafel plots of untreated Ti6Al4V, CHA and BHA films in Ringer's solution	117
Figure 6.8: The surface SEM micrographs of PEO treated films: (a) CHA, (b) BHA and (c) untreated Ti6Al4V after immersion in 7.3 pH SBF solutions for 14 days	120
Figure 6.9: EDS spectra of PEO treated films: (a) CHA, (b) BHA, and (c) Ti6Al4V substrate.....	121
Figure 6.10: ATR-FTIR patterns of (a) untreated Ti6Al4V, (b) BHA film, and (c) CHA film after soaking in SBF solution for 14 days	123

LIST OF TABLES

Table 1.1: Summary of mechanical properties of metallic biomaterials (Budinski, 1991; Kamachimudali et al., 2003)	2
Table 2.1: Designation and elemental composition of commercial titanium alloys (Welsch et al., 1993)	13
Table 2.2: Summary of physical properties of titanium (Aliasghari et al., 2016; Liu et al., 2004).....	14
Table 2.3: Compositions of low modulus β alloys developed for biomedical applications (Lütjering & Williams, 2007)	23
Table 2.4: Plasma electrolytic oxidation coating parameters for the coatings produced in different solutions (Durdu et al., 2013).....	42
Table 3.1: Elemental chemical composition of bovine bone powder particles.....	50
Table 3.2: Chemical composition of Ti6Al4V substrate material (Grade 5).....	51
Table 3.3: Details of the PEO condition	51
Table 3.4: PEO elemental powder composition/concentration.....	55
Table 3.5: The reagent grade used to prepare 1L SBF.....	64
Table 4.1: Electrolyte formulation for PEO process.....	65
Table 4.2: Elemental chemical compositions of the PEO coatings produced at different concentrations	70
Table 5.1: PEO parameters for BHA deposition.....	89
Table 5.2: Elemental chemical composition of the PEO-BHA coatings produced at varying voltages (at. %)	92
Table 5.3: Average thickness of PEO-BHA coatings produced at varying voltages.....	99
Table 5.4: COF test results obtained under dry conditions for untreated Ti6Al4V and PEO coatings at different applied voltages	103
Table 6.1: PEO parameters for CHA and BHA deposition	109
Table 6.2: Elemental chemical composition of the PEO coatings with two different hydroxyapatite (at.%).....	113

Table 6.3: Electrochemical corrosion parameters of untreated Ti6Al4V and PEO films in Ringer's solution 118

Table 6.4: Elemental composition of the PEO coatings with different hydroxyapatite particles (at.%) 122

University of Malaya

LIST OF SYMBOLS AND ABBREVIATIONS

PEO	:	Plasma Electrolytic Oxidation
NAP	:	Tri-sodium phosphates dodecahydrates
SEM	:	Scanning Electron Microscope
FESEM	:	Field Emission Scanning Electron Microscope
CHA	:	Conventional hydroxyapatite
BHA	:	Bovine hydroxyapatite
CaP	:	Calcium phosphates
Ra	:	Surface roughness (μm)
EDS	:	Energy Dispersive X-ray Spectroscopy
OM	:	Optical Microscope
XPS	:	X-ray photoelectron spectroscopy
FTIR	:	Fourier Transform Infrared Spectroscopy
XRD	:	X-Ray Diffraction
EDM	:	Electrical Discharge Machining
Anatase	:	Titanium oxide
CP-Ti	:	Commercial purity titanium
CoCr	:	Cobalt chromium
FeTiO ₂	:	Ilmenite
HA	:	Hydroxyapatite
Ti-Mo	:	Titanium Molybdenum
Ti-Nb	:	Titanium Niobium
BHN	:	Brinell Hardness Number (kgfmm^{-2})
CP-Ni	:	Commercial purity Niobium
EPD	:	Electrophoretic deposition

HDR	:	High Diffusion Rate
Ni	:	Nickel
Ti	:	Titanium
Al	:	Aluminum
Zr	:	Zirconium
Mg	:	Magnesium
AC	:	Alternating current (A)
DC	:	Direct current (A)
PBC	:	Pulse Bipolar Current (A)
ZnF ₂	:	Zinc fluoride
CaF ₂	:	Calcium fluoride
MAO	:	Micro-Arc Oxidation
SiC	:	Silicon carbide
HSP	:	Scratch hardness (GPa)
P	:	Normal force (N)
L _{C3}	:	Critical load for coating failure (mN)
W	:	Scratch hardness (μm)
SE	:	Scanning Electron
L _{ep}	:	Critical load for onset of plasticity (mN)
SBF	:	Simulated Body Fluid
NaCl	:	Sodium chloride
KCl	:	Potassium chloride
CaCl ₂	:	Calcium chloride
SCE	:	Saturated Calomel Electrode
CR	:	Corrosion rate (mmyear ⁻¹)
PE	:	Protection efficiency (%)

I_{corr}	:	Current density (μAcm^{-2})
E_{corr}	:	Electrode potential (V_{SCE})
B_a	:	Anodic Tafel ($V\text{dec}^{-1}$)
β_b	:	Cathodic Tafel ($V\text{dec}^{-1}$)
R_p	:	Polarization resistance (Ω)
Ti	:	Titanium
TCP	:	Tricalcium phosphates
OH^-	:	Hydroxyl
O	:	Oxygen
P	:	Phosphorus
Cl^-	:	Chloride ion
COF	:	Coefficient of friction
CO_2	:	Carbon dioxide
Ca	:	Calcium
Na	:	Sodium
C	:	Carbon

CHAPTER 1: INTRODUCTION

1.1 Introduction

Titanium and its alloys are transition metals and the fourth most occurring structural metal on Earth. It exists in several minerals such as rutile (TiO_2) and ilmenite (FeO.TiO_2) which are well dispersed over the Earth's crust. Titanium and its alloys are extensively used in a number of fields, including power generation, automotive, dental and biomedical devices. The broad variety of applications are due to its alluring and desirable properties, mainly high strength to weight ratio, good biocompatibility, complete inertness to body environment, low Young's modulus and enhanced corrosion resistance. Among the contending metallic materials for medical applications, titanium and its alloys are fast emerging as the most suitable candidate material because they satisfy the property requirements better than any other competing materials, like stainless steel, commercially pure niobium, tantalum and CoCr alloy (Jackson et al., 2016; Long & Rack, 1998). Their low Young's modulus, good corrosion resistance and superior biocompatibility offer them as an ideal material for biomedical applications. Because of these outstanding properties, titanium and its alloys are widely employed as hard tissue replacements in artificial bones, dentals and joints. Figure 1.1 shows the application of titanium and its alloys as artificial hip joints consisting of femoral head, cup and stem.

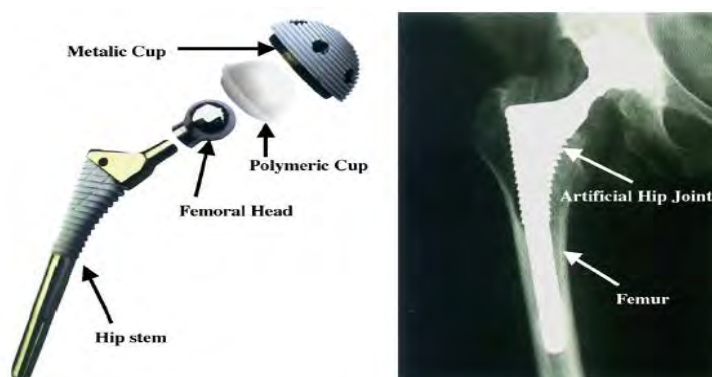


Figure 1.1: Schematic view of artificial hip joint (Liu et al., 2004)

Several grades of titanium and its alloys exist, the most commonly used in biomedical field are the commercially pure titanium (CP-Ti) (ASTM B348 Grade 2) and the Ti6Al4V (ASTM B348 Grade 5) alloy. Aside from their biocompatibility, the mechanical properties of titanium material are much closer to that of human bone compared with other metallic biomaterials. Table 1.1 shows summary of the comparison of mechanical properties of titanium and its alloy with other metallic implants.

Table 1.1: Summary of mechanical properties of metallic biomaterials
(Budinski, 1991; Kamachimudali et al., 2003)

Materials	Density (g/cm³)	Elastic modulus (GPa)	Compressive strength (MPa)	Tensile strength (MPa)
Cortical bone	1.8-2.0	5-23	164-240	35-283
Titanium	4.5-4.5	100-105	130-170	710
Ti6Al4V	4.4-4.5	110-117	758-1117	830-1025
Stainless steel	7.9-8.1	189-205	170-310	480-260
Co-Cr alloy	8.3-9.2	230	450-1000	1000

Thus, titanium materials remain the most popular utilized alloy because of their high level of mechanical strength and a significant assortment of microstructures (Cimenoglu et al., 2011). However, there are some problems associated with the titanium implants including poor bioactivity, poor implant fixation due to lack of osteoconductivity, corrosion and wear in physiological environment. Although titanium alloy exhibits high strength and toughness, they are susceptible to chemical and electrochemical degradation (Antônio et al., 2014; Surmenev, 2012). To overcome these surface originated problems, a range of physical and chemical surface modification techniques have been used, including sol-gel, plasma spray, electrophoretic deposition, magnetron sputtering, and thermal spray. However, there are many drawbacks associated with

these coating methods which include non-uniformity of coating formation, sluggishness of the process and poor adhesion of coating on the substrate (Rad et al., 2014).

Plasma electrolytic oxidation (PEO), also called micro-arc oxidation or spark plasma anodization, has been gaining attention as a novel and unique technique for surface modification of metallic implants because it can produce porous and firmly adherent micro-pore oxide film layer as pointed out by Sowa and Simka (2018). Besides low cost, the PEO process is flexible and there is no limitation on the geometry of the components made of light materials. Moreover, the PEO process allows utilization of benign and non-toxic compounds, thus can be considered as an environmentally friendly technique compared with other counterpart coating processes. The coating obtained through PEO can have a wide range of thickness, providing superior wear and corrosion protection to the substrate.

Over the last three decades, biomaterials research has been focusing on the improvement of titanium implant in an attempt to accelerate bone healing at early implantation. Considering that titanium surface is the first part of the implant that interacts with the host. Titanium material is bio-inert (non-bioactive) material and lacks the ability to directly bond to the surrounding tissues. Hydroxyapatite (HA, $Ca_{10}(PO_4)_6(OH)_2$), the inorganic constituent of bone has been widely employed as a bioactive material on metallic implants. HA is an important mineral to bond chemically with bone and it exhibits excellent bioactivity and biocompatibility with hard tissues without any toxic interaction. Metallic implants containing HA are usually designed to combine the favourable mechanical properties of the implant and biological properties of HA (Narayanan et al., 2008; Pillai et al., 2018).

Earlier works showed that HA was produced on titanium alloys using PEO process (Faghihi-Sani et al., 2013; Teng et al., 2016). In these studies, titanium material was coated by PEO at the first stage and then hydroxyapatite was formed on the oxide film

surface by secondary processes. After PEO, TiO₂-based coatings were placed in a pressure controlled reactors containing neutral or alkaline aqueous solution and treated hydrothermally within the temperature range of 100-250 °C for 2-24 hrs at pH 7-11 in order to obtain HA on the oxide layer (Alsaran et al., 2011; Kossenko et al., 2013). In another study, coated samples were placed in the simulated body fluid (SBF) at 36.5 °C for up to 56 days (Cimenoglu et al., 2011; Dinçer et al., 2013). After these secondary processes, hydroxyapatite was then formed on the TiO₂ coated samples. The existence of calcium and phosphorus containing phases on PEO surfaces exposed to hydrothermal or SBF test assisted the induction and recrystallization of HA layer. Incorporation of HA was also investigated on the titanium alloy in a solution containing Ca and P under different processing parameters (Abbasi et al., 2011; Han et al., 2008; Sowa et al., 2015). The obtained oxide coatings showed an improvement in the bioactivity of HA after few weeks of immersion. These efforts demonstrated that PEO can allow a significant amount of Ca and P ions incorporation either via hydrothermal or SBF treatment into the porous TiO₂ layer. Most of the previous studies have directed the efforts towards increasing the amount of Ca and P elements or recrystallization of HA in the porous oxide layer. However, there have been very few literature reports on how the level of these elements affects the mechanical performance of the PEO-derived oxide film layer. In the present work, a single PEO process was employed to deposit various concentrations of HA on the anodic film in order to identify the influence of Ca and P elements on the morphology and mechanical performance of the oxide coatings. Subsequent work also investigated the formation of coatings using a newly developed biologically friendly electrolytes containing natural bovine bone derived HA. An appropriate voltage regime for this electrolyte has also been studied. This will further help in mimicking the unique composition and structure of human bone tissues. A corrosion and bioactivity test have been undertaken for the titanium coated in a solution

containing conventional HA and bovine bone, derived-HA to examine the performance of the two coatings.

1.2 Problem statement

Several attempts have been made to improve the bioactivity of the titanium alloy through deposition of hydroxyapatite in the oxide film by plasma electrolytic oxidation. There is a strong indication that deposition of HA using a single PEO process has been considered as a difficult process and infrequently reported till date. As a result of this, secondary process either via hydrothermal or SBF treatment are usually employed to produce HA on the PEO-oxide film layer. These efforts have focused on increasing the level of elements in the oxide film. An increase in the amount of HA in the oxide film may have a detrimental effect on the mechanical properties of the PEO coatings. However, the range of HA concentrations to deposit without compromising the mechanical properties of the PEO-coatings has not been satisfactorily investigated and identified. As a source of bioactive elements, calcium and phosphorus inorganic compounds solution are widely selected as PEO electrolyte. From the perspective of biology, bone is a typical inorganic-organic composite. In order to further improve the bioactivity of titanium alloys, selection of an environmentally friendly, containing combination of organic-inorganic electrolytes, especially, natural bovine bone (source from cortical bone) is of critical importance. It has not been possible to harness the various possible attributes of natural bovine bone material to improve the performance of titanium alloy. Therefore, the following challenges still persist in the PEO deposition of HA on the titanium alloy material:

- i. The identification of the range of the PEO parameters such as concentration and voltage for the HA deposition.

- ii. The relationship of HA incorporation and mechanical performance of the film before and after infiltration of HA in the oxide film.
- iii. Sourcing of coating material from natural bovine bone to mimic the biological portion of human bone.
- iv. The in vitro corrosion and bioactive performance of conventional HA and natural bovine HA has not been reported elsewhere.

1.3 Objective of the study

The main objective of this project is to use a single process PEO to produce film, incorporating HA and studying the effect of various HA concentrations in the oxide layer. In order to facilitate the development of novel titanium alloy, a natural bovine HA was also selected to enhance the bioactivity of PEO-based coatings. This involves deposition of BHA on the PEO coatings under different applied voltages. Upon completion of the research at this stage, the following progressive objectives are intended to be achieved.

- To synthesize the hydroxyapatite micron particles from bovine bone cortical bone.
- To study the influence of HA concentrations in the oxide film and its effect on the mechanical performance of the PEO coated layers.
- To develop an experimental set up providing working ranges of PEO input parameter for BHA deposition and investigation of the various responses of the coated layer.
- To make a comparative evaluation on the in vitro corrosion and bioactive performance of the conventional hydroxyapatite and bovine hydroxyapatite PEO coatings.

1.4 Research scope

The research work consists of three parts: (i) investigation of the influence of HA concentration in the TiO₂ film and studying the mechanical performance of the PEO coating before and after incorporation of HA (ii) production and characterization of bovine hydroxyapatite micron particles from cortical bone; (iii) determination of the range of PEO voltage parameters for the deposition of BHA in the PEO coatings (iv) evaluation of the in-vitro corrosion and bioactive performance of PEO coatings processed in a solution containing conventional HA and bovine HA. The first part involves the selection of appropriate electrolyte solutions for various HA concentrations through preliminary study. The second part involves synthesis and characterization of the bovine bone powders produced from cortical bone material (ball milling, XRD, FTIR, sieving, micron size particle etc). The second part consists of two elements: (a) selection of concentration of BHA particles and a PEO voltage regime for the deposition of BHA, and (b) fabrication and characterization of the coatings developed with PEO voltages to investigate the surface morphology, coating thickness, surface roughness, adhesion strength, EDS/elemental mapping analysis, XRD, XPS analysis, coefficient of frictional forces and wear test analysis. The third part compares the in vitro corrosion and bioactive performance of conventional HA and natural bovine HA developed under the same processing condition.

1.5 Research methodology

This research commences with literature review in the general and specific areas of titanium based materials and surface engineering coating techniques. The general survey highlighting the challenges of the calcium phosphate (CaP) coating on titanium alloys, and various previous efforts aimed at deposition of CaP on the titanium implants were evaluated. This includes the areas of hydroxyapatite, the titanium alloys as well as

the surface treatment techniques. Following the literature survey, a scheme for carrying out the research is designed and this consists of the following specific activities:

- a. Identification and selection of the suitable electrolyte for HA deposition through preliminary study.
- b. Development of coatings using PEO process parameters and the most appropriate range was selected for the investigation.
- c. Specification and preparation of coupon material used for experimental PEO:
 - EDM wire cut titanium sheet to suitable dimension and surface preparation via mechanical grinding, polishing and chemical cleaning.
 - Pattern design of the counter electrode
 - Electrolyte bath design/coating formulation
- d. Characterization:
 - Surface structure characterization using FESEM, OM, XRD, EDX, surface roughness, XPS, FTIR and elemental mappings.
 - Mechanical characterization using profilometer, scratch tester and wear analysis.
 - Biological evaluation via corrosion test and apatite forming ability.
- e. Analysis of the results to establish the influence of the input parameters on the output of the PEO coated surface.
- f. Correlation of the output response with the input parameters.

The flow diagram of the research methodology is presented in Figure 1.2.

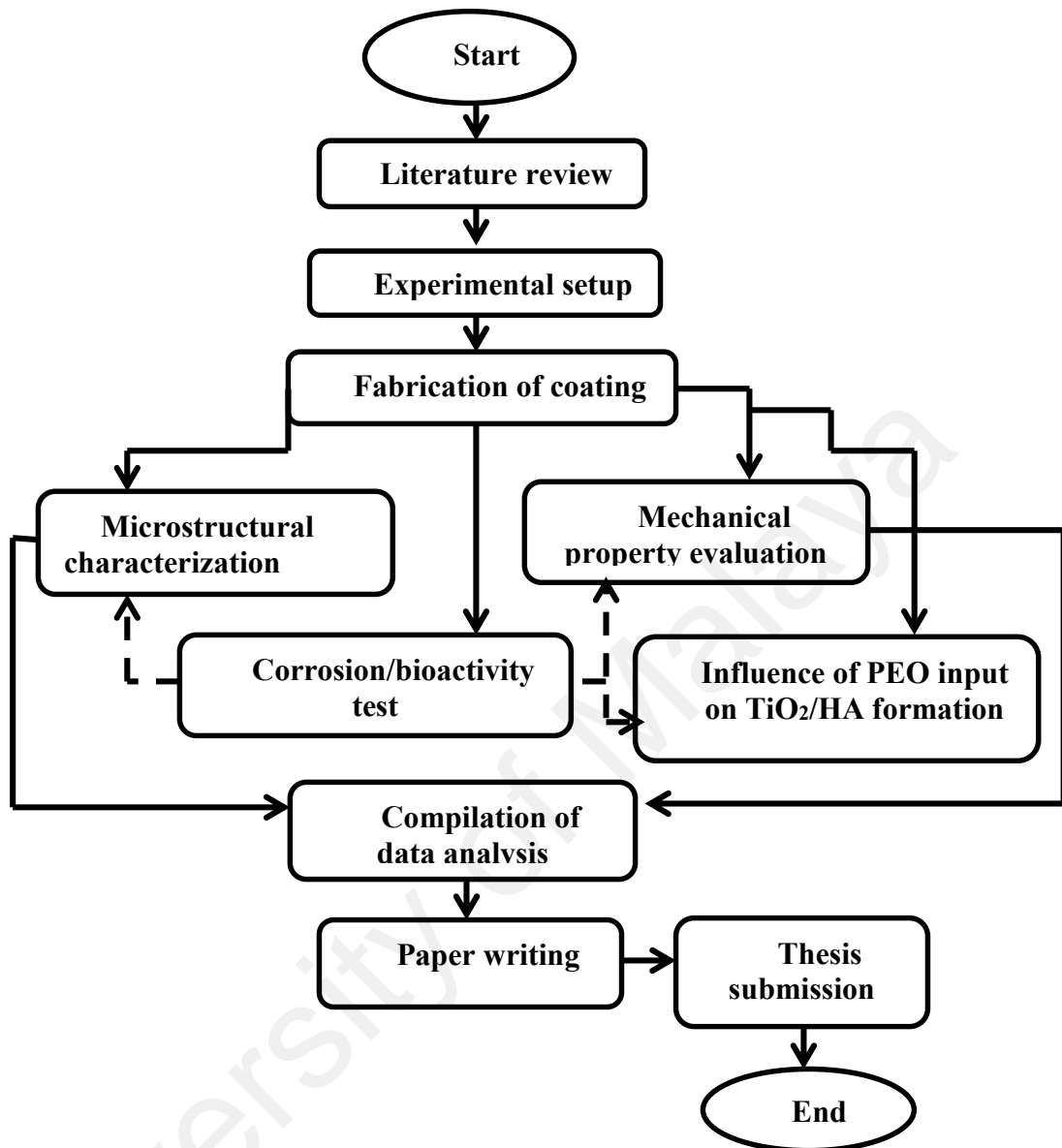


Figure 1.2: Work flow of the research work

1.6 Organization of the thesis

In order to meet the aforementioned objectives various studies are included in this work, which is distributed into seven chapters. The elements of the thesis chapter by chapter are shown in Figure 1.3.

Chapter One is the introduction which gives the trajectory of the thesis. This includes the background of the research, problem statement, objectives, methodology, scope and the thesis structure.

Chapter Two presents the literature survey giving the background discussion necessary for understanding calcium phosphate deposition on titanium alloys implant. The review was also made on the development of PEO process and features, which include specifications, microstructures, applications and corrosion of titanium and its alloy, tribological and biomedical behaviour of titanium implants. Some unresolved issues related to PEO deposition of HA were raised and these issues provided the basis for the research documented in this thesis.

Chapter Three describes the experimental work in terms of experimental regime of the process parameters, the experimental method used for coupons preparation, the materials and electrolyte employed for plasma electrolytic oxidation, surface roughness measurement, FESEM-EDX, X-ray photoelectron spectroscopy (XPS), FTIR and XRD phase. The analytical techniques used for coupons characterizations, and the procedures used for corrosion, mechanical properties, wear and biological test are described in details.

Chapter Four investigates the influence of hydroxyapatite concentration in the oxide film and mechanical behaviour of the film before and after HA incorporation.

Chapter Five analyses the influence of PEO electrical parameter on BHA deposition and the morphological/mechanical characterization of the coated layers.

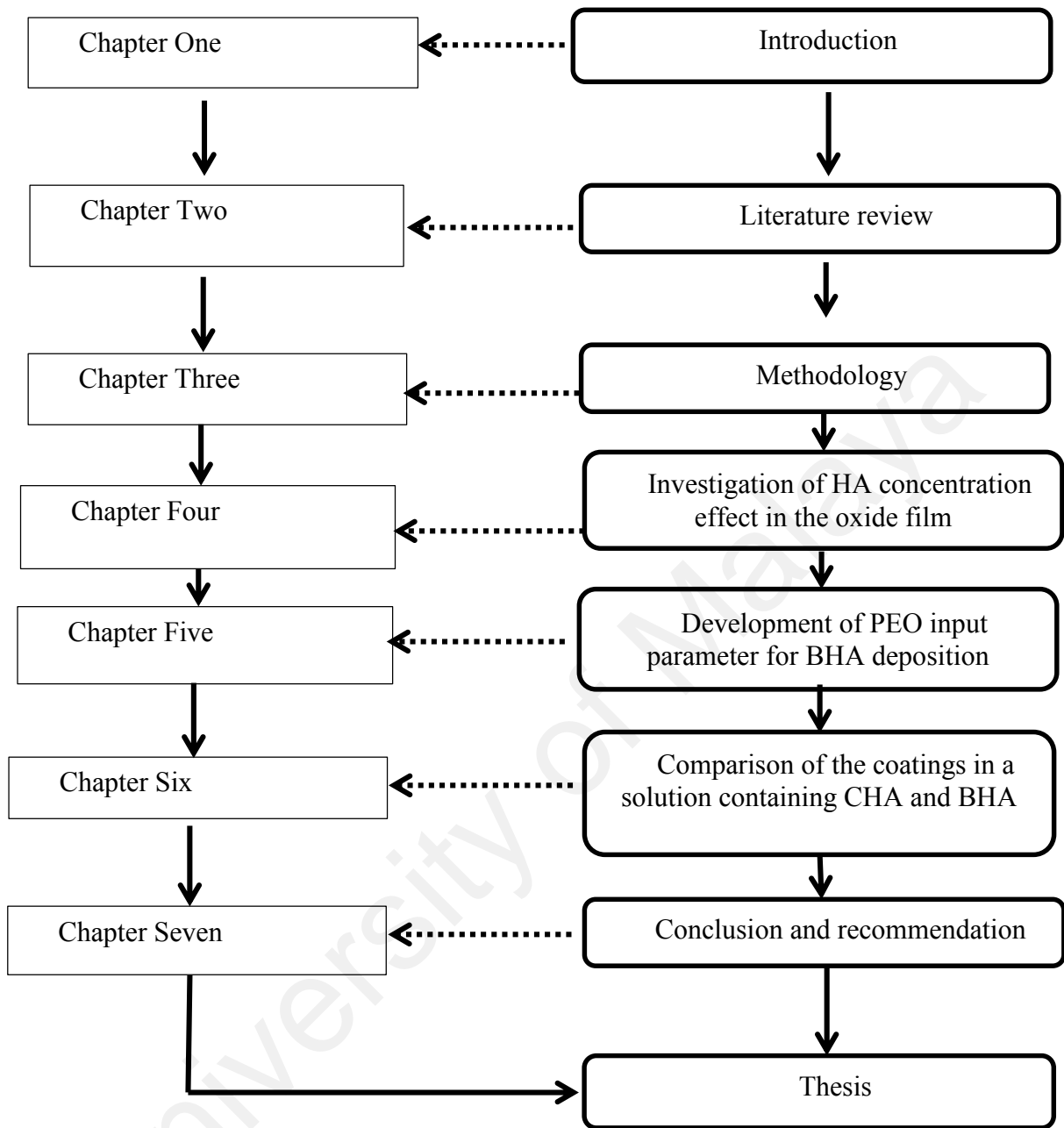


Figure 1.3: Structure of the thesis

Chapter Six studies the microstructure-property performance of coating developed in a solution containing bovine HA and conventional HA

Chapter Seven summarizes the findings of the research, enumerates the contribution to the frontier knowledge and suggests directions for future research on HA-PEO coatings.

CHAPTER 2: LITERATURE REVIEW

2.1 Introduction

The main thrust of this research is to use the advantage offered by the high plasma discharges event of PEO to modify the surface of titanium so as to achieve high quality bioactive coating. Toward this end, the PEO parameters such as concentration, voltage, and electrolyte compositions are involved. Therefore, this chapter reviews the research developments on calcium phosphates based coatings taking cognizant of the aforementioned areas, different efforts made in treating the alloy through PEO. Finally, pertinent issues associated with the subject of this research were reviewed in this chapter.

2.2 Researches on titanium alloys

2.2.1 Titanium alloys

Titanium-based alloy materials were firstly developed in the early 1950s for aerospace applications. The combination of high strength to weight ratio, low density and good biocompatibility were the attractive properties that determine the applications of titanium in such industries. Titanium alloys are very important for biomedical because of the superior corrosion resistance and passive thin oxide layer formation on its surface. Arising from reducing cost and increasing availability, these materials have become standard materials for various engineering applications (Schutz & Grauman, 1986). The typical designation, elemental chemical composition, and physical properties of titanium alloy and CP-Ti used for implant have been summarized in Tables 2.1-2.2.

Table 2.1: Designation and elemental composition of commercial titanium alloys

(Welsch et al., 1993)

Titanium materials	ASTM Grade	UNS designation	Nominal composition wt. %	Alloy type
CP-Ti 1(a)	1	R50250	Unalloyed titanium	α
CP-Ti 2(a)	2	R50400	Unalloyed titanium	α
CP-Ti 3(a)	3	R50500	Unalloyed titanium	α
CP-Ti 4	4	R50700	Unalloyed titanium	α
Ti-Pd(a)	7/11	R52400,R52250	Ti-0.15Pd	α
Ti-lean Pd(a)	16/17	R52402,R52252	Ti-0.06Pd	α
TiRU or TiRU (a)	26/17	R52404/R52254	Ti-0.1Ru	α
SMI-ACE(a)	30/31	...	Ti-0.3Co-0.05Pd	α
AKOT(a)	33/34	...	Ti-0.4Ni-0.015Pd0.025Ru.15Cr	α
Grade 12(a)	12	R53400	Ti-0.3Mo-0.8Ni	α
Ti-3-2-5	9	R56320	Ti-3Al-2.5V	Near- α
Ti-3-2-5 Ru(a)	28	R56323	Ti-3Al-2.5V-0.1Ru	Near- α
Ti-3-2-5 Pd(a)	18	R56322	Ti-3Al-2.5V-0.06Pd	Near- α
Ti-6-2-1-1	Ti-6Al-2Nb-1Ta-0.8Mo	Near- α
Ti-5-2-5	6	R54250	Ti-5Al-2.5Sn	α
Ti-5-1-1-1	32	R55111	Ti-5Al-1Sn-1Nb-1Zr-0.8Mo	Near- α
Ti-8-1-1	...	R54810	Ti-8Al-1V-1Mo	Near- α
Ti-6-2-4-2-S	...	R54620	Ti-6Al-2Sn-4Zr-2Mo-0.1Si	Near- α
Ti-6-4-2	5	R56400	Ti-6Al-4V	$\alpha - \beta$
Ti-6-4-ELI	23	R56407	Ti-6Al-4V (0.13 max O)	$\alpha - \beta$
Ti-6-4-Ru(a)	29	R56404	Ti-6Al-4V-0.1Ru (1.13 max O)	$\alpha - \beta$
Ti-550	Ti-4Al-2Sn-4Mo-0.5Si	$\alpha - \beta$
Ti-6-6-2	...	R56620	Ti-6Al-6V-2Sn-0.6Fe-0.6Cu	$\alpha - \beta$
Ti-6-2-4-6	...	R56260	Ti-6Al-2Sn-4Zr-6Mo	$\alpha - \beta$
Ti-6-22-22	Ti-6Al-2Sn-2Zr-2Mo-2Cr-0.15Si	$\alpha - \beta$
Ti-17	...	R58650	Ti-5Al-2Zr-2Sn-4Mo-4Cr	$\alpha - \beta$
Ti-10-2-3	Ti-10V-2Fe-3Al	Near- β
Ti-5-5-5-3	Ti-5Al-5Mo-5V-3Cr	Near- β
Ti-15-3-3-3	Ti-15V-3Sn-3Cr-3Al	β
Beta-C(a)	19	R58640	Ti-3Al-8V-6Cr-4Zr-4Mo	β
Beta-C/Pd(a)	20	R58645	Ti-3Al-8V-6Cr-4Zr-4Mo-0.06Pd	β
Ti-13-11-3	Ti-3Al-13V-11Cr	β
Beta-21S(a)	21	R58210	Ti-15Mo-2.7Nb-3Al-0.25Si	β
Ti15-5-3(a)	Ti-15Mo-5Zr-3Al	β
Ti45Nb	Ti-45Nb	β

Due to the relatively limited properties of titanium material, different alloy elements are added to improve its strength for biomedical applications. The phases of titanium material are stabilized when alloying elements are added. The addition of these elements causes the phase transformation from hexagonal closed-packed to body centered cubic phase. Generally, phases of titanium have been categorized into three different types such as alpha (α), beta (β) and alpha-beta (α - β) phases based on the crystalline structure; however, near-alpha and near-beta can also be obtained depending on the type and alloying elements being added (Table 2.1). The α -phase contains hexagonal closed packed structure, while β -phase is body centered cubic structure. The α -alloy contains neutral alloying elements such as aluminium and tin, and cannot be heat treated.

Table 2.2: Summary of physical properties of titanium (Aliasghari et al., 2016; Liu et al., 2004)

Property		Typical value
Atomic weight (g/mol)		47.9
$c(\text{\AA})$		4.6832±0.0004
Alpha (\AA)		2.9504±0.0004
Beta, cubic, body centered		
Alpha (\AA)		3.28±0.003
Density (g/cm ³)	CP- titanium, Grade 2	4.5175
	Beta-titanium, at 1000°C	4.302
	Amorphous titanium	3.54
Coefficient of thermal expansion	CP-Ti, Grade 2	16.3
Melting point (°C)	CP-Ti, Grade 2	1668
Boiling point (°C)	High purity	3210
Phase transformation temperature (°C)	CP-Ti, Grade 2	882.5
Electrical resistivity ($\mu\Omega\text{cm}$)	High purity	42
	CP-Ti, Grade 2	55
Elastic modulus (GPa)	CP-Ti, Grade 2	103
Yield strength/Density (Nmkg ⁻¹)	CP-Ti, Grade 2	78
Ultimate strength/Density (Nmkg ⁻¹)	CP-Ti, Grade 2	107
Fatigue strength/Density (Nmkg ⁻¹)	CP-Ti, Grade 2	54
Hardness, BHN	CP-Ti, Grade 2	160

The near α -alloys have higher strength compared to the full α -alloy and possess good creep resistance. The α - β alloys contain a combination α and β stabilizers and can be heat treated to strengthen and enhance their properties. The most common alloy in this category for orthopaedic implant is Ti6Al4V (Cimenoglu et al., 2011; Freese et al., 2001). β -alloys contain stabilizers such as molybdenum, vanadium and can be treated to obtain a higher strength.

2.2.2 Corrosion resistance of titanium alloys

The excellent corrosion resistance of titanium-based materials arises from the formation of self-healing thin passive film. The presence of oxide film, which is between 3-10 nm has been considered as a very effective barrier to corrosive media (Andreeva, 1964; Golestani-Fard et al., 2011). It is known that titanium material permits passage of electric current and allows electrochemical reduction of ions in a corrosive environment. Due to the interaction between the passive film and aggressive ions, the electrolyte solution can access to the titanium surface by defects the film. The breakdown of the oxide film and resultant corrosion of titanium material may occur. This can lead to generation of particulate debris, which may in turn aggravate the physiological environment and elicit both local and systemic biological responses. Aside the corrosive medium, chemical compositions of the implant material play a vital role in determining the corrosion rate of titanium implant material. As soon as the passive oxide film is broken, the release of metal ions will be easier which can be a toxic contaminant inside the human body. For instance, the vanadium ion release on titanium alloys that is preceded with corrosion process (Morais et al., 2007).

The corrosion resistance of titanium material can be improved by the addition of alloying element. It has been shown that addition of molybdenum can improve both the mechanical properties and corrosion resistance of titanium (Kumar et al., 2010).

However, in a separate study conducted by Kumar and Narayanan (2008), they observed that the corrosion resistance of Ti15Mo is strongly dependent on several factors in solution rather than molybdenum addition.

Besides alloying, another appropriate method to reduce the corrosion rate and metal ions release from titanium material is via surface modification by protective bioceramic coatings (Chaturvedi, 2009; Hermawan et al., 2011; Kamachimudali et al., 2003). Coating can separate the metallic implant from its surrounding corrosive environment, hence reducing the corrosion rate. Surface treatment via traditional methods such as physical vapour deposition, diffusion process, sol-gel, electrodeposition, etc. often imparts satisfactory corrosion resistance to implant materials with intrinsically inadequate properties (Kamachimudali et al., 2003). They have only limited use for protecting metallic implants since many are subjected to abrasion and wear in biomedical implant applications.

Plasma electrolytic oxidation is a versatile electrolytic process for producing thick, stable oxide film on the metal surface. Because of the excellent corrosion and wear resistance offer by this technique, the PEO process has been widely studied. Various plasma assisted anodizing process such as HAE and Keronite, Anomag and Magoxid have been currently commercialized (Blawert et al., 2006; Gray & Luan, 2002). More importantly, it can form ceramic coatings composed mainly of substrate metal oxides and electrolyte ingredients. With this technique, a porous surface morphology is formed due to plasma discharge during PEO process, which provides a potentially favourable layer for corrosion prevention. It has been well established that the PEO process produced higher adhesion strength between the coating and substrate compared to conventional coating methods (Cakmak et al., 2010). In fact, PEO process has been considered as one of the most suitable treatment for titanium implant applications as it

offers a favourable biological environment (Aliasghari et al., 2014). PEO technique has been given major attention in the present work.

2.2.3 Wear characteristics of titanium materials

Wear is another surface degradation problem that limits the use of titanium alloys in several applications. Although titanium based alloy is used in several critical areas including biomedical field, aerospace and automotive industries, it has poor tribological properties and thus tends to seize under relative sliding contact. The removal of thin oxide film, which intrinsically formed on the titanium surface in turn caused wear process (Komotori et al., 2007). Since wear is a surface phenomenon and it is considered as a surface failure that occurs due to surface contact, thus surface treatment is an appropriate method to improve the wear resistance. An improvement of the wear properties of titanium alloy was reported due to the formation of calcium phosphate coatings (Durdu & Usta, 2014). The coating structure predominantly contained high amounts of TiO_2 and HA_p phases and crater-like (Durdu et al., 2016). Gordienko and Gnedenkov (1997) investigated the development of wear resistance and anti-frictional coatings on titanium implant via PEO method. It was found that the coatings produced in phosphate electrolyte solution not only exhibit better corrosion resistance but also reduce the friction coefficient in the titanium, because the wear product (pliable fine powder) acts as a lubricant.

Different types of wear based on wear mechanism have been developed and categorized into sliding, impact and rolling contact (Figure 2.1). The wear mechanism is a classification of the process by which material is removed from the contact surface. In wear mechanism, a real contact more than one mechanism acts at the same time.

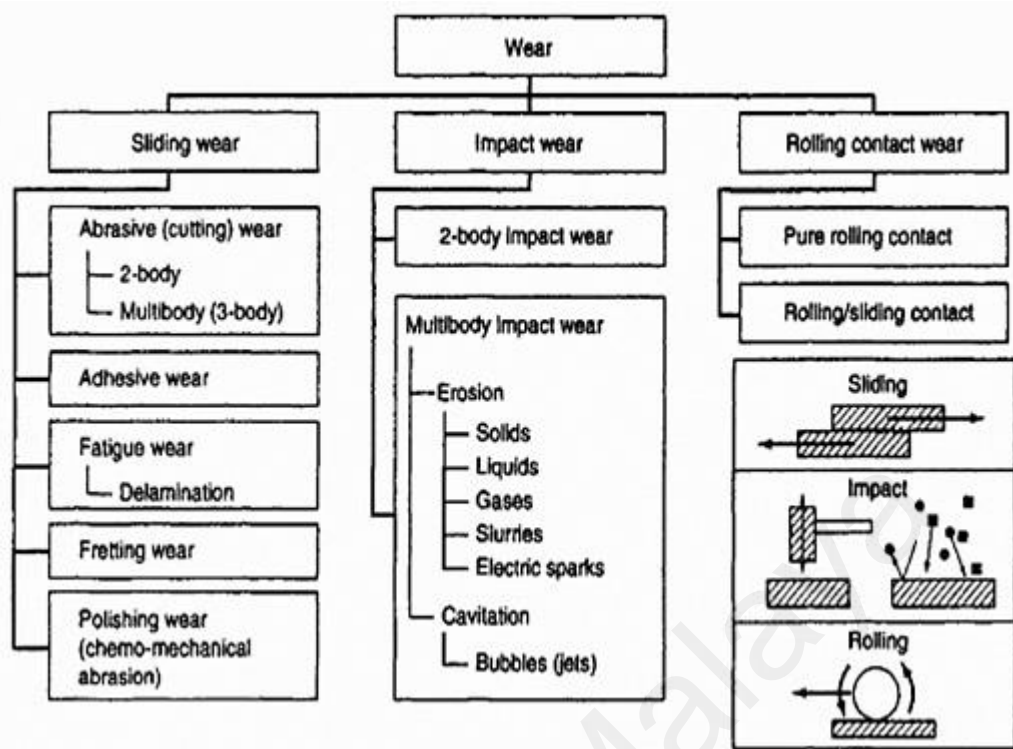


Figure 2.1: Wear classified by the type of relative motion, such as sliding, impact and rolling contact (Davis, 2001).

The precise combination of wear mechanism depends on the contact conditions which results in a specific type of wear. There are different types of wear in the industry and in our daily life. Different methods are used to categorize the wear process. For examples, wear can be divided as lubricated wear and unlubricated wear, severe wear, mild wear, sliding wear, rolling contact wear and impact wear. However, all wear process involves one or a combination of wear mechanisms, including abrasion, adhesion, fatigue and oxidation or other tribo-chemical actions. In order to solve a wear problem, it is necessary to understand the underlying wear mechanism. Basically, there are mainly four types of wear mechanisms available which are recognized by the industry such as abrasive wear, adhesive wear, fatigue wear and chemical wear (Holmberg & Mathews, 1994). The two most frequently encountered wear mechanisms in the industry are wear by abrasion and wear by adhesion. In the classification of Blau

(1997), galling, scuffing and scoring are not considered as types of wear since the material is not removed (Figure 2.2).

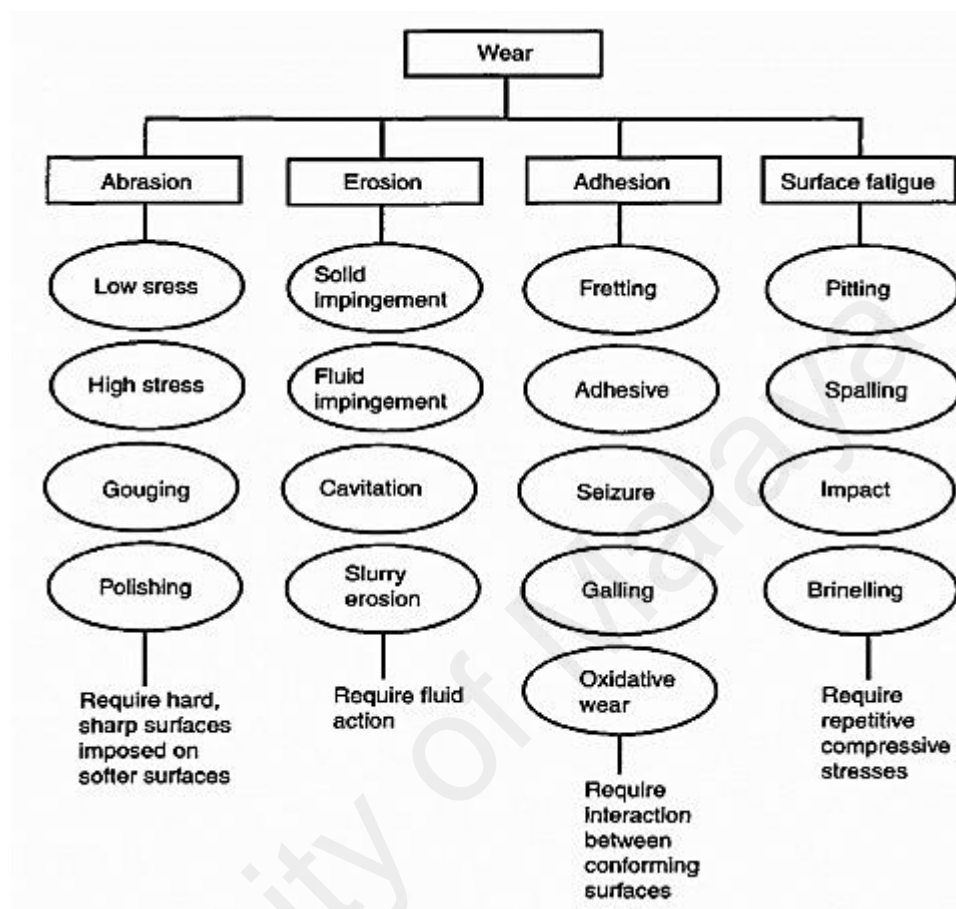


Figure 2.2: Various categories of wear based on abrasion, erosion, adhesion and surface fatigue (Davis, 2001).

Fatigue and chemical wear are also addressed as they are considered as part of the wear mechanism.

2.2.3.1 Abrasive wear

There are two types of situation where abrasive wear may occur. The first is two body abrasion which occurs when metal-on-metal contact protuberances (asperities) on a hard surface plough or cut through the other surface while in the three-body abrasion the wear hard particles are free to roll and slide between two sliding surfaces causing the hard particles to be trapped between two sliding surface and abrading one or both

surfaces (Hutchings, 1992). In abrasive wear mechanism, the hard asperities or particles penetrate into the softer surface under normal contact pressure. The tangential motion imposed caused the materials on the soft surface, to be removed by combining effect of micro-ploughing, micro cutting and micro cracking which makes the worn surface to be characterized with particles, grooves and scratches.

2.2.3.2 Adhesive wear

Generally, most engineering surfaces is not perfectly flat, the wear by adhesion is mostly characterized by the appearance of junctions between surfaces that are subject to friction (Takadom, 2013). When two such surfaces that are brought into contact becomes weak, plastic deformation occurs at the junction of the two surfaces and when the interface (junction) is strong the softer material is subject to shearing which later transferred to harder material. Most metallic materials show an appreciable tendency of adhesion. The relative motion between the two contact surfaces usually paves way for the tearing to take place at the cold junction inside the original material depending on which is weaker. If the strength of adhesion is relatively low, in case of metallic surface which are usually separated by oxide films, it gives way for the tearing to take place at the junction and material loss is minimal. However, if the tearing occurs inside, the material, a fragment of softer material is dragged away and adhering to the harder body.

2.2.3.3 Fatigue wear

Fatigue wear of a material occurs when a material is subject to a cyclic loading during friction. It is the progressive and localized structural damage that occurs when a material is subjected to cyclic loading. Fatigue occurs if the applied load is higher than the fatigue strength of the material. As a result of repeated cyclic stresses that are subjected to the material, strain is introduced in the superficial layers of the material caused the surface of the material to be dented and resulting in cracking (Takadom,

2013). These cracks spread after repeated stress by the bearing load, even without additional particulate damage. As a result, the surface fails, producing a spall. Contamination reduces bearing life significantly through fatigue, abrasion and roughening of operating surfaces.

2.2.3.4 Tribochemical wear

Tribochemical wear is a phenomenon which involves the growth of a film of reaction products due to chemical interactions between the surfaces in contact with each other and the surrounding environment. Tribochemical wear mechanisms involve a coupling between the mechanical and thermal processes occurring at the interface and the environment (Takadom, 2013). The corrosiveness or reactivity of the environment is generally enhanced due to these mechanical and thermal processes. In all environments, corrosion follows the wear process except in an inert atmosphere and vacuum. Combination of wear and corrosion on a material surface leads to severe damage of an implant material. As depicted in Figure 2.1, wear and corrosion can proceed by many mechanisms. The synergistic relationships that exist between abrasion, impact and corrosion that significantly increase the degradation of the material in aqueous environment have been determined (Natarajan et al., 1984; Stachowiak, 2006).

2.2.4 Titanium alloy as an orthopaedic implant

Titanium based alloys have been widely accepted in the biomedical industry because they perform property requirement than any other competing materials (CoCr, commercial purity niobium (CP-Ni), commercial purity tantalum and stainless steel). One important yardstick in metal selection for biomedical application is the consideration of their properties such as biocompatibility, bio-adhesion, modulus of elasticity etc. The combination of good mechanical characteristics and corrosion resistance make the titanium material very attractive for medical devices, automotive,

aerospace and marine applications. There are several types of prosthetic devices using titanium materials, e.g. hip joint implants, heart valves, bone plates and other kind of fixtures employed in dental area.

As biomedical implants, CP-Ti, α - β alloys Ti6Al4V and β -alloys are used. CP-Ti and Ti6Al4V were the first titanium materials used as hard tissue replacements and up till today, they are widely used in most applications. Figure 2.3 shows the first usage of titanium as bone plate. The X-ray radiographs reveal the broken bone before and after attaching the bone plate. Owing to the suspicion of a toxicity problem with vanadium, Ti6Al7Nb and $\alpha + \beta$ TiAl2.5Fe were developed in the 1980's. The microstructure and properties of the two alloys are similar to the $\alpha + \beta$ Ti6Al4V alloy. In an application where higher strength is desired for bone plates, either the Ti6Al4V or the Ti6Al7Nb is used (Perren et al., 2001).

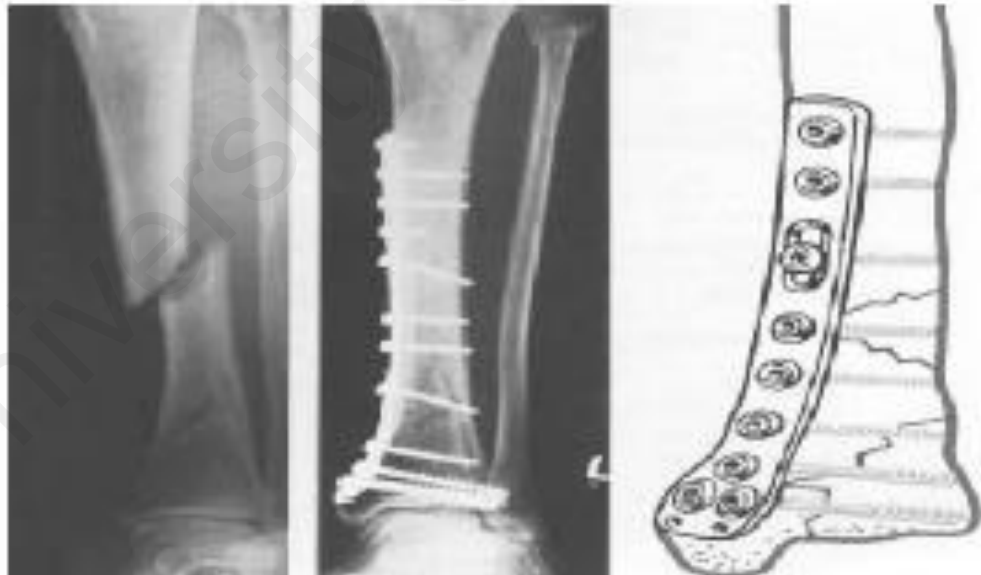


Figure 2.3: Example of a bone plate implant, CP titanium grade 3 (Donald et al., 2001).

Because of the need for higher fatigue strength and lower modulus of elasticity, different types of β -alloys were developed in the 1990's. The compositions of various types of β -alloys used for hard tissue replacement are shown in Table 2.3.

Table 2.3: Compositions of low modulus β alloys developed for biomedical applications (Lütjering & Williams, 2007)

Composition	ASTM standard	Alloy type	Country developed
Ti13Nb13Zr	F1713	β	USA
Ti-12Mo-6Zr-2Fe	F1813	β	USA
Ti-15Mo	F2066	β	USA
Ti-16Nb-10Hf	-	β	USA
Ti-15Mo-5Zr-3Al	-	β	Japan
Ti-15Mo-2.8Nb-0.2Si-0.26O	-	β	USA
Ti-35Nb-7Zr-5Ta	-	β	USA
Ti-29Nb-13Ta-4.6Zr	-	β	Japan

However, the aforementioned properties of titanium material can only provide temporary protection in the human body environment, as it is known when implant material is placed within the bone for repairing, there are various biological, physical, chemical and other factors that determines whether material can easily bond or not. Despite reports of direct bond, titanium alloys do not form chemical bonds with bone tissues (Durdu et al., 2016). The poor bonding ability and possible corrosion/wear problems have led to the development of bioactive calcium phosphates (CaP) on its surface to accelerate bone bonding formation.

2.3 Research trends in CaP coating on titanium alloy implant

Over the years, effort has been made to improve the performance of titanium implants through bioactive coating. Literatures have presented different views on CaP coating research at different periods. A state of the art review of CaP coating research showed that the performance measures, process variables and surface integrity were the major focus of the researches (Surmenev et al., 2014). Progressive investigations

together with advances in biological science and biomedical engineering have led to the increasing demand of bioactive substances, which is of significance not only in terms of similarity in composition to natural bone but also from the economic aspect. Recently, Qiao et al. (2016) introduced organic-inorganic composites bioactive materials to achieve an early and functional bone apposition of the titanium implant. Additionally, other variants of CaP were presented with the aim of improving the surface integrity and bone bonding formation with the surrounding tissues. The research trends in CaP are seen to be changing over time to address the challenges in practice as they are encountered, and thus prompting the introduction of new coating material or new surface engineering methods. The growing demands as well as to improve life quality have been stimulating the development of novel coating materials for orthopaedic applications. However, the main objective of this new coating material being introduced continues to remain the same: to mimic the biological portion of human bone and to provide a good surface for anchorage of new bones.

In this review, the research developments of CaP coating on titanium alloy implants would be evaluated in terms of improvements and popular surface treatment techniques for CaP coating.

2.3.1 Fabrication of bioactive CaP on titanium alloy implant

Generally, biomedical implants should exhibit sufficient bioactivity and proper osseointegration in the human body. The bioactivity of titanium material and other alloys are poor and this prevents them from performing their biological function. Enhancing its bioactivity has been the primary focus; however, in recent times, attention has gradually moved towards bioactive coating which can promote direct interaction between the implant and tissue components. Based on this requirement, considerable research efforts have been devoted towards producing coatings containing Ca and P

element in the oxide film layer (Aktuğ et al., 2017; Antônio et al., 2014; Qiao et al., 2016). Hydroxyapatites $\text{Ca}_{10}(\text{PO}_4)_6(\text{OH})_2$, has been widely used as the most bioactive material for orthopaedic and dental bio-metallic implants due to its chemical composition, biological and crystallographic similarity to human bone. HA is the most stable of CaP compounds and has intrinsic osseointegration potential which makes it a better candidate material of choice in orthopaedic and dental applications. Aside from its high bioactivity, HA possesses high stability in human body fluid and thus can protect the implants by hindering the corrosive medium from penetrating into the substrate. A strong and durable bone to implant connection can be achieved by the formation of a stable bone tissue in bone-implant interface by various surface engineering techniques as can be sol-gel, electrophoretic deposition, thermal spray, magnetron sputtering and plasma electrolytic oxidation.

2.3.2 Surface engineering techniques of producing CaP coatings

The possibility of modifying the surface area of metallic implants by tailoring the composition and structure using various surface engineering techniques available has grown wider recently in the fields of biomedical industry. CaP coatings, especially, hydroxyapatite coating is commonly employed in orthopaedic applications. Many surface engineering methods have been developed for the deposition of CaP coatings on metallic implants. Generally, coating fabrication methods can be broadly classified into two: chemical and physical deposition. Chemical deposition involves chemical treatment of metallic materials in an electrolyte solution. Three techniques are presented here: sol-gel, micro-arc oxidation and electrophoretic deposition. On the other hand, physical deposition includes those methods which involve atomization or vaporization of a material from a solid source and the deposition of these materials onto the substrate to form a dense coating. Physical deposition methods are classified into plasma spray, magnetron sputtering and physical vapour deposition, of which plasma spray is the most

widely used for the deposition of CaP coatings because of its ability to produce a higher deposition rate and coating thickness of 30–200 μm (Liu et al., 2004), which improves the biological properties of the material.

2.3.2.1 Thermal spray for CaP coating

Thermal spray allows production of HA onto metallic substrates with a thick layer ranging from 30 to 200 μm . Studies on the coatings of HA formed by thermal spray show that the particle size is an important factor to obtain a good quality coating (Smith et al., 2015). The interaction between the molten HA particles and the plasma beam have strong influences on the way the particles in the plasma beam melt and transform both physically and chemically. Generally, the HA particles should be of the similar shape and the uniformity of the size should be maintained. This is due to the fact that thermal sprayed HA particles of different sizes caused overheating and subsequent evaporation owing to a high thermal energy and kinetic effect of the plasma beam. The use of pure crystalline HA particle size is important, but does not necessarily guarantee good quality of the desired mechanical and biocompatibility properties of thermal spray HA coatings. Ntsoane et al. (2016) investigated the size and the crystalline effect of pure HA powder on the microstructure and mechanical properties of plasma spray. They found that at a larger particle size, there are numerous un-melted particle sizes, cavities and macropores with attendant poor mechanical properties due to poor interlamellar adhesion and cohesion of the coating. The use of weak agglomerated HA powder particles can further worsen coating inconsistency by allowing fragmentation of HA particles to take place during plasma particle interaction (Ntsoane et al., 2016). Figure 2.4 shows a typical scanning electron micrograph of an as-sprayed HAp coating formed. From the result, it is evident that the micrograph of that HAp coating is characterized by partially melted and unmelted particles with a mild crack running across the surface

(Figure 2.4a). The formation of pores and gaps across the coating thickness layer was attributed to poor mechanical interlocking between coating and substrate (Figure 2.4b).

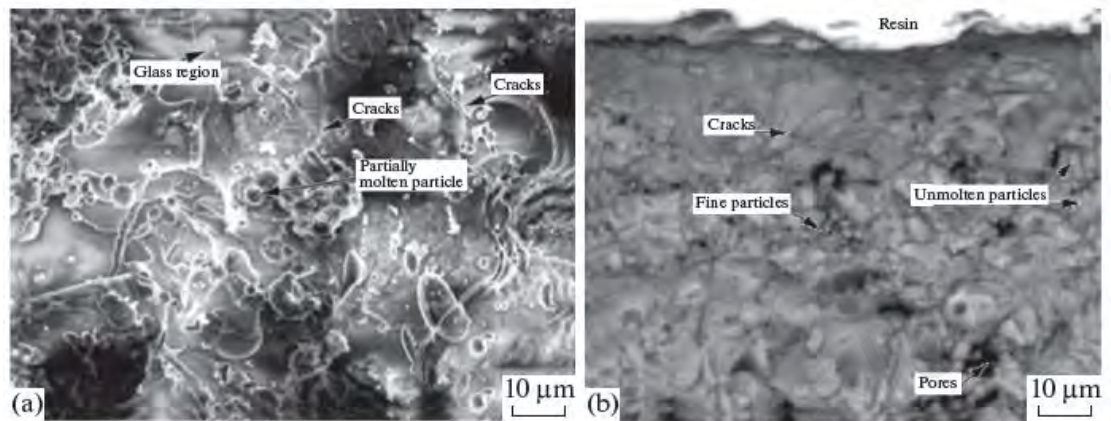


Figure 2.4: Scanning electron micrograph of a typical as-sprayed HAp coating: (a) top surface; b) cross-section (Ntsoane et al., 2016).

Recent findings have revealed that thermal spray HA particles of various sizes can be produced under certain processing conditions and the problem that arises from variations of particle sizes can be avoided. However, the technique requires a high sintering temperature, which produces cracks on the surface of the coating. In addition, the coating deposited by thermal spray suffers from poor interfacial bonding strength and non-uniformity of the coating, which reduces the life span of metallic implant (Mohseni et al., 2014).

2.3.2.2 Radio frequency magnetron sputtering for CaP coating

The deposition of CaP thin film coatings by Radio frequency (RF) magnetron sputtering is usually in the form of the amorphous phase and post heat treatment is usually carried out which is typically in the range of 400–700 °C (Nelea et al., 2003; Takahashi et al., 2008), thus ensuring highly crystalline and better stability on metallic implant materials. However, the CaP thin films produced under a lower post heat treatment temperature $\leq 400^{\circ}\text{C}$ displayed poor crystallinity and greater phosphates as

compared to as sputtered at higher temperatures as pointed out by Yang et al. (2005). RF magnetron sputtering allows preparation of CaP thin films with a composition close to that of the initial target by keeping the substrate temperature at 100°C (Shukor et al., 2010) or 250 °C (Hayakawa et al., 2004). The coating thickness deposited from RF magnetron sputtering is typically in a range of 0.5–4 µm while the surface roughness varies from 0.05–0.28 µm. It is a well-known fact that the surface morphology plays a vital role in the overall success of metallic implant materials (Variola et al., 2011). RF magnetron sputtering allows the preparation of homogeneous continuous coatings that are highly dense, uniform, of lower porosity and without any micro-crack. The typical pattern of the surface morphology of CaP thin film coating prepared by RF magnetron sputtering is presented in Figure 2.5. The figure shows the surface morphology of the etched titanium surface (Figure 2.5a) and the SEM cross-sectional view of the CaP grown on titanium etched surface (Figure 2.5b–d). Various thickness of the surface of CaP 170 ± 20 ; 250 ± 40 ; and 440 ± 50 nm grown via magnetron sputtering revealed a thin, fine layer of CaP (~ 30–50 nm thick) with a regular grain-like morphology. An increase in the average grain size is noticed as well as an increase of the thickness. Despite the remarkable success, RF magnetron sputtering for deposition of CaP coatings requires post heat treatment in order to obtain highly crystalline and dense coatings. Moreover, magnetron sputtering is expensive and time consuming (Shukor et al., 2010).

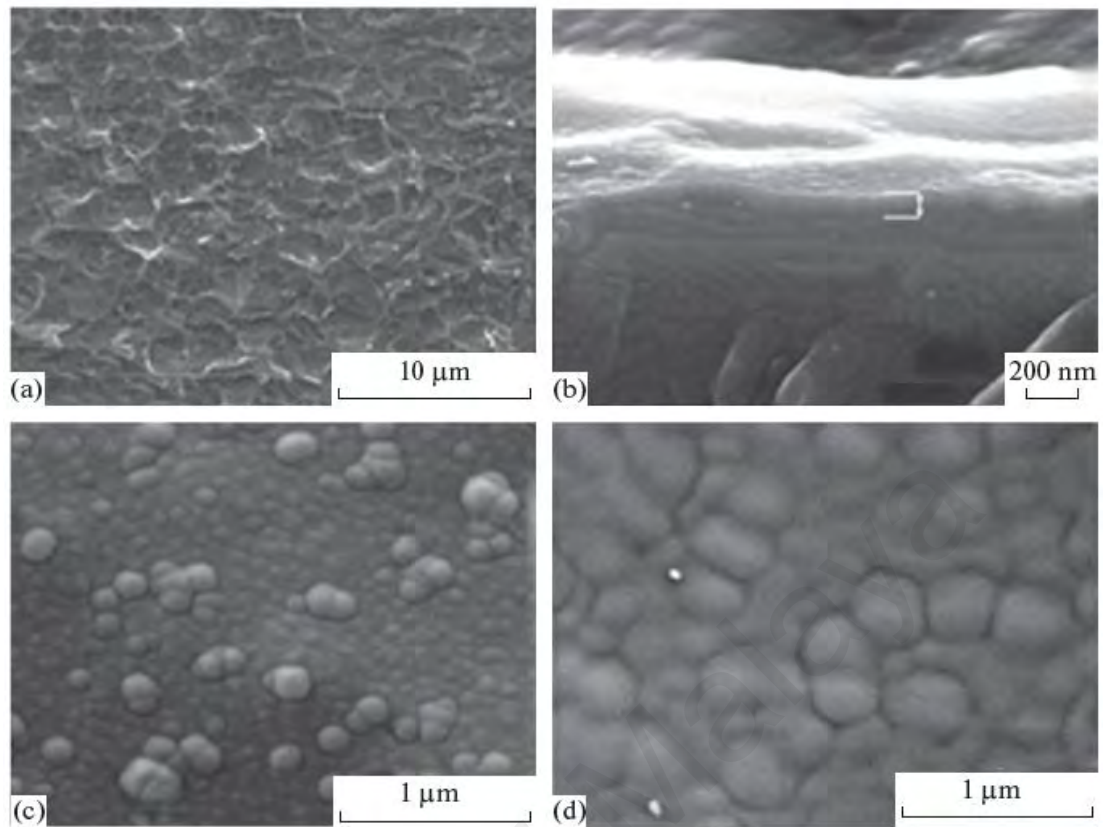


Figure 2.5: SEM image of: acid-etched uncoated titanium surface (a), cross-section of the deposited CaP coating (b) and the surface morphology (c, d) of the CaP coating deposited on acid-etched titanium surfaces over different amounts of time. Thickness: (b,c) 170 nm, (d) 440 nm (Surmenev et al., 2014).

To guide against the post-heat treatment, the geometry of magnetron sputtering can be altered using right-angled radio frequency magnetron sputtering to produce thin, highly stoichiometry crystalline films at room temperature (López et al., 2015; Mello et al., 2007).

2.3.2.3 Electrophoretic deposition of CaP coating

Basically, electrophoretic deposition (EPD) of CaP coatings is mostly carried out at the cathode as high anodic potentials may adversely affect the metallic material surface (Kwok et al., 2009). Several standard anodic electrode materials have been used during the deposition of CaP coatings on titanium implants, including graphite, platinum, lead,

carbon rod and stainless steel (Kaya, 2008). Higher deposition and uniformity of the coatings on implant materials can be obtained during EPD by keeping the separating distance between the electrodes within a range of 6–20 mm (Farnoush et al., 2013; Xiao & Liu, 2006). Deposition time used by investigators varies depending on the electrolyte ingredients, current, voltage and dispersed in suspension. The deposition time from 1 min to 2 h has been reported to have successfully produced a highly dense, adherent thin layer (~ 0.1–2 mm) and a homogeneous coating on prosthetic devices (Ágata de Sena et al., 2002; Chen et al., 2007). The coatings obtained by EPD have been described as rough and porous and densification at higher temperature has been suggested to create a more uniform, dense and well adhered coatings on metallic implants (Dumelié et al., 2005). However, a higher sintering process improves densification and the bonding of coatings formed via EPD, but also promotes HA decomposition as well as a high degree of shrinkage and micro-cracks within the coating layer (Figure 2.6) while lower densification leads to inadequate adhesion strength (Kaya, 2008).

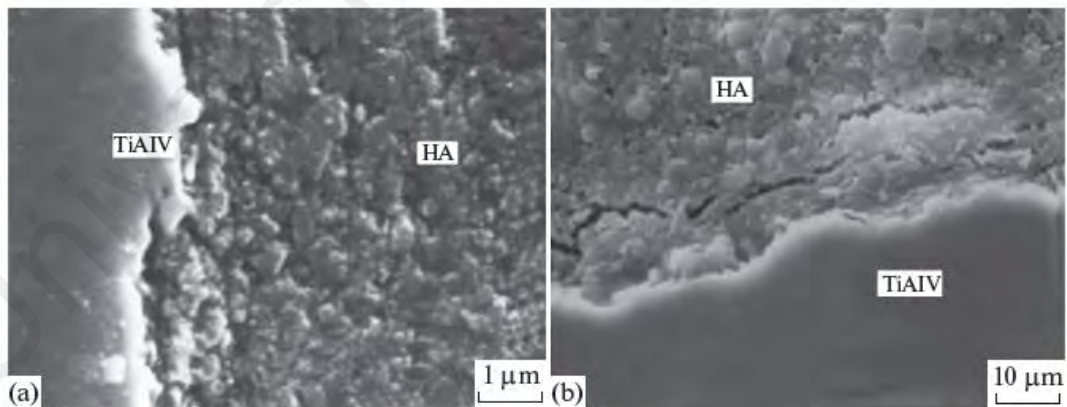


Figure 2.6: SEM images of sintered HA coatings on TiAlV substrates (Zhitomirsky & Gal-Or, 1997).

To solve the problem of HA decomposition and cracking of CaP coatings obtained using EPD, Kollath (2016) investigated the effect of Alginate incorporation in HA on

Ti6Al4V scaffolds. Figure 2.7 shows the optical microscopic images of bare and HA Alginate coated Ti6Al4V scaffolds.

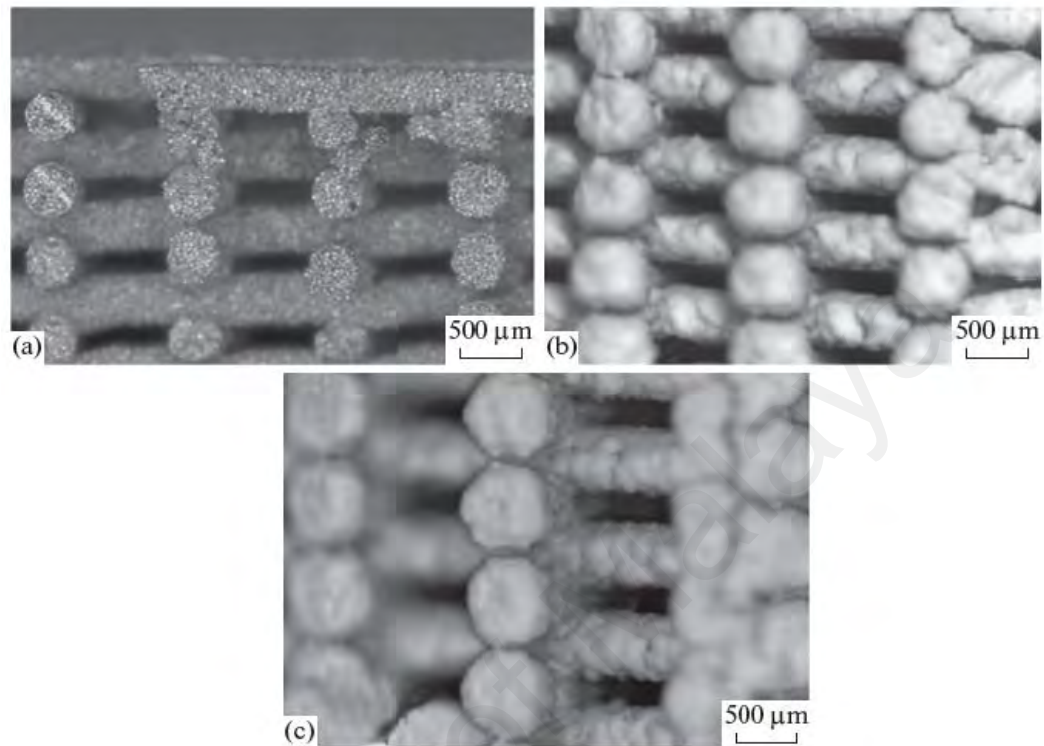


Figure 2.7: Optical micrographs of (a) uncoated and HA–Alg-coated sample (0.4 mm; 1,1) before (b) and after (c) sintering (Kollath et al., 2016).

In general, it was shown that the presence of Alginate improves the homogeneity of the coating and eliminates the microstructural defects. However, then the coating is not smooth, which was attributed to the roughness of the bare Ti6Al4V.

2.3.2.4 Sol-gel deposition for CaP coating

The sol-gel method is a relatively simple way to prepare hydroxyapatite coatings on metallic implants because of the easy formation of the compound coatings at a relatively low temperature. Jafari et al. (2016) investigated the production of sol-gel deposited HA coating on a Ti-14Zr-13Nb alloy substrate using calcium chloride ($\text{CaCl}_2 \cdot \text{H}_2\text{O}$) and $\text{Na}_3\text{PO}_4 \cdot 12\text{H}_2\text{O}$. X-ray diffraction of the coatings heated to different temperature and within different time span indicated that raising the sintering temperature from 500 to 700°C

increased the crystallinity of nano HA. However, sintering at high temperatures introduces Ti ions into the thermally insulated HA coating layer leading to the formation of the oxide layer. The reaction of Ti ion with HA led to the formation of TiO_2 on Ti alloy surface, which eventually led to decomposition of HA into TCP, CaTiO_3 and CaO. Thus, for the sol-gel technique, it is suggested that the processing temperature should be below 700°C to prevent phase transformation and ion migration from the Ti alloy substrate into the coating layer. Sol-gel allows preparation of nano-grained HA coatings.

Figure 2.8 shows a field emission scanning electron microscope (FESEM) of the coating obtained at three different sintering temperatures for the sintering time of 10 and 30 min. The sintered coating obtained at 500°C for 30 min appeared more compact than that sintered for 10 min. At the sintering temperature from 500 to 600°C and the sintering time span from 10 min to 30 min, broad crack was conspicuously seen at a shorter time period; the crack become narrower at a higher sintering time. At above 600°C , the sintering time span shows no significant impact on the coating morphology. The absence of a crack at a higher sintering temperature was attributed to a higher diffusion rate (HDR) of Ti ions into the HA coating. With a HDR, more TiO_2 is formed as evidenced by high sharp peaks in Figure 2.8c. The formation of an oxide layer enhances the coating grain interface and subsequently suppresses coating crack propagation. Production of sol-gel derived HA on metallic implants requires very stringent process parameters, especially for the thermal processing phase such as sintering time and temperature, chemical composition of the precursor and substrate type.

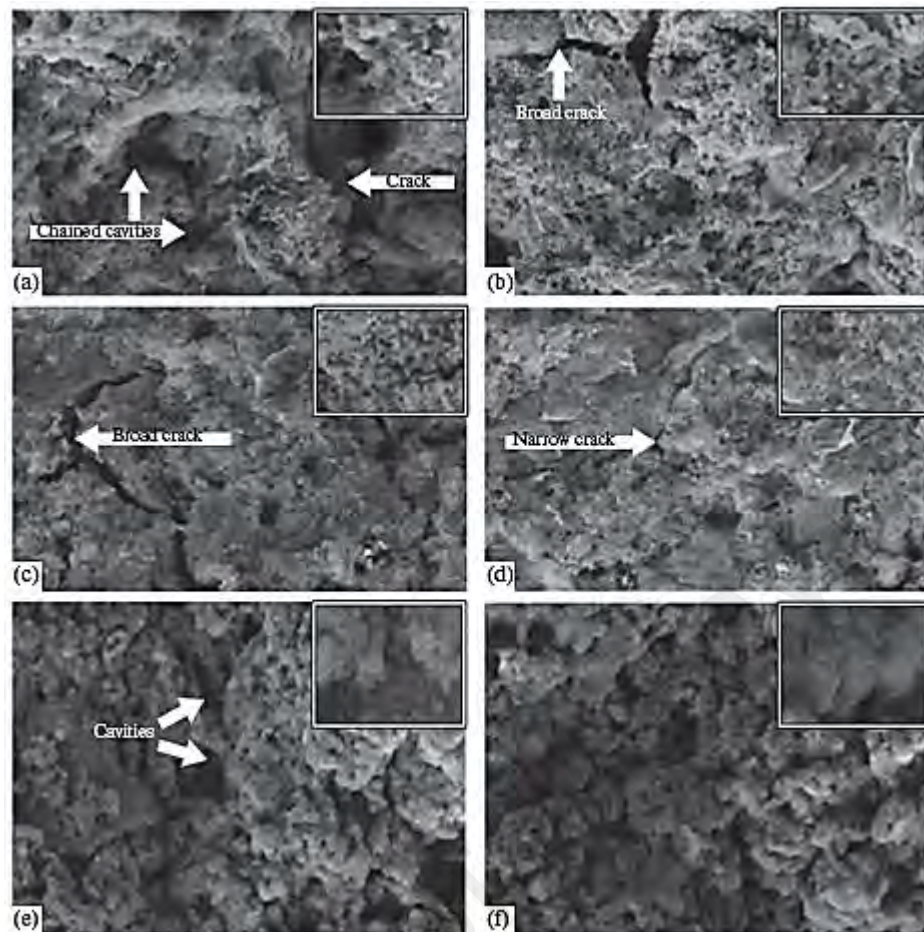


Figure 2.8: FESEM images of nano-HA coatings after sintering at: (a) 500 °C for 10 min; (b) 500 °C for 30 min; (c) 600 °C for 10 min; (d) 600 °C for 30 min; (e) 700 °C for 10 min, and (f) 700 °C for 30 min (Jafari et al., 2016).

The major issue includes the crystalline nature of the phase, porosity control, bonding strength and biocompatibility of the obtained coatings (Mohseni et al., 2014). In addition, it uses an expensive raw material so this technique is not suitable for industrial use (Olding et al., 2001).

2.3.2.5 Plasma electrolytic oxidation for CaP coating

In recent years, researchers have made attempts to see the possibility of enhancing the bioactivity and biocompatibility of titanium materials through incorporation of Ca and P ions into the surface oxide layers by controlling the composition and concentration of electrolytes. Ishizawa et al. (1995) and Ishizawa and Ogino (1995)

were the pioneers to make use of PEO to prepare HA layers on Ti; however, unfortunately, they were not successful using only PEO technique to produce HA layers. The incorporation of Ca and P into coatings and the preparation of CaP coating via PEO on the surface of metallic materials have been considered to be difficult and complex and infrequently reported so far. Preparation of CaP into the surface of titanium alloy has recently been proven effective by Yang et al. (2014). It is found that the Ca/P ratio in the PEO coating is dependent on the processing parameters. By changing the Ca/P ratio concentration, different phase structures were obtained. An appreciable amount of Ca/P ratio was incorporated into the microporous oxide film layer.

In an effort to improve the bioactivity of titanium alloy, CaP was deposited onto titanium surface using the single PEO process under a high voltage and prolonged time. With the increased in the PEO voltage and time, a significant amount of Ca and P element were incorporated. The PEO coating produced at higher voltage and time improved the surface roughness, porous structure and HA crystallinity. However, the incorporation of CaP which was accomplished using a high voltage and time has some limitations, because increased in electrical parameters caused cracks and failure within the coating. Though the addition of Ca and P containing compounds into the PEO coating was successfully deposited into the PEO coating by other researchers (Faghihi-Sani et al., 2013; Song et al., 2005). The results are quite encouraging from the aspect of successful incorporation of Ca and P element; however, the XRD results cannot identify the Ca and P containing phases in the PEO coating.

Sowa et al. (2015) investigated the bioactivity of anodic oxide coating on Ti₁₃Nb₁₃Zr by PEO process in a solution containing Ca and P. They observed that the thick oxide surfaces were essentially amorphous, with small amount of crystalline phases,

depending on the PEO process parameters. The obtained oxide coatings were reported to improve after 4 weeks of immersion in SBF. The available reports showed that PEO can allow the incorporation of Ca and P ions into the surface of the TiO₂ in the form of an amorphous phase, and further hydrothermal treatment can successfully transform the amorphous phase into crystalline HA. However, little work is available that systematically studies the influence of HA deposition in the oxide film and the mechanical performance of the coating before and after incorporation of HA.

Moreover, the attention is mainly focused on using Ca and P inorganic compounds electrolytes in the preliminary efforts, and production of bioactive coating from natural bovine bone hydroxyapatite is not highlighted in the literature. Therefore, it would be of great interest to employ bovine bone material as electrolyte solution for PEO coating to further improve the bioactivity and corrosion resistance of the implant material. In addition to this, it appears that the PEO processing parameters regime to deposit CaP is very essential in controlling the amount of CaP and crystallinity in the TiO₂ film and unfortunately, this has not been satisfactorily identified.

The deposition of CaP coating via PEO process is much better than the aforementioned surface coating processes in the following aspects. The adhesion strength between the coating and substrate is higher than the conventional coating owing to the conversion of the substrate during PEO process. The electrolyte solution used in PEO is more environmentally benign than the conventional coatings. Moreover, it is much easier to prepare the substrates. More importantly, there is no limitation to the size and shape of the workpiece in PEO coating, which makes the process quite flexible. Compared to conventional processes, the set-up for PEO is much cheaper. PEO process has been considered as one of the most suitable surface engineering techniques for biomedical implants application by offering a biological favourable environment (Cengiz et al., 2016). This technique has been given major attention in the present work.

2.4 State of the art on the PEO coating process

2.4.1 Plasma electrolytic oxidation

Plasma electrolytic oxidation process (PEO) is a versatile surface treatment method widely employed in various industrial sectors such as aerospace, automotive, oil and gas due to the good coating properties, including wear and superior corrosion resistance. In recent times, the application of PEO has been extended into the biomedical areas owing to its ability to produce biocompatible and bioactive coatings.

2.4.2 Characteristics features of PEO

PEO is a plasma assisted anodic surface process for the production of ceramic coatings on the light metals substrate in a benign electrolyte solution. The light metals that have attracted the most interest are aluminium, magnesium, zirconium and titanium but they do not represent an exhaustive list of the materials which can be processed by PEO. An alternative term for PEO can include: micro-arc oxidation, anodic spark deposition, electrolytic plasma processing, and micro-plasma discharging as pointed out in the work of Yerokhin et al. (1999) and Matykina et al. (2016). In a typical PEO process, the working electrode (anode), together with the counter electrode (cathode), usually stainless steel of a larger surface area is immersed in a suitable electrolyte of interest. An external power supply is connected to the two electrodes providing the energy necessary for the coating process. PEO evolved from hybrid of conventional low voltage and high energy plasma arc discharges; therefore the basic equipment layout is similar and is schematically depicted in Figure 2.9. At a sufficiently high potential difference of a few hundred volts, the electrolyte compound dissociates into anions and cations. The anions drift towards the working electrode (e.g. Ti, Al, Zr and Mg) while the cations migrate towards the cathode. At the anode, the oxidation of the surface starts by forming an insulating layer on the working electrode which causes a slight drop in the applied current. With a further increase in the applied voltage, the intense electric

field between the electrodes generates a micro-arc plasma discharge on the anodic surface, transforming it to a micro-porous thin oxide layer.

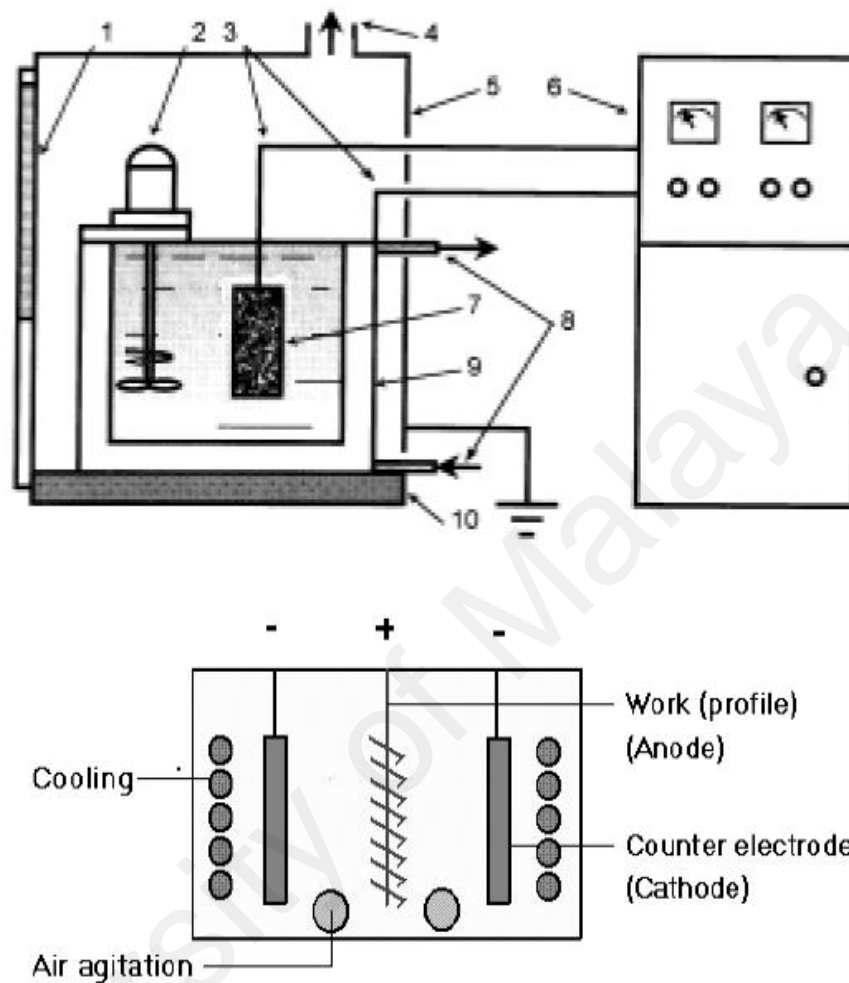


Figure 2.9: (a) Typical arrangement of the equipment used for PEO treatment (1. window, 2. mixer, 3. connecting wires, 4. exhaust/ventilation system, 5. grounded case, 6. power supply unit, 7. workpiece, 8. cooling system, 9. bath, 10 insulating plate). (b) Electrolyte bath (Yerokhin et al., 1999).

The deposition of electrolyte ingredients then follows. The coating is formed on the entire substrate (anode) immersed in the electrolyte solution without altering the bulk properties of the substrate material. PEO can confer a firmly adherent ceramic coating on light metal alloy surface. An essential feature of PEO coating is that the ceramic oxide layer actually grows inward from the light metal surface. Thus, superior adhesion

and dimensional stability of the part is possible and more importantly the geometric complex part can be easily coated. Contrary to other conventional surface engineering techniques (Sol-gel, electrophoretic deposition, magnetron sputtering and thermal spray), a thick layer of up to 100 μm can be obtained by PEO process.

2.4.3 PEO coating procedure

After light metals (substrate) pretreatment consisting of abrading, degreasing and cleaning. The substrate sample is attached to the current supply (Alternating current (AC), Direct current (DC) or pulse bipolar current (PBC)) of the PEO unit and typically immersed in the electrolyte bath at a depth of 10 mm to 50 mm beneath the electrolyte surface. The working voltage can be applied to the electrolyser terminal and adjusted at the power supply system in accordance with the desired processing treatment regime. PEO treatment is typically conducted between 2 min and 120 min at current densities of 500 to 2000 mAcm^{-2} and voltages regime of up to 800 V. The electrolyte is usually maintained at a temperature in the range 20 °C to 70 °C via an external heat exchanger. The effect of electrolyte composition/concentration on the PEO process may include changes in the sparking voltage and incorporating of elemental ingredients in the electrolyte (Walsh et al., 2009).

In PEO process, the composition of the substrate is probably the most important parameter in describing the effect of PEO inputs and the morphology. The interaction between the base material and processing parameters results in a series of physical and chemical interactions that culminates into the final coating composition, structure and properties. The profile of the PEO coating process and hence the morphological features of the PEO coatings are determined by the variables of PEO process and these are:

- i. The substrate composition and property
- ii. Electrolyte composition/concentration

- iii. Deposition time
- iv. Deposition voltage/current density regime

2.4.3.1 Influence of substrate composition and property

The material composition and properties influence the PEO process and coating formation. Currently, PEO coatings have been conducted on various types of metallic light materials, it is clear that the substrate composition and morphology of the metals affect both the PEO process and the coatings from various aspects. Moreover, PEO treatment of similar metals containing different alloying elements also presents different characteristic features. For instance, Cimenoglu et al. (2011) systematically studied the PEO coatings on different titanium alloys and found that the surface oxide layer of Ti6Al4V was porous while grainy appearance was noticed on the surface of Ti6Al7Nb. In a similar study conducted by Apachitei et al. (2011), more micro-porous oxide layer was also obtained on the surface of Ti6Al4V as compared with those produced on its counterpart.

The chemical phase content of the coatings was also affected by the PEO oxidation. Incorporation of the elemental constituents of the substrate material in the PEO coating has been reported. Apachitei (2009) also investigated the effect of shot peened Ti6Al4V alloy with that of unpeened alloy. It was found that the shot peened alloy revealed a significant voltage transient behaviour compared to unpeened alloy. The PEO coatings fabricated on different ultrafined grained sizes AZ91D magnesium alloy substrate showed a more dense structure, a little porous and better protection in a sodium chloride solution (Jiang et al., 2013). It can be said that the growth rate of PEO coating has relation with elemental compositions of the substrate; phase content of the coating is also affected by the oxidation of the light substrates and incorporation of the elements into the PEO coating.

2.4.3.2 Influence of electrolytes

Apart from the substrate type, electrolyte is another vital factor influencing the PEO coatings and determines coating properties (Khan et al., 2010; Kim et al., 2009; Shokouhfar et al., 2012). The composition and concentration of electrolyte solution are the two most important factors affecting the PEO coatings because of the incorporation of electrolyte borne elements such as calcium and phosphorus from the electrolyte solution. The electrolyte concentration has been reported to influence coating characteristics, including roughness, thickness, chemical composition, surface structure and performance. Bai et al. (2011) fabricated PEO coatings on commercial grade 2 titanium in a solution containing 0.2M NaOH and different concentration of hydroxyapatite particles. They found that the surface morphology of the PEO coating was significantly affected by the HA concentration dispersed in the solution. The surface roughness of the coating reached 1.5 μm for 20 g/L formed coatings (Figure 2.10).

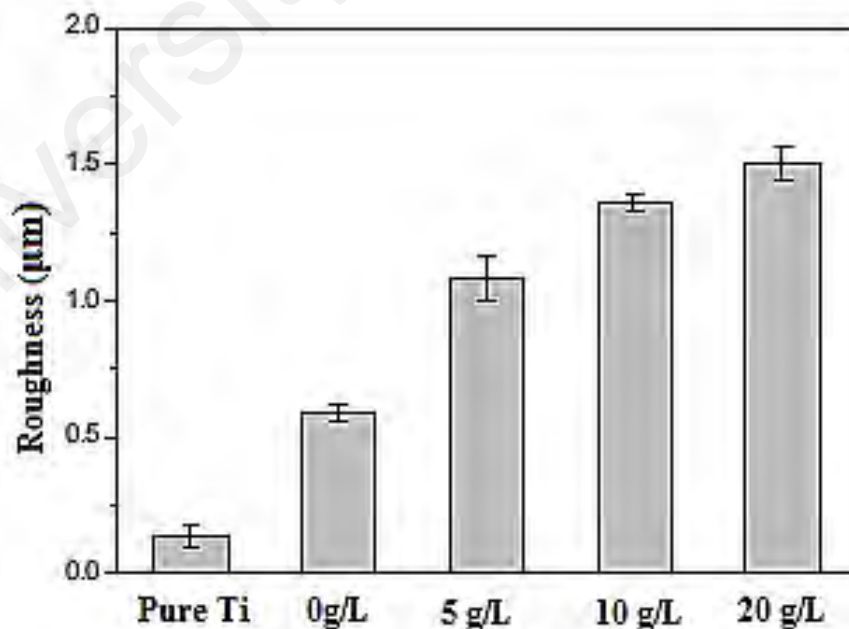


Figure 2.10: Roughness of the sample produced using MAO&EPD process in the NaOH electrolyte solution with different HA concentrations (Bai et al., 2011).

Pan et al. (2013) produced PEO coatings on ZK60 magnesium alloy in the electrolyte containing different concentrations of electrolyte (E₁ and E₂) containing calcium acetate and disodium hydrogen phosphate and the same additives. The results showed that the coating with higher concentration gave higher thickness of about 38 μm while the lower concentration had a thickness of about 32 μm. A maximum adhesive strength of 95.5 MPa was achieved in the PEO coating (Figure 2.11). Moreover, the coating produced in two different concentrations contained different phase constituents, with MgO, MgF₂, ZnF₂, CaF₂ and β-Ca₃(PO₄)₃. The effect of electrolyte composition may also influence the surface morphology. For example, during the PEO of titanium alloy, it was found that the presence of magnesium element in the electrolyte composition improved the surface roughness, surface energy, adhesion, and wettability of the PEO coating, thus giving a compact coating, with a higher thickness value (Harun et al., 2017).

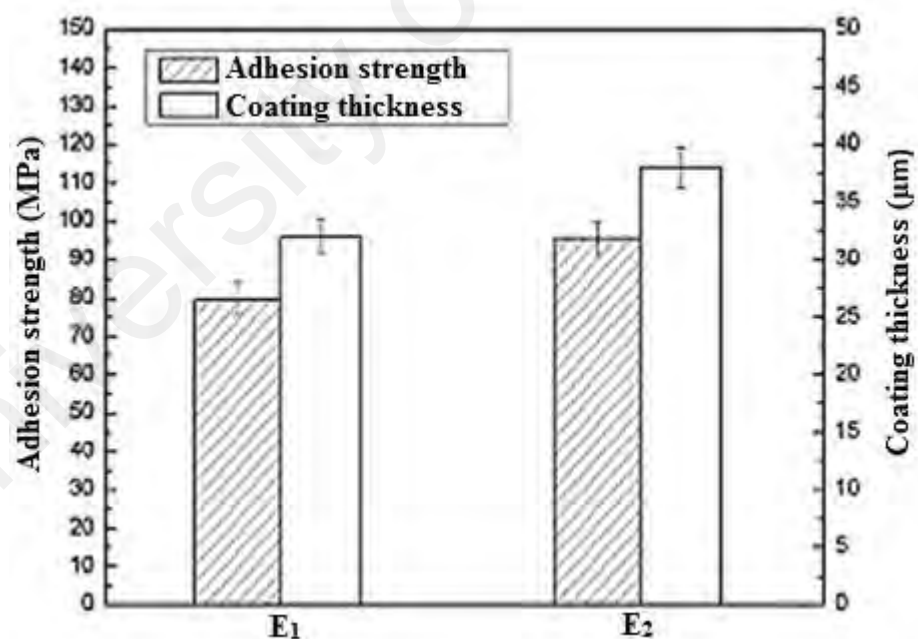


Figure 2.11: Thickness and adhesive strength of MAO coatings formed in electrolyte E₁ and E₂ (Pan et al., 2013).

The PEO coatings produced in the same electrolytes with different additives can also have different characteristics. It is established that increase of an electrolyte

concentration would result in thicker, more adherent and micro-porous PEO coatings (Khan et al., 2010; Krishna et al., 2010).

2.4.3.3 Influence of deposition time

The deposition time has also been demonstrated as a prominent factor on the PEO coatings. The coating thickness is found to increase with prolonged deposition time, however, with a staggered incremental behaviour (Table 2.4). For example, Durdu et al. (2013) (Table 2.4) and Hussein et al. (2013) reported a direct linear relation in coating thickness with deposition time (Figure 2.12a), whereas non-linear relation behaviour is reported by Wang et al. (2004) (Figure 2.12b).

Table 2.4: Plasma electrolytic oxidation coating parameters for the coatings produced in different solutions (Durdu et al., 2013).

Electrolyte	Current density (A/cm ²)	Duration time (min)	Average coating thickness (µm)	Average pore size (µm)
(CH ₃ COO) ₂ Ca C ₃ H ₅ (OH ₂)PO ₄ Ca, Pure water	0.123	1	16.1 ± 0.32	1
		5	22.1 ± 0.48	3
		10	28.2 ± 0.57	4
		20	33.0 ± 0.72	6
		40	42.7 ± 1.70	7
		60	47.0 ± 1.90	8
		120	63.4 ± 4.10	20

Generally, longer deposition time, usually results in average larger pore diameter as shown in Table 2.4 which is consistent with the results reported by Duan et al. (2012) and Sundararajan and Krishna (2003).

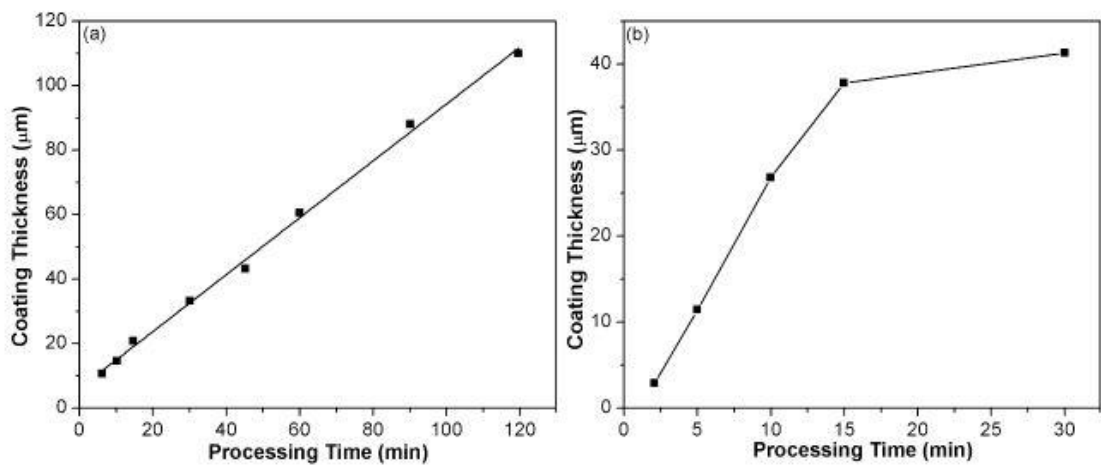


Figure 2.12: (a) Linear (Hussein et al., 2013) and (b) non-linear growth (Wang et al., 2004) of the PEO coating with different deposition time.

Variation in the PEO deposition time also has a substantial effect on the roughness of the PEO coating. The coating roughness increased considerably at the beginning of the PEO process and thereafter remains almost constant as found by Rožić et al. (2013). Apart from surface morphology, other aspects of the PEO coating are also influenced by the deposition time. In an investigation of wear resistance of PEO coatings on titanium alloy, Durdu and Usta (2014) reported that the wear rate of the coatings improved with increasing in deposition time. The significant improvement was attributed to a different evolution of phase structure formed under various duration times.

2.4.3.4 Influence of deposition voltage

As depicted in Figure 2.13 an external power DC supply to the PEO system which provides a direction for the investigation of the PEO process. Several PEO variables, including voltage magnitude, pulse frequency, duty cycle and current density would affect the PEO coating properties (Martin et al., 2013). The coating structure and morphology are notably influenced by the applied voltage magnitude and current density. Montazeri et al. (2011) investigated the effect of voltage magnitude on the morphology and corrosion properties of PEO coatings on titanium alloy, revealing that,

with the same deposition time of 10 min, when the voltage increased from 350 – 500 V the corresponding pore diameter and porosity of the PEO coatings were increased. The increase was attributed to discharge activity and gas evolution during the PEO process. Their studies also showed that the coating produced at a higher voltage magnitude of 500 V had the best corrosion resistance and bioactivity compared with those produced at lower voltages. Effect of deposition voltage has also been studied on the surface roughness and thickness of the PEO coatings (Li et al., 2004; Sowa et al., 2015). The corresponding thickness and roughness were found to almost double with increased applied voltage (Figure 2.13).

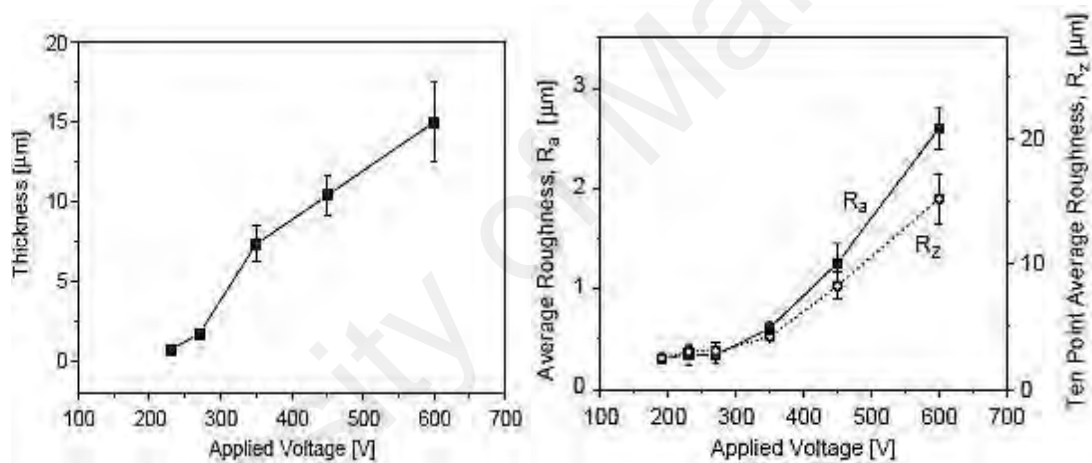


Figure 2.13: Thickness of the PEO coated layer and (b) Surface roughness as a function of the applied voltages (Li et al., 2004).

Aside from surface roughness and coating thickness, residual stress is also influenced by the applied voltage/current density. In an investigation on residual stress of PEO coatings on titanium material, Huang et al. (2007) reported that the coatings produced at high voltage contained more titania compared with that at low voltage, and the resultant residual stress tended to increase with the increase in applied voltage. Similar results were also published by Khan et al. (2010), the internal stress produced on Al alloy decreased significantly when the applied current density increased from 5 Adm^{-2} to 20

Adm⁻². The effects of voltage on the coating morphology and structure undoubtedly influence the final PEO coating properties. Gan et al. (2013) studied the effects of DC voltage on the final properties of the PEO coatings on commercially pure magnesium, and found that the coating produced at an intermediate voltage of 360 V exhibited superior corrosion resistance compared with those produced at 450 V and 410 V.

Investigation on the influence of various PEO processing parameters on the characteristic features of PEO coating provide a substantial amount of information regarding the PEO process. The findings from different studies are consistent, i.e. the average pore diameter and coating porosity can be increased by either increasing the voltage/current density, deposition time or by altering the composition/concentration of the electrolyte.

2.5 Mechanisms of PEO coating formation

Investigating the phenomenology of the coating process during PEO process gives an understanding of the complex coating formation mechanism. The mechanism of the coating formation, such as electrical transient (Duan et al., 2012), gas evolution (Guo et al., 2005; Snizhko et al., 2007), micro-discharge events (Moon & Jeong, 2009; Yerokhin et al., 2003), acoustic emission (Boinet et al., 2005), which are generally observed during the PEO process have been widely studied.

2.5.1 PEO electrical transient phenomena

The electrical transient analysis includes current and voltage transient during PEO processing. The electrical transient is generally acknowledged as prominent parameters for describing the PEO coating formation kinetics. Electrical transient behaviour of the PEO process has been widely reported in the literatures (Arrabal et al., 2009; Hwang et al., 2012; Liang et al., 2007). During the PEO process, the voltage is generally increasing with the deposition time. The behaviour of voltage-current transient is

attributed to the growth of the oxide film layer on the substrate material, as claimed by Yerokhin et al. (2000). A typical voltage-time response during the PEO process of Al 6082 is shown in Figure 2.14. As can be seen, different stages can be identified according to the slope of the voltage-time response. At the outset of the PEO process (stage I), when the voltage is linearly increased with the current, the substrate material is immediately encapsulated by an insulating layer, which conforms to the ohm's law.

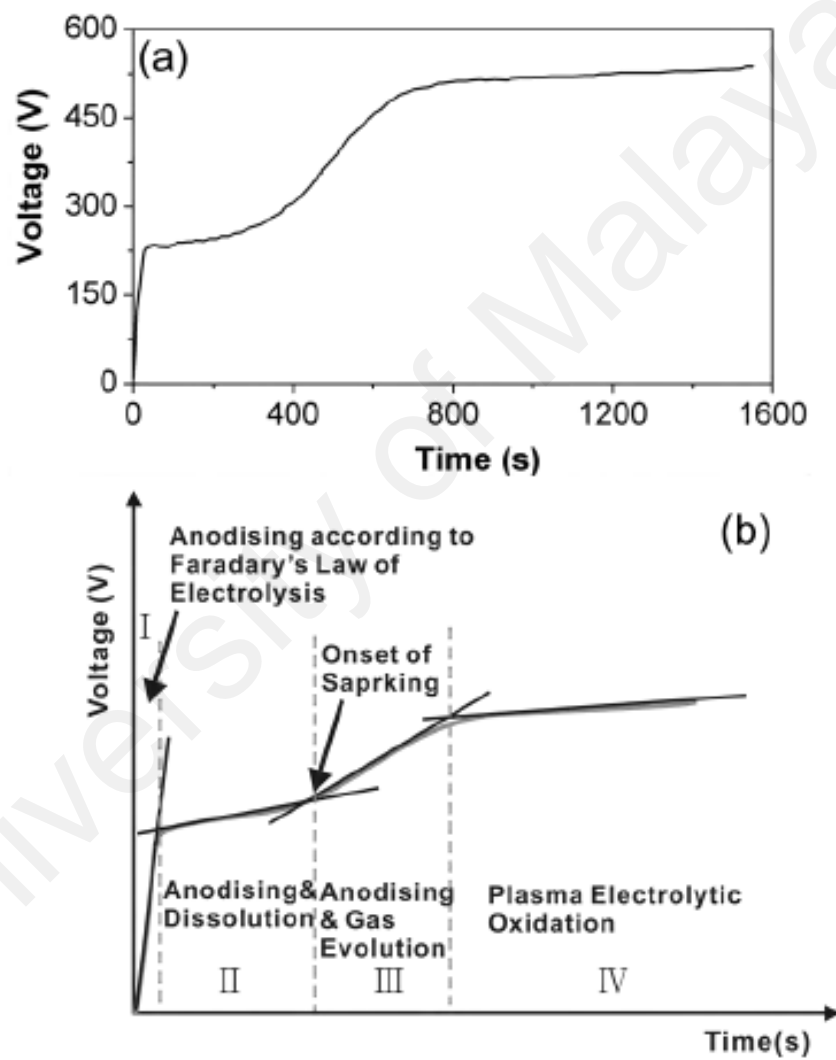


Figure 2.14: Voltage-time response of the PEO treated Al 6082 alloy under the current density 467 A.m^2 and electrolyte concentration 1 g/L KOH . (a) Voltage-time response (Yerokhin et al., 2004) (b) identification of different PEO stages based on voltage transient (Gao, 2014).

After this stage, the rate of voltage is low due to the oxidation/dissolution of the coatings (stage II). Thereafter, the behaviour of the current/voltage changes greatly. This is followed by thickening of the PEO coating, which accompanied by a substantial amount of micro-sparks traversing on the substrate surface. At the stage (IV), the rate of voltage is slower, indicating a steady growth of the PEO coating thickness. During this stage, micro-spark becomes less intense compared to the previous stages. In this stage, the PEO coating is characterized with large defects.

University of Malaya

2.6 Summary

To put this research into perspective, PEO process and associated features in terms of input parameters and the performance measures have been reviewed in this chapter. The review discusses the titanium alloy's properties, capabilities in service, corrosion/wear resistance, biomedical applications, and efforts in surface treatment of the alloys with CaP based ceramics. A general overview of current development in the PEO treatment process covering important parameters and treatment conditions with CaP are deliberated. The influence of PEO parameters, substrate type material, voltage, deposition time, and electrolyte concentration and the mechanism of the PEO coatings were discussed.

The review showed that most work on CaP coating via PEO method have not employed natural bovine hydroxyapatite to enhance the bioactivity of the titanium alloy. Also, the ranges of PEO process parameters that fall within low electrical input parameters have not been well identified. Beside these, published works have not considered the influence of mechanical performance of the PEO coating before and after incorporation of CaP.

The literature review suggests that the titanium implant encapsulated with CaP improved the bioactivity of the implant. Hence, the current effort which seeks to use PEO features and natural bovine material with the aim of mimicking the biological portion of human bone is being explored.

CHAPTER 3: METHODOLOGY

3.1 Introduction

This chapter presents the experimental set-up, investigation of the PEO process, including electrolyte concentration, voltage regime, and method of data analysis adopted in this present work. The basic materials and equipment used in this study are also contained in the chapter. Specifically, experimental designs are used to identify the PEO input parameters and the required formulation for the hydroxyapatite deposition used in investigating the process outputs of elemental composition, surface roughness, adhesion strength, scratch hardness, wear, bioactivity test and in vitro corrosion. The equipment used in the fabrication of PEO coatings is consisted of three parts: DC Power Supply System, Electrolytic cell and Data acquisition controlling system.

3.2 Materials

3.2.1 Bovine hydroxyapatite derived from cortical bone

The materials used in formulation of calcium phosphates are trisodium phosphate dodecahydrate (NAP), commercial hydroxyapatite (CHA) and bovine bone HA powders (BHA). The trisodium phosphate and commercial HA powder are of 99.5 % and 99.9 % purity with particle size of 44 μm and 45 μm , respectively. The hydroxyapatite powders were derived from cortical bovine bone. The procured cortical bones collected from the local slaughterhouse were cleaned to remove adhering impurities such as tissues and ligament attached to the bone surface. The cortical bones were cut into rectangular size of dimension 10 x 10 x 5 mm^3 using hack saw. Based on the literature findings (Niakan et al., 2015; Ooi et al., 2007), the bone samples were heat treated in an electric furnace to a temperature of about 900 $^{\circ}\text{C}$ with a heating/cooling rate of 5 $^{\circ}\text{Cmin}^{-1}$ and 2 h holding time. To obtain a homogeneous distribution and required particle size, the BHA powders were ball-milled with a stainless steel balls in a 250 ml stainless steel mixing jars at 250 rpm. The ball-to-powder weight ratio was 10:1 and the milling time was set

to 5 h. The as-milled powders were then measured using a particle size analyzer (Malvern Instruments, MAL32913, UK). BHA powder with a particle size of 45 μm was used in this study. The phases present in the BHA powder was examined by XRD and Attenuated total reflectance-Fourier transform infrared spectroscopy (ATR-spectrum 400 FTIR). Figure 3.1 shows the XRD and FTIR spectrum of the prepared BHA powder.

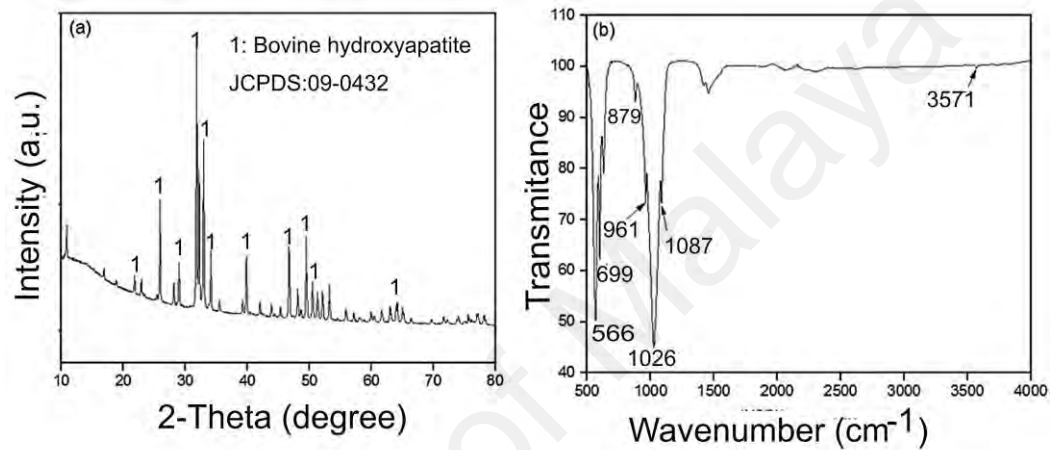


Figure 3.1: XRD pattern (a) and FTIR spectrum (b) of the BHA powder.

Table 3.1 shows the chemical composition of the bovine hydroxyapatite obtained from cortical bone powder particles. The bovine bone pieces were then crushed and sieve to obtain bovine hydroxyapatite of particle size 45 μm , which was used in this study.

Table 3.1: Elemental chemical composition of bovine bone powder particles

Element	Ca K	Mg K	P K	Na K	O K	C K
Wt. %	33.42	07.85	19.59	01.08	32.89	05.17
At. %	16.96	07.83	15.02	01.12	48.84	10.23

3.2.2 Substrate preparation

Ti6Al4V alloy (Grade 5; Cenco Sains Special Materials Co. Ltd, Malaysia) was used as the substrate material in the present study. The material received in the form of 2 mm

thick sheet is cut into specimen coupons of dimensions 20 mm x 10 mm using electrical discharge machining (EDM) wire cut machine. The chemical composition of the Ti6Al4V is given in Table 3.2.

Table 3.2: Chemical composition of Ti6Al4V substrate material (Grade 5)

Element	Al	V	Fe	O	C	Ti
Weight (%)	5.65	3.93	0.13	0.11	0.08	90.1

Before the PEO treatment, the surfaces of the specimen were ground with silicon carbide (SiC) emery papers (with 7 grades: 240, 320, 600, 800, 1200, 1500 and 2000 grit) and ultrasonically cleaned for 10 minutes with acetone and distilled water to remove dirt and surface contamination.

3.2.3 Electrolyte preparation

Hydroxyapatite aqueous suspension was prepared by adding bovine bone, derived HA and NAP simultaneously to 1 litre of distilled water taken in a conical flask. The aqueous BHA suspension was then sonicated using an ultrasonic vibrator for 60 mins to obtain a homogeneous dispersion. Since the electrolyte composition for the PEO treatment of Ti6Al4V is to be optimized, various electrolytes were prepared in the present study. The details of the PEO conditions and electrolyte formulation are provided in Table 3.3.

Table 3.3: Details of the PEO condition

Process condition	PEO working ranges
HA concentration (g/L)	0-2
Trisodium phosphate concentration (g/L)	3.8-12.5
Voltage (V)	200-350
Deposition time (minutes)	2-20
Current density (mAcm ⁻²)	250-500
Electrolyte temperature (°C)	30-35 °C
Current (A)	1

In general, the electrolyte formulation commences with the measuring of the reagent chemicals (BHA powders, $\text{Na}_3\text{PO}_4 \cdot 12\text{H}_2\text{O}$ and commercial HA powders) as specified in the design with an electronic balance (OHAUS Adventurer and precision balancer); and mixing/stirring on a hot plate. The mixing/stirring on the hot plate ensures homogeneous distribution of the particle suspension. Figure 3.2 illustrates the detail formulation of the electrolyte formulations.

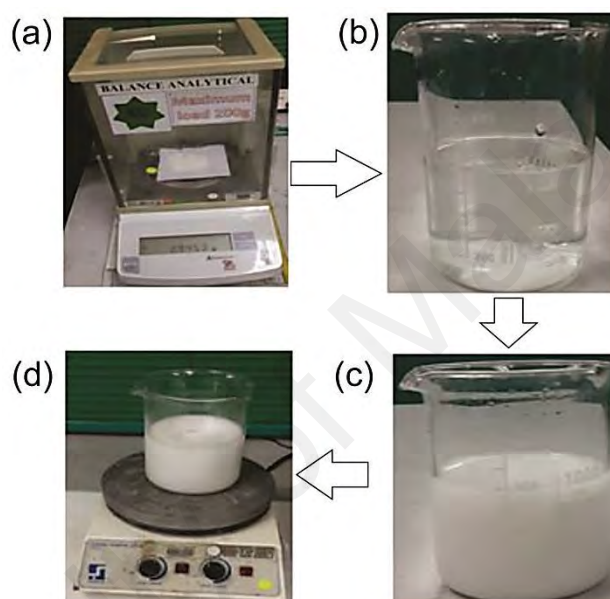


Figure 3.2: Illustrative outline of the apparatus for the electrolyte formulation:
(a) Weighing balance, (b) NAP dissolution, (c) NAP+BHA particle suspension, and
(d) Magnetic stirrer of the particle suspension.

After complete suspension of the chemicals in distilled water, the conductivity and the pH of the electrolyte were measured using a conductivity meter (HANNA H19835) and pH meter (HANNA 211).

3.3 Characterization

The direct current (DC) power supply unit is used as a source of power for coating development. Examination of the surface roughness (R_a) of untreated Ti6Al4 V and coated samples was measured using a Mitutoyo SurfTest SJ-201 profilometer. The

surface morphology and elemental composition of the samples were analysed using a high-resolution field emission scanning electron microscope (FESEM) and an energy dispersive spectrometer (EDS) (FESEM-EDS, FEI Quanta 450 FEG). Before FESEM analysis, PEO coated samples were sputtered with a thin gold conductive layer to prevent charging and improving the image of the coating surfaces. The X-ray photoelectron spectroscopy (XPS) was used to confirm the bonding structure and elemental coating compositions. The phase composition of the samples was studied by X-ray diffraction (XRD; PANalytical X'Pert High Score Empyrean, 45 kV, 40 mA) with a Cu K α ($\lambda=1.54 \text{ \AA}$) radiation over the scanning range (2θ) from 10° to 80° with a scan speed of 1° min^{-1} and a step size of 0.02° . Attenuated total reflectance–Fourier transform infrared spectroscopy is employed for further confirmation of the phase structures. A micro-scratch tester (Micro Materials Ltd., Wrexham, UK) was used to measure the adhesive strength of the coating by applying a load ranging from 0 to 2500 mN. The *in vitro* corrosion test of the samples were carried out by a potentiodynamic polarization method using a potentiostat/galvanostat/frequency response analyser from Metrohm (Model: AutoLab PG STAT30) while *in vitro* secondary apatite bioactivity was evaluated in Simulated body fluid (SBF) following the procedure suggested by Kokubo and Takadama (2006). The mechanical behaviour of the coating layer formed was examined by a commercially available scratch tester machine. The friction and wear tests on the PEO coatings and untreated Ti6Al4V were carried out using Reciprocating frequency wear tester. The working ranges of the PEO processing parameter for coating deposition are found using different applied voltages.

3.3.1 PEO coating

The PEO coating unit used for the development of the film layer consists of the DC power supply system, electrolytic cell and data acquisition controlling computer. The DC power supply unit (Keysight Technologies Deutschland GmbH, Model No:

N89757A, Germany) of 1500 V/30 A capacity is powered by a 3-phase mains supply. The Autogeneous DC units are remotely controlled by the host computer through a LAN cable interface, while the current and voltage transient behaviour during the PEO treatment are monitored by BenchVue software installed on the system. This monitoring is critical as it provides insights into the coating development, coating morphology and final properties. It is also vitally important to monitor the temperature variation because the electrolyte temperature can adversely affect the coating morphology. Measurement of the temperature variation during the PEO process is performed with the aid of thermocouple. Figure 3.3 shows the experimental setup for the PEO process.

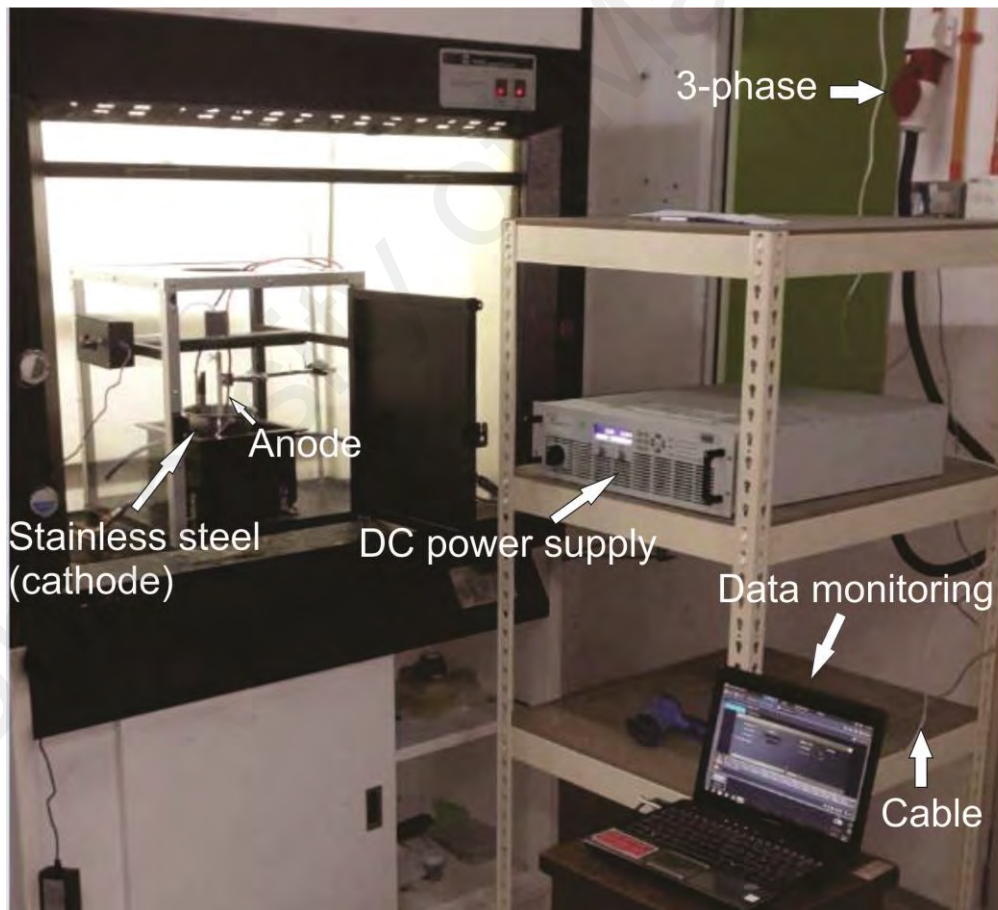


Figure 3.3: Experimental setup for the PEO process.

A cylindrical stainless steel ($\varnothing 140 \times 130 \text{ mm}$) is used in the electrolytic cell system, which serves as the cathode (counter electrode) and container for the electrolyte suspension. The stainless steel cathode is beneficial to the PEO treatment as it allows a symmetrical electrical field, which is a condition for achieving uniform coating thickness. A magnetic stirrer is applied through the PEO process to achieve uniformity in the electrolyte composition. The electrolyte temperature is maintained within the desirable range during the PEO treatment by passing cool water through a hosepipe made of rubber.

3.3.2 Development of films by PEO treatment

The ranges of individual bovine derived HA powders, commercial available HA and NAP and their mixture used in this study is determined through preliminary investigation and is given in Table 3.4. An electrolyte containing different amount of either BHA powder or NAP or mixture of these two is separately prepared in 1 L of distilled water.

Table 3.4: PEO elemental powder composition/concentration

Type of powder	Amount (g)	Concentration (g/L)
Bovine-derived HA	0	-
	1	-
	1.5	-
	2.0	-
NAP	3.8	-
	4.0	-
	4.2	-
CHA + NAP	0+3.8	3.8
	1+3.8	4.8
	1.5+4.0	5.5
	2.0+4.2	6.2
BHA+NAP	0	0
	1+3.8	4.8
	1.5+4.2	5.7
	2.0+4.2	6.2

For PEO process, the electrolyte prepared (Figure 3.2) was taken into a cylindrical stainless steel container which serves as the cathode and Ti6Al4V coupons immersed in the electrolyte was used as the anode. For the present investigation, the PEO process was performed at current density 250-500 mAcm⁻², current 1.0 A, and electrolyte temperature was maintained at the range of 30-35 °C. After the PEO process, the treated coupons were removed from the electrolyte, washed with distilled water, air dried at room temperature for subsequent characterization.

3.4 Morphological characterization of the PEO coatings

The PEO structure produced under different combination of voltage and electrolyte concentration are subjected to microstructural, X-ray, and mechanical testing in order to correlate the PEO parameters to microstructures and properties. The procedures for each of these characterizations are presented in subsequent sub-sections.

3.4.1 FESEM microstructural/XPS examination

Scanning electron microscope (SEM) is an electron microscope that is widely employed in various areas of materials science, biology, chemistry, geology etc. In SEM, the electron beam is generated by a biased element and directed towards the surface of the specimen, where the atoms of the specimen and the high electrons generated will interact and causing different signal emission. The scanning electron (SE) is the most common SEM mode and is very sensitive to characteristics of surface topographies such as roughness, porosity, cracks and the interpretation of SE images is of significance to reveal the surface morphologies (Lyman et al., 1990). Figure 3.4 shows the schematic diagram of an SEM instrument.

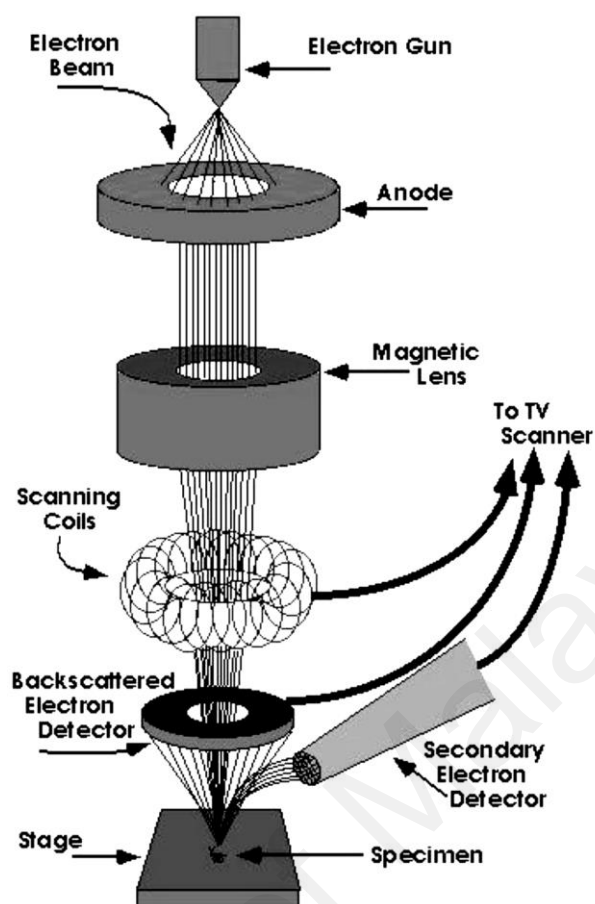


Figure 3.4: Schematic view of the operation of SEM

In the present study, the characteristics of the plane surface and cross-sectional morphologies of the coatings were examined using FEI Quanta 450 FEG FESEM instrument at an accelerated voltage of 15-20 kV. The elemental chemical compositions and distribution were determined by the energy dispersive X-ray spectroscopy attached to the FESEM. The exact elemental composition analysis and chemical state of the specimen was determined by X-ray photoelectron spectroscopy (XPS, ULVAC-PHI Quanterra II).

For the cross-sectional observation, the specimen is prepared by cutting the coated sample into halves using the Isomet 5000 precision saw with cutting speed of 1.5 mm/min to prevent the risk of damaging the coating layer. Thereafter, the sample was cold mounted in resin (epoxy: hardener is 5:1) before being subjected to grinding and polishing. The mounted samples were ground progressively on water cooled (to prevent

temperature increase and eliminating the oxidation of titanium substrate) using silicon carbide papers of varying grit sizes (400-4000 grit). Polishing is done in disc polishing machine using polycrystalline diamond suspension (6 μm , 3 μm , and 1 μm) to achieve a fine surface finish.

For plane surface FESEM examination, the samples were stuck on aluminium stub using a conductive carbon tape. The cross-sectional and plane surface samples were sputter coated with carbon tape to prevent accumulation of charges during SEM observation.

3.4.2 XRD and FTIR analysis

The phase structure of the PEO coatings was characterized using X-ray diffraction method. The basic principle of X-ray techniques relies on the interaction of X-ray beam with atomic crystals. When the incident ray impinges on the crystals, it is reflected by different atomic planes. The interaction of the incident ray with the sample generated a constructive interference and a diffracted ray. Figure 3.5 shows the schematic view of the XRD principle.

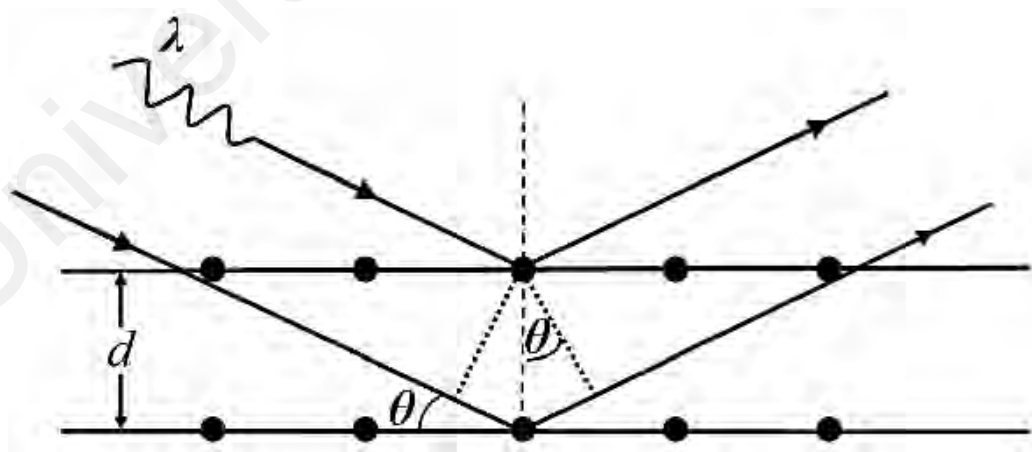


Figure 3.5: Schematic view of XRD principle

The relationship between the crystal lattice, wavelength and the incident angles is depicted by the Bragg's formula:

$$2d\sin\theta = n\lambda \quad 3.1$$

Where d is the plane spacing of the crystal lattice, θ is the angle of the incident ray, and λ is the X-ray of the wavelength. The Bragg's equation illustrates the interference pattern of the X-ray scattered by the crystals. The equation 3.1 guarantees the specific diffraction for each phase. XRD is used to identify the phase composition of the PEO coatings. The PANalytical Empyrean X-ray diffractometer system was used for phase identification and structural determination of the coating layer. The operating parameters were $Cu K_{\alpha}$ (45 kV/40 mA), divergence slit of 0.05° , receiving slit width of 0.1 mm, step scan of $0.02^{\circ} s^{-1}$ and a 2θ (10° to 80°) scan rate of $1^{\circ} min^{-1}$. The chemical bond structure was verified using Attenuated Fourier transform infrared spectroscopy-400.

3.5 Mechanical characterization of PEO films

The mechanical properties of the PEO coated samples in response to the PEO input parameters are assessed in terms of surface roughness, Micro-scratch examination and wear characteristics.

3.5.1 Surface roughness of the PEO films

The surface roughness is determined in terms of the arithmetic mean Ra of the PEO film surface. In this study, SJ-Mitutoyo surfstest SJ-210 profilometer tester is employed to measure the roughness. The instrument allows a stylus to pass over the surface of the sample and the surface roughness is measured by comparing all the peaks and valleys with the mean line and then averaging them all over the entire surface. Averages of five measurements taken on each specimen are recorded.

3.5.2 Micro-scratch examination

A micro-scratch tester (Micro Materials Ltd., Wrexham, UK) was used to measure the adhesive strength of the PEO film by applying a load ranging from 0 to 2500 mN, which generated scratches with a conical Rockwell diamond tip of radius 25 μm . The indenter was drawn across the coated surface to be tested under progressive loading at a fixed rate of 1.2 $\mu\text{m/s}$. The scratch length during the scratch test was 1000 μm . In the micro-scratch test, critical load (L_c) was used to quantify the adhesive strength of coating/substrate combinations and it was defined as the load that caused the coatings to detach completely from the substrate. The critical load value was confirmed by the scratch tracks. The chronology of the abrupt changes along the profile determined the critical loads on the scratch track, which were defined as (a) L_{e-p} : critical load for the onset of plasticity; (b) L_{c1} : critical load to indicate onset of edge cracking; L_{c2} : critical load to indicate delamination of film from the substrate; L_{c3} : critical load of total coating failure as indicated by complete exposure of the substrate surface. To determine the magnitude of the critical load, the frictional curve and penetration depth as a function of critical load were also measured. After the scratch test, the scratch tracks were observed using the FESEM and optical microscope to evaluate the damage and changes in morphology on the as-deposited coatings.

3.5.2.1 Scratch hardness of PEO coatings

To measure the resistance of the films to deformation, the scratch hardness test was conducted on the PEO-coated samples. This test provides a different combination of the surface as the stylus moves tangentially along the coated surface. The method is applicable to a variety of engineering materials including ceramics, metals and polymers. It involves measurements of the leftover scratch width after the stylus has been removed to calculate the hardness number. Owing to the fact that, the stress state at the diamond tip is a function of the contact area and applied force, the scratch

hardness depends solely on the diamond tip radius and applied load. The hardness is obtained by dividing the applied load on the diamond tip by the projected area of the contact scratching surface. In the present work, a constant normal force is applied by the stylus and track formed by relative movement of the stylus against the coated surface. The average width of the scratch track was measured with the aid of optical microscope. The scratch hardness H_{SP} was determined following the specification of ASTM G171-03 (ASTM, 2009):

$$H_{SP} = \frac{8P}{\pi w^2} \quad 3.2$$

where H_{SP} is the scratch hardness number, P is the normal force (N) and w is the scratch width (mm).

3.5.3 Wear resistance

The wear behaviour of the PEO samples and untreated substrate was studied using a ball on plate configuration (Ducom Reciprocating Friction Monitor-TR 282 Series). The machine is designed to assess both the friction and wear characteristics of the samples under reciprocating sliding motion. A bi-directional motion is created between the samples by a reciprocating engine, while a loading mechanism applies the desired load upon the test samples. In addition, a friction measurement system allows the instant frictional force to be measured during the operation. The coefficient of friction and a variety of optional facilities are calculated and obtained on the *WinDucom* software. Prior to the test, the samples were thoroughly cleaned with distilled water and degreased with acetone. AISI 52100 steel ball with the diameter of 6 mm and nominal hardness of 62 HRC was tightly fixed in the ball holder as the static friction partner against the stationary PEO coated and untreated substrate plate. The test was performed at normal room temperature of 25 °C. The tribological wear test was carried out at a normal load of 5N with a reciprocating frequency of 10 Hz and amplitude stroke of 1 ± 0.02 mm

were applied to the disc, where the tangential force was incessantly calculated using a load cell sensor attached to the loader. The kinetic coefficient of friction was determined by dividing the recorded frictional force by the normal load and displayed in the instrumentation output. Moreover, optical microscope and field emission scanning electron microscope were utilized to assess the wear scars.

3.5.4 In vitro corrosion resistance

As stated in Chapter 2, the application of Ti6Al4V alloy in the biomedical application area is limited by its corrosion performance. Therefore, investigating the effect of PEO coatings on corrosion behaviour Ti6Al4V alloy comprises the major research activity within this project. The *in vitro* corrosion measurements of the samples were carried out by a potentiodynamic polarization method using a potentiostat/galvanostat/frequency response analyser from Metrohm (Model: AutoLab PG STAT30). The polarization behaviour was recorded during immersion in Ringer's solution (8.6 g/L NaCl, 0.3 g/L KCl and 0.33 g/L CaCl₂) for 7 days using a three-electrode cell. The sample, a platinum wire and a saturated calomel electrode (SCE) were the working, counter and reference electrodes, respectively. The corrosion potential and corrosion current density were obtained from the Tafel plots with the scan rate of 2 mV/s. Figure 3.6 depicts the data interpretation via Tafel extrapolation method. The corrosion rate, CR of the PEO treated and untreated substrate could be derived from Stern-Geary equation:

$$I_{corr} = \frac{1}{R_p} \frac{\beta_a \beta_c}{2.3 (\beta_a + \beta_c)} \quad 3.3$$

Protection efficiency (*P.E*) was also determined to evaluate the effectiveness of the corrosion protection of the film layers using the equation (Rafieerad et al., 2016):

$$P.E(\%) = \frac{I_{corr}(untreated\ Ti6Al4V) - I_{corr}(treated\ Ti6Al4V)}{I_{corr}(untreated\ Ti6Al4V)} \times 100$$

3.4

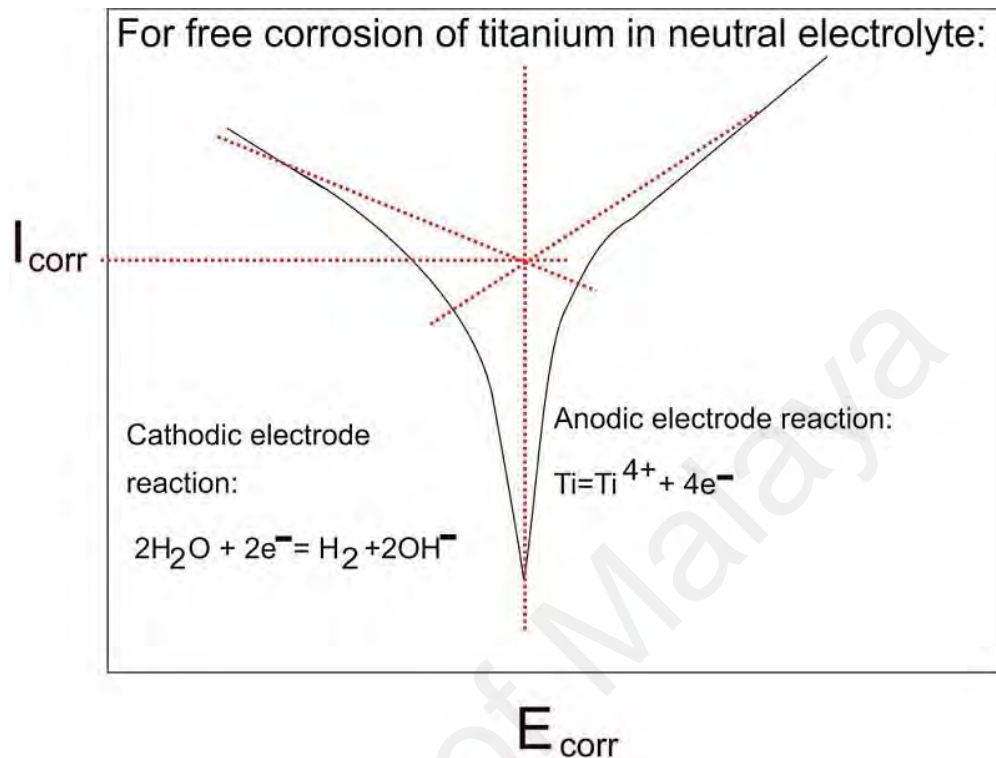


Figure 3.6: Schematic view of potentiodynamic polarization curve using Tafel plots.

where β_a is the anodic Tafel slope while β_b the cathodic Tafel slope, and R_p (Ω) the polarization resistance.

3.5.5 In vitro bioactivity test

In-vitro bioactivity of the Ti6Al4V substrate and coated samples was evaluated by assessing the possibility of forming bone like apatite layer. The samples were submerged in simulated body fluid (SBF) with ion concentrations almost similar to those in human blood plasma. The SBF utilized previously in Kokubo & Takadama (2006) was prepared according to the procedure suggested by Kokubo et al. (1990). The solution was prepared by dissolving the reagent grades NaCl, NaHCO₃, KCl, K₂HPO₄.3H₂O, MgCl₂.6H₂O, CaCl₂ and Na₂SO₄ in ion-exchanged water and the pH

adjusted to 7.3. Table 3.5 presents the composition of the reagent grade used to prepare 1 liter of SBF.

Table 3.5: The reagent grade used to prepare 1L SBF

Order	Reagent	Mass (g)
1	NaCl	8.035
2	NaHCO ₃	0.355
3	KCl	0.225
4	K ₂ HPO ₄ .3H ₂ O	0.231
5	MgCl ₂ .6H ₂ O	0.311
5	CaCl ₂	0.292
6	Na ₂ SO ₄	0.072
8	Tris	6.118
9	1.0M-HCl	Adjust to pH 7.3

Each sample was immersed in a smooth plastic vial containing 50 ml of SBF solution and was kept in a biological incubator at 36.5 °C for a predetermined number of days. The prepared SBF solution was refreshed every 24 h to maintain the ion concentration similar to that of human body blood plasma.

3.6 Summary

In this chapter, the materials, equipment and experimental procedures adopted in the investigation are described. The experimental and procedures mentioned in this chapter are essential to achieve the objectives listed in Section 1.3. The range of voltage regimes and concentration of bovine HA and commercial HA is presented as well. The detailed experimental parameter is not described here, but presented in each specific chapter. In order to have a clear picture of PEO treatment parameters, the reader is recommended to refer to the specific chapter of interest. Specifically, the procedures and conditions for the characterization of PEO-coated surfaces and untreated Ti6Al4V in terms of phase structure, morphology, corrosion resistance, in vitro bioactivity, mechanical property testing, etc. are presented.

CHAPTER 4: RESULTS AND DISCUSSIONS

4.1 Introduction

This chapter presents the results and discussion of the influences of the HA concentration on the morphological features and properties of HA coating produced using PEO on the titanium alloy. The PEO features discussed include phase structure, elemental composition, coating thickness, porosity while the properties analyzed are surface roughness, scratch hardness, and adhesion strength. The mechanism of the formation and failure modes associated with each of the HA concentrations was also discussed as well.

4.2 Influence of electrolyte concentration on PEO

4.2.1 Coating fabrication

The PEO coatings were formed on Ti6Al4V substrates, the preparation of which involves cutting, degreasing, and rinsing according to the procedure described in Chapter 3. The PEO treatments were carried out for 5 minutes at a current density of 500 mAcm⁻² and voltage of 300 V. The coatings were produced under DC current with the electrolyte concentration ranging from 0-2 g/L. The electrolyte preparation has been mentioned in Chapter 3. Table 4.1 shows the formulation for electrolyte concentration for PEO coatings.

Table 4.1: Electrolyte formulation for PEO process

PEO processing parameters	Quantity
HA concentration (g/L)	0, 1, 1.5, 2
Na ₃ PO ₄ .12H ₂ O (NAP) (M)	0.12
Voltage (V)	300
Current density (mAcm ⁻²)	500
Deposition time (mins.)	5

4.2.2 Characteristics of PEO process

Monitoring the voltage-time response is important to understand the electrochemical behaviour of the samples during the PEO process. The voltage-time plots obtained during the PEO processing of Ti6Al4V alloy under various electrolyte concentrations are shown in Figure 4.1. During the first 30-50 s, the voltage rises fast and increases linearly with time at a constant rate, which is consistent with the voltage-time response analysis discussed in Section 2.5.1. This initial rise in voltage is due to dissolution of the substrate and formation of a thin oxide layer at the electrolyte/anode interface.

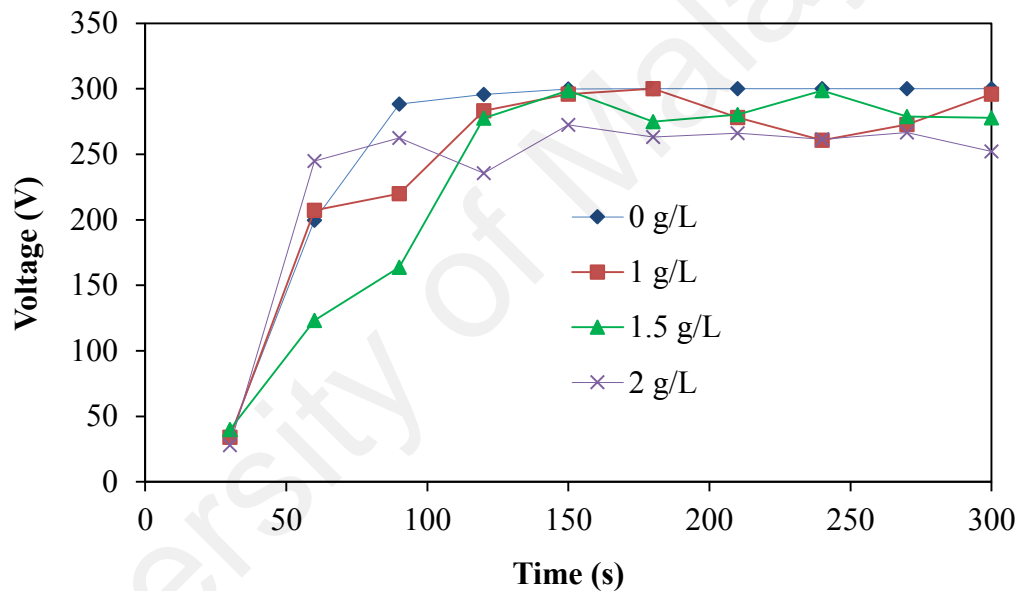


Figure 4.1: Voltage-time plots obtained during the PEO process in different electrolyte concentration

For the sample 0 g/L, the dissolution-oxide film formation is observed up to approximately 199 V, where dielectric breakdown of the film (normal oxide growth terminates) and numerous micro-arc sparks along with fine discharges were noticed on the sample surface. This was also accompanied by gas evolution. This behaviour continues until a final voltage of 300 V was registered. At this point, no significant increase in the intensity of the micro-sparks was observed on the substrate. The

emergence of high frequency ascending and descending oscillation of the cell voltage, observed for the 1 g/L, 1.5 g/L and 2 g/L HA samples, represents the stages of oxide breakdown and regrowth, which maintains the thickness of the layer approximately constant. The distinct deviation in the observed behaviour of the 1 g/L, 1.5 g/L and 2 g/L HA samples, compared to 0 g/L HA, is due to the electrolyte concentrations at the oxide interface. During the PEO process, when a current density flows through the anode/electrolyte interface, the charged electrolyte particles (HA) enter the initial growing oxide layer and release a current of electrons into the oxide film. The incorporation of ions into the oxide film induces a complex high-temperature reaction and causes the initial growth layer to lose its oxide coating (initial breakdown). This enables an avalanche of electrons injections into the broken spot, thus allowing the locally destroyed film to be rebuilt immediately. As soon as the breakdown is eradicated, the anodization proceeds further to a new breakdown voltage, when the ionic current in the oxide film predominates. This phenomenon continues until a final voltage is reached. It has been shown in Albella et al. (1987) and Jun et al. (2007) work, that the working voltage and the final voltage during the PEO process decrease with increasing electrolyte concentration due to the electrolytic composition, and therefore it is not surprising that the highest electrolyte concentration, 2 g/L HA, exhibited the lowest final voltage. While the increase in voltage during the PEO process up to the point of breakdown voltage is predominantly governed by the electrolyte concentration, the further increase in voltage is caused by the growth of the layer thickness and coating formation on the substrate surface. The final voltages reached at the end of coating of 0 g/L, 1 g/L, 1.5 g/L and 2 g/L HA in the present study were 300, 296, 278 and 252 V, respectively.

4.2.3 Surface morphology of PEO coated layers

The plan view of the PEO coatings produced under different electrolyte concentration is shown in Figure 4.2. It is obvious that the surface morphology was affected by the HA concentration in the NAP electrolyte solutions. Without HA, the coating surface is covered by many discharge channels appearing as irregular circular and elliptical spots distributed over the entire film surface (Figure 4.2a).

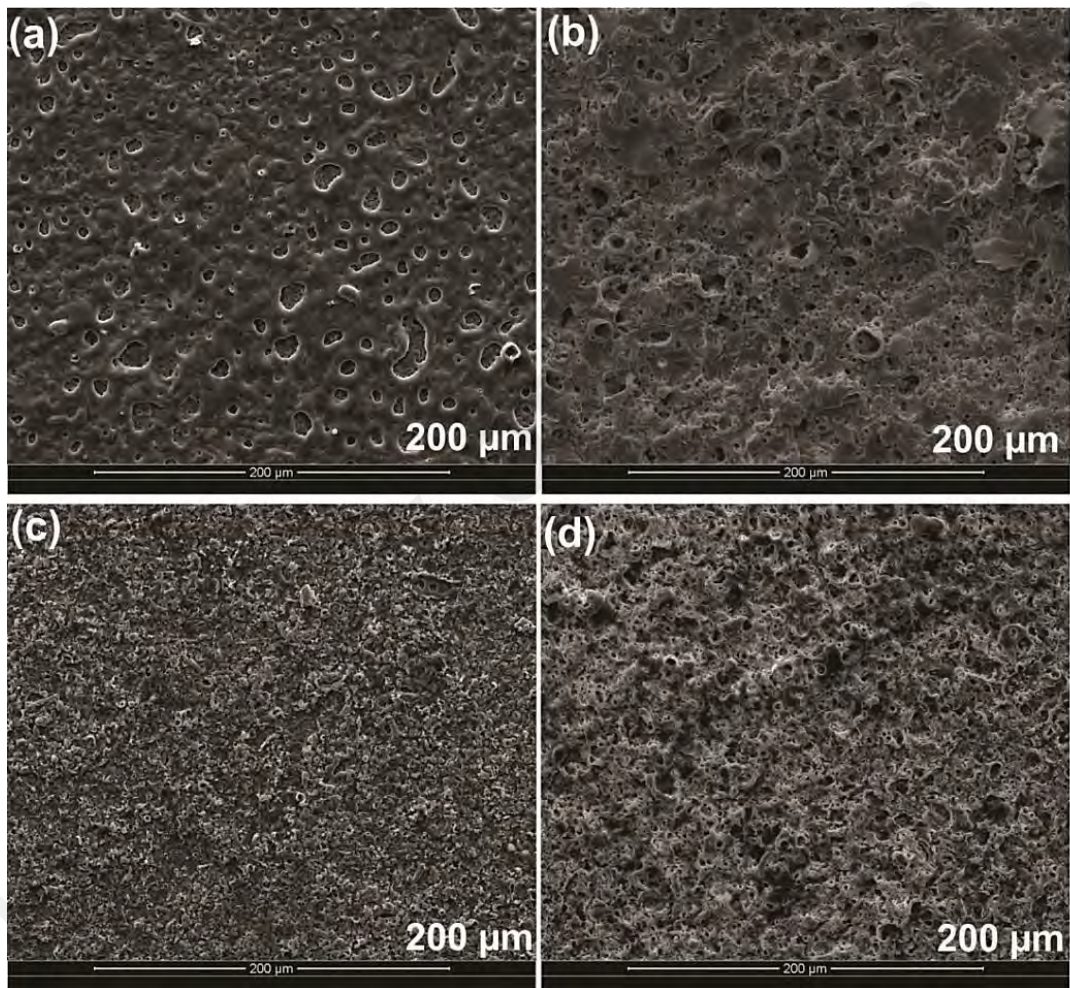


Figure 4.2: Surface plane SEM micrographs (a) 0 g/L, (b) 1 g/L, (c) 1.5 g/L, and (d) 2 g/L HA

The spots seem to be associated with the liberation of gaseous oxygen and micro-arc discharge occurring on the Ti surface. When the Ti surface was treated with a solitary NAP electrolyte solution, a careful observation of micro-arc discharge revealed that

oxidation of the surface started to occur at ~ 164 V and became more intense with increasing electrolytic voltage (up to 300 V). Consequently, the micro-porous rough region started to appear locally due to the formation of an insulating TiO_2 layer on the Ti surface. The Ti surface which was initially smooth became rough with numerous micro-pores due to the high spark discharges and gas evolution.

For the sample processed with a lower HA concentration (1 g/L), the film surface was seen to be rough and a number of micro-pores were observed. However, the micro-pores are not as prominent as those observed without HA addition. The large micro-pores noticed without HA addition became slightly smaller. This indicates that the pores have partially been sealed by the HA particles. Nevertheless, the surface appeared to maintain the initial surface morphology of the PEO-NAP treated layer. A tiny surface crack was found on the surface processed with 1 g/L HA concentration. The residual stress developed during the PEO process due to rapid solidification seems to be the main cause of cracking. With a further increase of the HA concentration (from 1.5 g/L to 2 g/L), micro-pores were hardly seen on the surface as they have been covered with HA particles. In addition, at higher HA concentrations, the electrolyte fluidity increased, and the gas evolution, which usually accompanied the PEO process, was suppressed. On the other hand, the evolution of gas from the less viscous solution used for the 1 g/L HA sample during the solidification process led to the formation of pores and the electrolyte was not sufficiently fluid to fill the pores.

4.2.4 Surface chemistry and phase compositions

The elemental chemical composition results indicate that, regardless of the HA concentrations, all coatings are composed of Na, Ca, P, Al, O, Ti; only the spectrum of the PEO-HA coating produced at 2 g/L HA is therefore presented in Figure 4.3. The

coating is mainly composed of Ca, P, Ti, O, Na, Al. This means that the substrate and modifying elements from the electrolyte participated in the formation of the coatings.

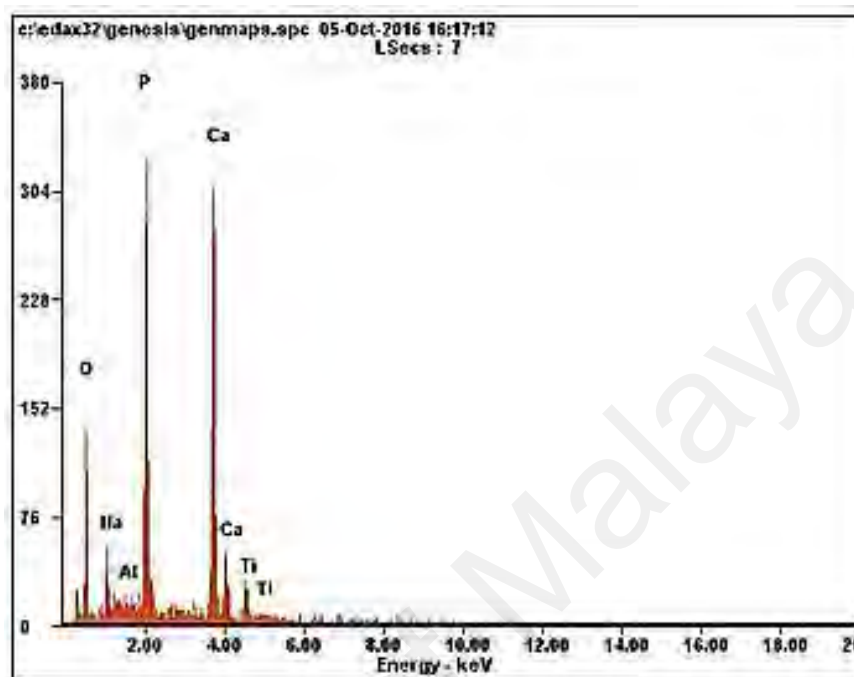


Figure 4.3: Representative EDS spectrum of the PEO coating produced at 2 g/L HA

Table 4.2 shows the atomic concentrations of the PEO-HA coatings produced at varied concentrations. As can be seen, the atomic concentrations of the elements are slightly different. The coating formed at higher concentrations tends to contain higher amount of Ca and P, which is consistent with previous results by Bai et al. (2011).

Table 4.2: Elemental chemical compositions of the PEO coatings produced at different concentrations

Concentration (g/L)	Ca	P	O	Ti	Al	Na	Ca/P
0	-	09.86	64.59	20.50	02.89	02.16	-
1	13.43	11.93	67.06	01.60	00.37	05.62	1.12
1.5	17.57	14.52	60.66	02.85	00.65	03.75	1.21
2	22.84	17.58	53.25	03.16	00.89	02.29	1.30

The higher content of Ti and O from the elemental composition indicates that oxidation of the substrate is predominant during the PEO process. With the samples produced in the HA-containing NAP electrolyte solutions, the EDS spectrum showed the presence of Ca and P peaks (Figure 4.3). This suggested that HA could be deposited in the film layers by PEO treatment in an aqueous electrolyte solution. The increase in Ca and P concentration in the 1 g/L, 1.5 g/L and 2 g/L HA samples confirm that HA has been incorporated into the PEO-TiO₂ coatings. The changes in the amount of Ca and P can be attributed to the different amount of HA particles in the electrolyte solution. Based on the atomic concentration from Table 4.2, it is found that Ca/P ratio was increased with increase of the HA concentrations.

XRD patterns of the PEO layers produced at varied concentrations are shown in Figure 4.4 to facilitate the understanding of how the elements identified by the EDS analysis are combined in the coatings. It can be seen that all coatings are composed of hexagonal hydroxyapatite, tricalcium phosphate (TCP), anatase, and titanium peaks corresponding to the metal substrate. During the PEO process, the temperature and pressure in the discharge channel could reach approximately 10000 K and 100 MPa (Walsh et al., 2009), which are high enough to promote the conversion of the titanium substrate into TiO₂. At a 0 g/L HA concentration, there were only titanium and anatase TiO₂ phase (Figure 4.4a). With the addition of HA powder particles, the peak associated with hexagonal HA, TCP were detected along with the anatase (Figure 4.4).

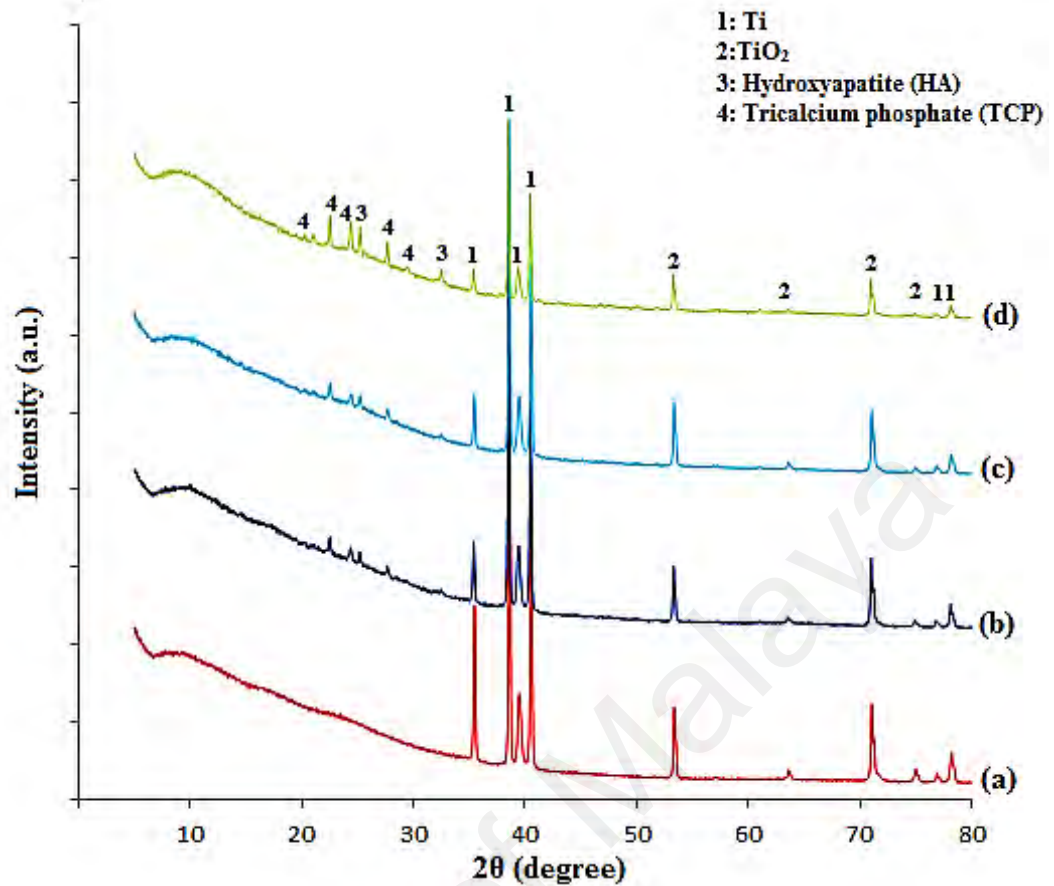


Figure 4.4: XRD patterns of the coating produced at varied concentrations: (a) 0 g/L, (b) 1 g/L, (c) 1.5 g/L, and (d) 2 g/L HA

Moreover, as the HA concentration increases from 0 to 2 g/L, the intensity of the HA and TCP peaks increase. The appearance of TCP at 5 min. deposition time has also been reported by Durdu et al. (2013), while studying hydroxyapatite and calcium apatite based coatings formation on Ti6Al4V alloy surface using PEO method. Abbasi et al. (2011) inferred that the decomposition of HA_p phase to TCP is as a result of anode temperature surge during PEO process. They found that the HA phase appeared at a deposition time of 3 min. and its decomposition start to occur when treated above 3 min. deposition time.

4.2.4.1 Porosity of PEO coatings

The porosity of the PEO coatings was examined using OLYMPUS Stream Micro-Imaging Software. The average pore size presented in Figure 4.5 tends to reduce with increasing HA concentration from 80.8 % at 0 g/L to about 54.1 % at 2 g/L.

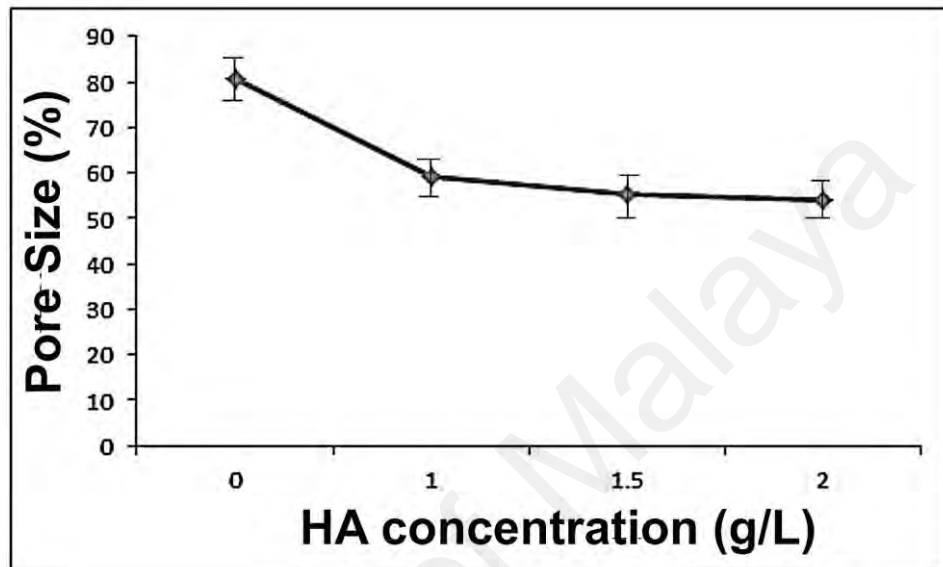


Figure 4.5: Dependence of pore size in the PEO coatings on the HA concentration

The PEO coating processed with 0 g/L HA had a large percentage of pores. These pores are characteristic features of the PEO coating and their formation is related to gases produced during the PEO process. The NAP solution (without HA addition) is less viscous, and the entrapped gases produced during the PEO process formed pores on the re-solidified titanium surface (Figure 4.2a). On the other hand, the PEO processed with the electrolytes with the HA addition had high fluidity due to the concentrations of HA particles. The evolved gases can escape during the solidification or sintering process when the electrolyte solution is sufficiently fluid. It is believed that the PEO coatings with HA addition yielded high fluidity liquids which assisted these gases to

escape. The porosity level of the 2 g/L HA decreases due to the HA incorporated into the film layer (Figure 4.2d).

4.2.5 Coating thickness

The polished cross-sectional views of PEO-coated surfaces of the samples prepared with different HA concentrations are shown in Figure 4.6. The coating thickness revealed that the thickness of the PEO-coated layers also depends on the HA content in the electrolyte. With increasing concentration of HA particles in the electrolyte during PEO treatment, a much thicker layer, ranging from 10-17 μm , was formed.

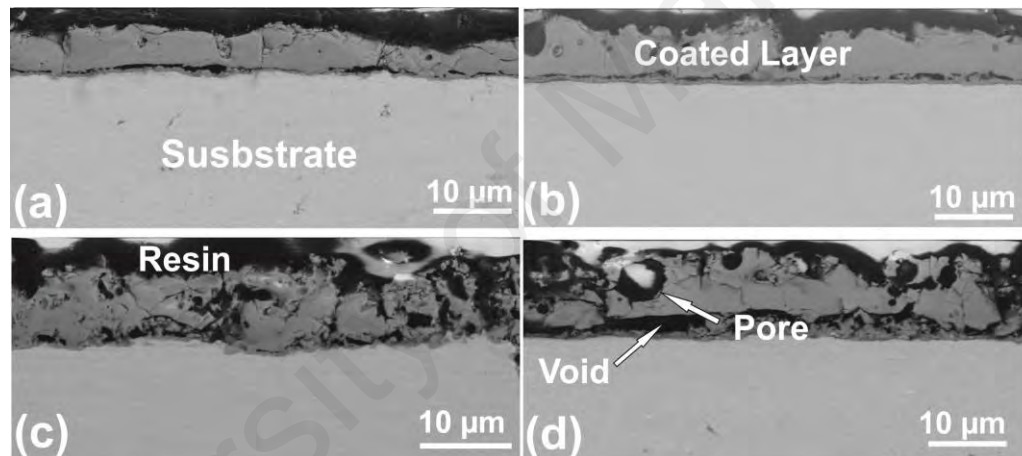


Figure 4.6: Cross-sectional morphologies of PEO coatings produced at varied concentrations: (a) 0 g/L, (b) 1 g/L, (c) 1.5 g/L, and (d) 2 g/L HA

The obtained coatings were significantly thicker when higher concentrations of HA were used. This finding is in agreement with the observation reported by Bai et al. (2011) and Simka et al. (2013) in their PEO treatment of titanium samples. They found that the thickness of oxide film was higher when larger amount of Ca and P were deposited into the porous oxide film. A significant amount of closed pores were also observed due to CaP enrichment in the porous oxide layer. This morphological change is attributed to the dielectric breakdown of the enriched oxide layer. It can be inferred

that during PEO process, an intense micro-arc discharge appears on a local area of the substrate to form micro-pores. As the micro-pores are formed, more openings are created for the entrance of electrolyte-borne particles. The micro-porous layer becomes filled with Ca and P ions. As the TiO₂ layer enriched with Ca and P becomes thicker, the resistance of the layer increases and more energy is required to break the dielectric layer. Owing to a series of thermochemical reactions and subsequent formation of complex compounds on the substrates, the thickness increase. The thickness of the PEO-coated layers depend on the electrolyte concentration and the coatings were significantly thicker when higher concentrations of HA were used.

Figure 4.7 shows correlation between the final voltage and coating thickness, which is consistent with the theoretical analysis of the voltage-time response discussed in Section 4.2.2

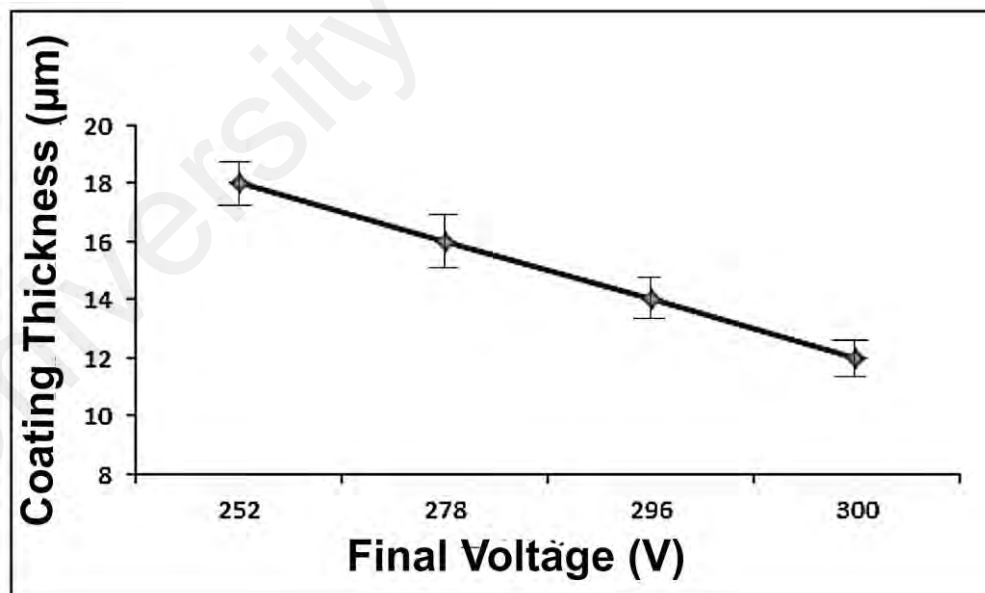


Figure 4.7: Correlation between the final voltage and coating thickness of the PEO coatings produced at varied concentrations

4.2.6 Mechanism of TiO₂/HA coating formation

The deposition of HA in the Na₃PO₄ solution was performed using an anodization process, and a TiO₂/HA layer is created on the Ti surface. In the PEO process, when the applied voltage is higher than the breakdown voltage, the micro-arc discharges rapidly build up on the anode surface which leads to the dissolution of Ti metal. According to Eq. (4.1), Ti plate has a strong tendency to release electrons to produce Ti⁴⁺ ions.



At a sufficient potential difference, the water molecules in the aqueous electrolyte solution dissociate and produce hydroxyl (OH⁻). The OH⁻ ion migrates towards the anode and produces O₂ gas via the following chemical reactions.



Thus, the main reactions occur on the anode via the combination of equations

(4.1 and 4.3) as follows:



In the next stage of the PEO process, the Na₃PO₄ compound in the electrolyte can ionize to Na⁺ and PO₄³⁻. The anion (PO₄³⁻) is not bound to any particular atom during the PEO process and are free to drift throughout the entire electrolyte bath, which finally form a sea of electrons on the HA particles. The PO₄³⁻ ion charges the HA particles negatively. The negatively charged HA particles in the electrolyte are attracted to, and migrated towards, the anode under the strong electric field and get deposited into the microporous oxide layer grown via the PEO process. The HA particle is thereafter

sintered onto the anodic surface by the high micro-arc plasma discharge produced at the anode. Thus, the incorporation of charged HA particles into the porous oxide film will occur concurrently, thereby forming the TiO₂/HA layer.

During the PEO process, the high temperature generated inside the micro-porous layer would promote migration of Ca and P ions from the inner porous layer into the outer layer and form tricalcium phosphate according to the following reaction:



According to reaction equations (2-6), TiO₂ is produced in the anodic coatings, and Ca and P elements are incorporated into the oxide films. In addition, anatase, TCP and HA are present in the PEO coatings.

4.2.7 Mechanical properties

4.2.7.1 Surface roughness

The surface roughness (R_a) measured using SJ-Mitutoyo surfstest SJ-201 profilometer are presented by the bar chart shown in Figure 4.8. The R_a of the PEO treated layers is significantly higher than that of untreated substrate. All the coatings are rougher than 1 μm ; the roughest ($2.3 \pm 0.5 \mu m$) corresponds to the HA concentration of 2 g/L, and the least roughness ($1.45 \pm 0.3 \mu m$).

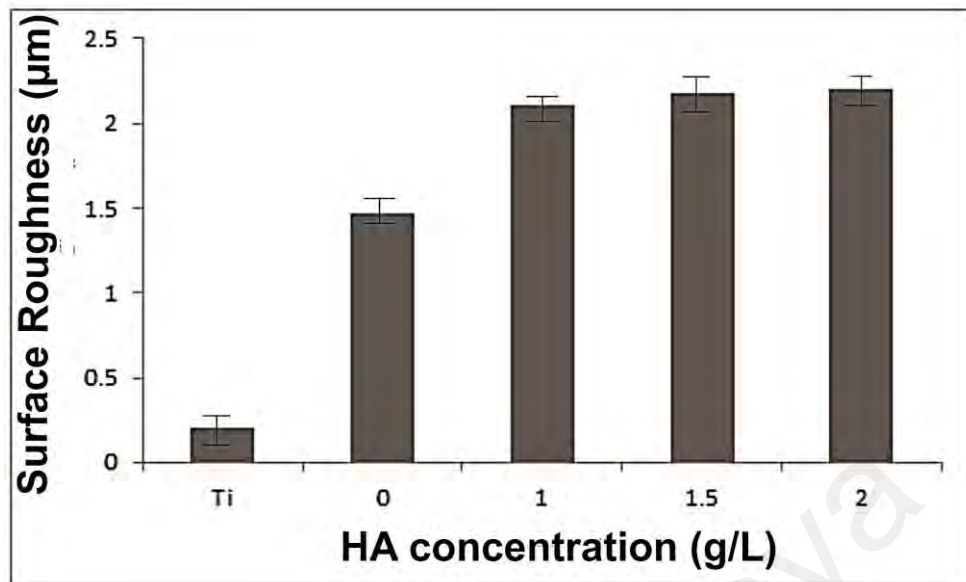


Figure 4.8: Dependence of PEO coating roughness produced on titanium at various concentrations

The overall trend is that higher HA concentration leads to rougher PEO coatings, although the coatings produced at 1.5 g/L HA is almost the same to that of 2 g/L HA. When the titanium was micro-arc oxidized with the electrolyte with no HA additions, the surface roughness increased steadily. The surface roughness of the 1.5 g/L HA and 2 g/L HA samples were much higher than the oxidized surface (0 g/L HA).

4.2.7.2 Adhesive strength of PEO coatings

Adhesion of the coatings to the substrates is critical to their function and determines the stability and durability of films. To detect the widest possible range of coating failure modes, scratch tests were performed on PEO-coated surfaces. Figure 4.9 shows the surface of the coating after the diamond indenter is drawn over the surface with a linearly increasing load (0-2500 mN) until failure occurs at the critical load. At the onset of the test, the coating was in the elastic-to-plastic region. As the normal load progressively increases, the indentation tip gradually sinks into the coated layer, indicated by a nearly linear change of penetration at the beginning of the test (Figure 4.9

(a-d)). Consequently, spalled regions of coating removed laterally from the edges of the scratch track grooves were observed.

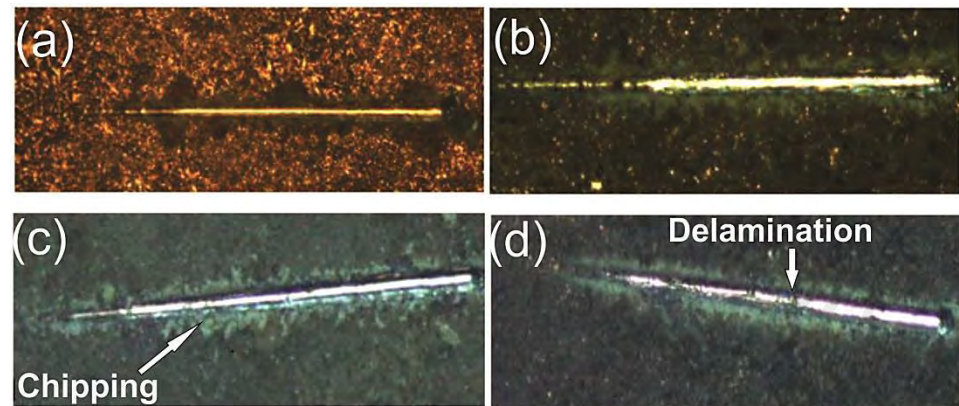


Figure 4.9: Residual scratch tract after scratch test: (a) 0 g/L, (b) 1 g/L, (c) 1.5 g/L, and (d) 2 g/L HA

The sample processed without the HA addition (0 g/L HA) was characterized with cohesive failure indicated by large periodic localized hemispherical chips, which remain attached to the coating at the outside edges of the trackside, indicating a weak cohesive strength of this sample. Such film failure is clearly seen as an increase in scratch depth (Figure 4.9a). This was subsequently followed by detachment of the coating and subsequent failure of the coated layer through complete exposure of the substrate material. It is to be noted that 0 g/L HA has the lowest coating thickness and a high level of porosity (Figure 4.6a and 4.2a), which are thought to be responsible for the low adhesive strength. The presence of the porous thin layer led to faster degradation of the adhesive strength and early fracture under the applied load. The stylus tip could penetrate the porous thin layer more easily and thus the durability of the oxide film coating was reduced. Therefore, the failure of 0 g/L HA can be attributed to the presence of a micro-porous thin layer on the surface of this sample which weakens the interface layer.

Comparing the samples processed without HA (0 g/L HA) with those processed with HA addition (1 g/L HA, 1.5 g/L HA and 2 g/L HA), the scratch length between the chipping region and the point of delamination suggests that the coatings processed with HA addition have adequate adhesive strength. The failure mode depicts different surface features. The first sign of failure observed with the samples processed with HA addition was intermittent delamination of the coating layer along the scratch path (Figure 4.9 (b-d)). As the load progressively increased, the coating was seen to completely fail from the substrate surface. The extent of delamination along the scratch path is more pronounced with the highest 2 g/L HA addition (Figure 4.9d). It is clear from the scratch test results presented here that the intermittent delamination and the area of uncovered substrate is greater and extends beyond the limit of the scratch track (Figure 4.9d) for 2 g/L HA, while the 1.5 g/L HA only had a small amount of exposed substrate that was confined within the track (Figure 4.9c).

Figure 4.10 shows the adhesive strength of PEO coatings formed in different concentrations of HA. It can be observed that the highest adhesion value is obtained for the coating processed with 1.5 g/L HA. The coating produced with the highest HA concentration showed a lower value in the adhesion strength compared to 1.5 g/L HA concentration. The reason for the decline in the adhesion value of the highest HA concentration is attributed to the morphological change of the TiO₂ film.

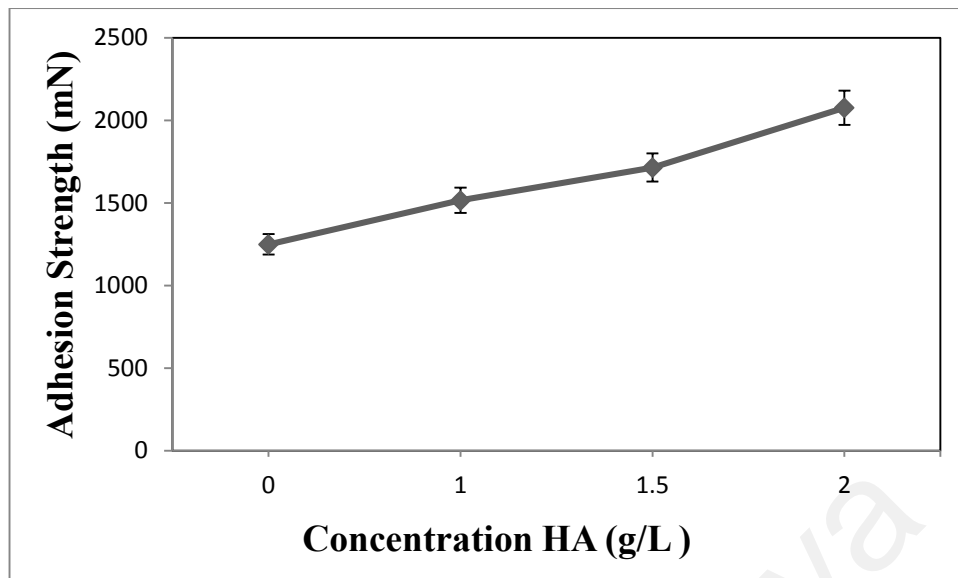


Figure 4.10: Adhesion strength of PEO coatings formed at varied concentration

The TiO₂ film enriched with the highest concentration of HA was not well formed due to the higher level of Ca and P in the anodic oxide film (Figure 4.6d). The incomplete breakdown of the anodic oxide/micro-arc discharges film due to high levels of Ca and P elements may have resulted in a poor network of micro-pore channel through the oxide section of the increased layer thickness (Figure 4.6d). As a result of this, the oxide film became unstable when the HA concentration increased beyond 1.5 g/L HA.

Although, 2 g/L HA has the highest coating thickness and showed the existence of strong intensity of Ca and P, its overall adhesive strength was lower than that of the sample processed with 1.5 g/L HA due to instability of the oxide film and higher levels of Ca and P in the oxide film. The reduction in adhesion strength of the thickest sample can be attributed to high levels of residual stress, which arises from the thermochemical reaction during formation of the coating. At a 2 g/L HA concentration at the anodic interface, higher incorporation of ions is expected, which will ultimately release larger exothermic energy. The gas generated during the reaction causes development of voids

area and pores at the interface and centre of the cross-section of the thick layer (Figure 4.6d). Thus, the adhesive strength decreases when the level of residual stresses present in the TiO₂/HA film increases. A similar result was reported when CaP was produced on Ti surface using the electrochemical deposition method. Higher thickness and surface roughness were recorded with low adhesive strength (Blackwood & Seah, 2009). Of all the samples, 1.5 g/L HA sample displayed high adhesive strength and cohesive resistance to the applied stress of the sliding indenter during the scratch test.

4.2.7.3 Elemental analysis of the PEO scratches

Further investigation was done to identify the elemental constituents in the scratches produced during the scratch test. The elemental profile for the samples prepared with 1.5 g/L and 2 g/L HA concentrations was also characterized by the FESEM line scan analysis as shown in Figure 4.11.

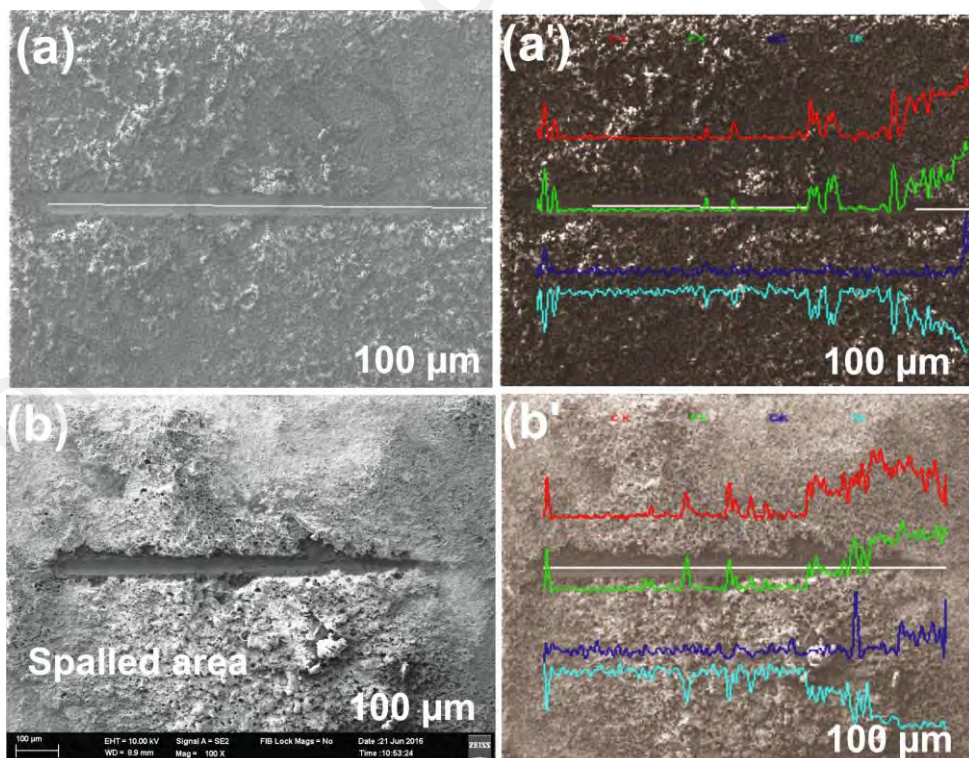


Figure 4.11: Elemental constituent analysis of the left over scratches (a) 1.5 g/L spalt region (a') profile and (b) 2 g/L HA spalt region, (b') profile

It can be observed from the spall region area of the scratch test (Figure 4.11b) that detachment of the coating in 2 g/L HA is more pronounced compared to 1.5 g/L HA. For sample processed with 1.5 g/L HA, some spallation is noticed on both sides of the scratch area (Figure 4.11a). Along the scratch length of the test, peaks for Ti and O were detected which indicates the existence of the oxide phase. The distribution of the oxide layer can be observed for 1.5 g/L HA almost along the entire scratch length of the test (Figure 4.11a). However, for the sample processed with 2 g/L HA, as the relative intensity of Ca and P ions increased, the peak of Ti decreased up to a certain limit, and this marks the beginning of the instability of the oxide film (Figure 4.11b). This may be associated with the incorporation of more HA particles from the NAP electrolyte aqueous solution.

4.2.7.4 Scratch hardness of PEO coatings

Figure 4.12 shows the scratch hardness measured for the PEO-coated titanium alloy under different HA concentration. The scratch hardness measured for the PEO-coated titanium reveals different scratch hardness number. It can be seen that the highest scratch hardness number was obtained for PEO-coating without HA ($5.03 \pm 0.8 \text{ GPa}$).

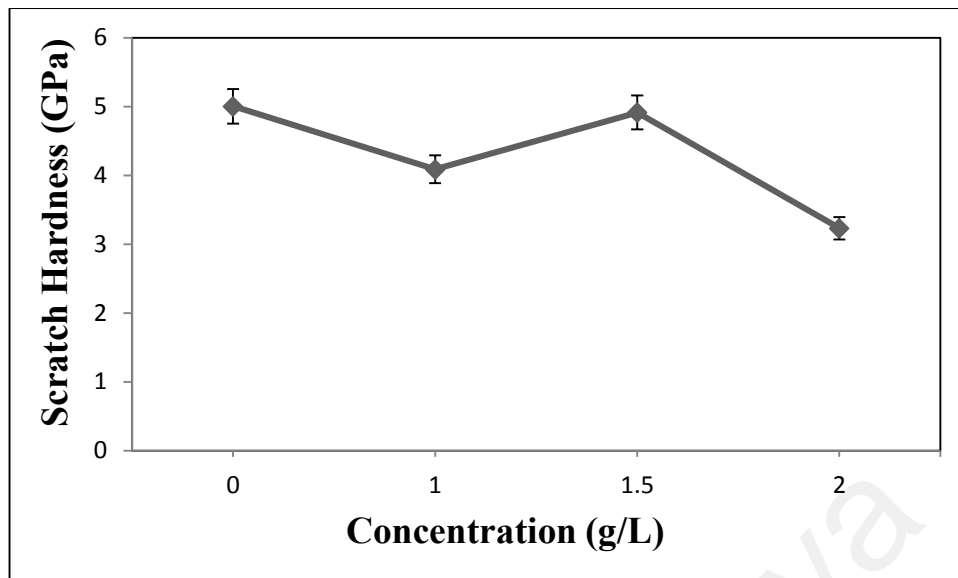


Figure 4.12: Scratch hardness number of PEO coatings formed at varied concentration

On the other hand, the coatings produced with HA addition were relatively lower. The coating processed with 2 g/L HA had the lowest scratch hardness number ($3.34 \pm 0.2 \text{ GPa}$). The results show that the oxide film layer had the highest resistance to scratching than coatings produced with HA addition. The relatively lower hardness obtained with HA addition could be associated with the brittle nature of HA, residual stress generated at the coating interface and the inconsistent formation of the oxide layer.

4.2.7.5 Failure mode of PEO coatings

In general, the failure modes mechanism observed in thin coatings is influenced by a number of internal and external factors. The internal factors are related to the testing conditions and are scratch test-dependent such as loading rate, indenter shape, scratch speed, machine calibration and others. The external factors are categorized as substrate material, coating properties, surface roughness, friction coefficient and testing environment (Bunshah, 2001). Previous studies revealed the existence of a number of

failure mode mechanisms, making the resulting behaviour of coatings subjected to the scratch test having a complex array of interaction of these factors (Nledengvist & Hogmark, 1997). In this study, the failure mechanism is divided into two stages. For the sample processed without HA addition, a chipping failure mode was observed, which implies that the TiO₂-PEO films on the Ti surface influence coating adhesion. The failure was seen to occur within the substrate, which leads to chipping and loss of coating along the scratch trackside (Figure 4.9a). This may be due to the interaction of the coating and the substrate. The oxide film is known to be brittle while Ti is ductile. As the diamond indenter contacts the coating during the scratch test, hemispherical chipping, which propagates outward from the centre line of the trackside, occurred due to compressive stresses generated ahead of the moving diamond indenter. Trackside chipping occurs due to compressive stresses that have been built up ahead of the moving diamond indenter. The stresses experienced by the coating are relieved through hemispherical chipping on both sides of the track.

For the sample produced with HA addition, the coating failure is characterized by partial and intermittent delamination (Figure 4.9b-d). The stresses responsible for the coating delamination are a combination of the stresses remaining in the coating and the localized tensile stresses generated by the diamond indenter stylus. The failure mode occurred ahead of the moving indenter. The shear force scrapes the coating off the substrate. The tensile crack first forms at the weak coating/substrate interface ahead of the moving indenter due to compressive shear stress. This is usually accompanied by the rise and fall of diamond indenter penetration depth. The continued forward movement of the indenter tip increases the stress and leads to the growth of an interfacial tensile crack (Figure 4.9c). Prior to failure mode, the space between the scratch widths becomes constant and the interfacial tensile crack decreases. At this particular point, the high compressive stress that had built up disappears and no delamination will be

observed. Eventually, the spallation is then replaced by chipping and detachment of the coating along the trackside. The spalled regions are usually smaller with a lower number of cracks. As mentioned earlier, the adhesive strength of TiO₂/HA was $2099 \pm 13.7 \text{ mN}$. Conversely, a value $1247 \pm 6.8 \text{ mN}$ was recorded with the microporous oxide film on Ti surface. These results show that by infiltrating Ca and P in the porous oxide film, the adhesive strength can be increased by about 68%.

4.3 Summary

This chapter has discussed the influence of HA concentration on the morphological features and properties of PEO coatings produced on Ti6Al4V implant, in connection with the mechanism of formation and failure modes, and resulted in the following findings:

- The PEO layers (10-17 μm) were rough and porous regardless of the HA concentration. However, the average pore size and thickness layer are concentration dependent, so that higher HA concentration results in coatings having a higher thickness and smaller porosity. This is due to enrichment of the TiO₂ film with larger amount of HA.
- Calcium and phosphorous were incorporated into all coatings treated with HA concentration. With increasing HA concentration, the content of CaP increased. Higher amount of Ca/P ratio of 1.3 was achieved with single PEO process.
- The phase structure were mainly composed of hexagonal HA, TCP, and anatase. The intensity of HA and TCP increased with increasing HA concentration. The appearance of TCP is due to high temperature generated inside the microporous layer.

- Higher scratch adhesive strength was achieved using 1.5 g/L HA suspension with a critical load of 2099 mN, while coatings without HA produced a critical load of 1247 mN.
- The failure of the PEO coatings was characterized by large periodic hemispherical chipping, while intermittent delamination was noticed with the coating embedded with HA particles.

It emerges from the analysis of the results presented in this chapter that HA concentration of 1.5 g/L can be considered as low concentration condition for PEO coating, which produced higher adhesion, high resistance to scratching and relatively good rough porous surface in relation to other ranges of HA concentration.

CHAPTER 5: INVESTIGATION OF VOLTAGE REGIME EFFECT ON THE PEO COATINGS CONTAINING BOVINE-HA PARTICLES SOLUTION

5.1 Introduction

As stated in Chapter 4, PEO coatings were formed in the HA concentration ranging from 0-2 g/L. The effects of HA concentration on the PEO process and final coating characteristics were discussed. It was concluded that the PEO coating produced at 1.5 g/L HA presented the best in adhesion performance compared with its counterparts produced at other concentration. As stated in Chapter 2, apart from commercial HA, PEO coatings can also be produced using natural bovine HA in order to mimic the biological portion of human bone. However, the effects of PEO parameter (voltage) to deposit BHA have not been established. The effects of the voltage regime of the PEO coating using the concentration optimized in Chapter 4 are studied in the present chapter.

5.2 Influence of applied voltage on BHA film

5.2.1 Coating fabrication

PEO coatings were fabricated on Ti6Al4V alloy, and the details of the substrates including elemental composition, dimension and preparation procedures were described in Chapter 3. The PEO coatings were conducted in the familiar, inexpensive and benign compound electrolyte containing 1.5 g/L BHA and 4 g/L NAP, as identified in Chapter 3 and 4. The current density was also set at 500 mAcm⁻², with deposition voltage varied from 225 to 325 V. Table 5.1 summarizes the PEO parameters.

Table 5.1: PEO parameters for BHA deposition

PEO parameters	Quantity
BHA concentration (g/L)	1.5
Na ₃ PO ₄ .12H ₂ O (g/L)	4.0
Voltage regime (V)	200-325
Deposition time (min)	5
Current density (mAcm ⁻²)	500
Electrolyte temperature	35 °C

All the treatments were carried out for 5 mins. The electrolyte temperature did not exceed 35 °C.

5.2.2 PEO process characterization

As mentioned in the Chapter 4, monitoring the voltage transient during PEO treatment is vital to study the PEO process and predict the coating characteristic features including structure and in vitro corrosion behaviour. The voltage-time response during the PEO process recorded in the present study is presented in Figure 5.1.

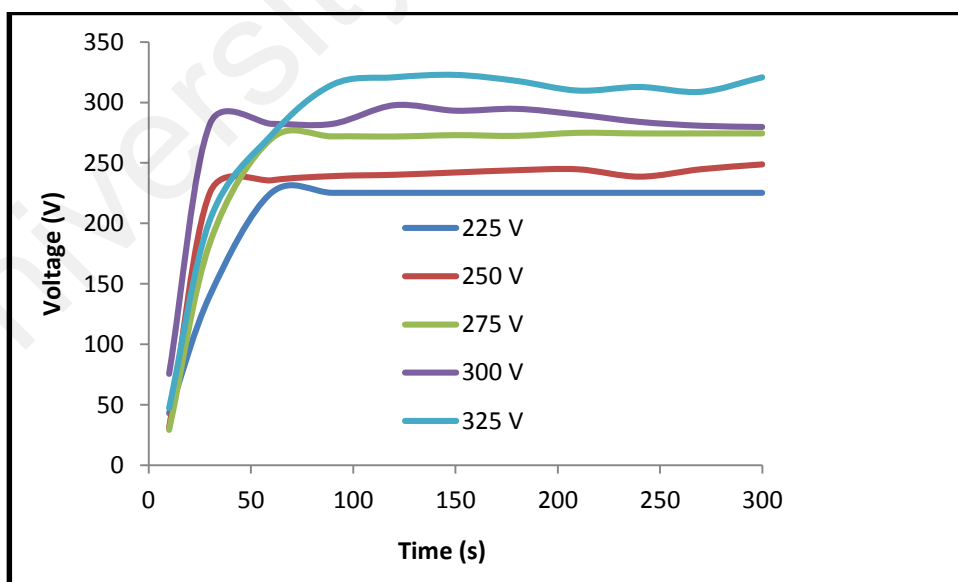


Figure 5.1: Voltage-time behaviour during PEO process at varying voltages

For all the applied voltages, the trend of the voltage-time curves was the same. Similar to the results reported in Chapter 4, the voltage-time experienced a steady increase after the start of PEO process. In the first (0-10 s), the voltage increased linearly, suggesting a rapid passivation of the titanium substrate. Thereafter, the voltage incremental behaviour continued at a lower rate, which was accompanied by vigorous gas liberation, and micro-tiny sparks traversing on the sample surface. The gas produced during PEO process has been independently verified to be oxygen by Snizhko et al. (2007) and Guo et al. (2005). The appearance of the micro-spark is due to the local breakdown of the preformed oxide layer because of high energy intensity. Afterwards, the voltage was slightly increased to the final voltage within the period of 45-300 s.

5.2.3 Surface morphology of PEO-BHA coated layers

The surface morphologies of PEO coatings produced at varying applied voltages for 5 mins are shown in Figure 5.2. It can be seen that the sample processed at low voltage is bereft of micro-pores. The absence of pores is probably due to low discharges caused by low energy injection. Increasing the applied voltage from 225 to 325 V, a typical porous morphologies are observed, which are attributed to the discharge activity and effervescence of gas during the PEO process, as described in Chapter 2. The smallest pore diameter ($< 0.5 \mu\text{m}$) is recorded for the sample processed with low voltage, the pore diameter increased from $\sim 8.5 \pm 0.3 \mu\text{m}$ at a voltage of 275 V to $\sim 11.3 \pm 1.1 \mu\text{m}$ and $12.8 \pm 0.9 \mu\text{m}$ for a voltage of 300 and 325 V, respectively. The increased in pore size at higher voltages is due to formation of sparks with the higher energy. Moreover, mild cracks were detected in the coating formed at highest applied voltage (325 V). It is believed that the appearance of crack was due to temperature difference between the coating and the electrolyte.

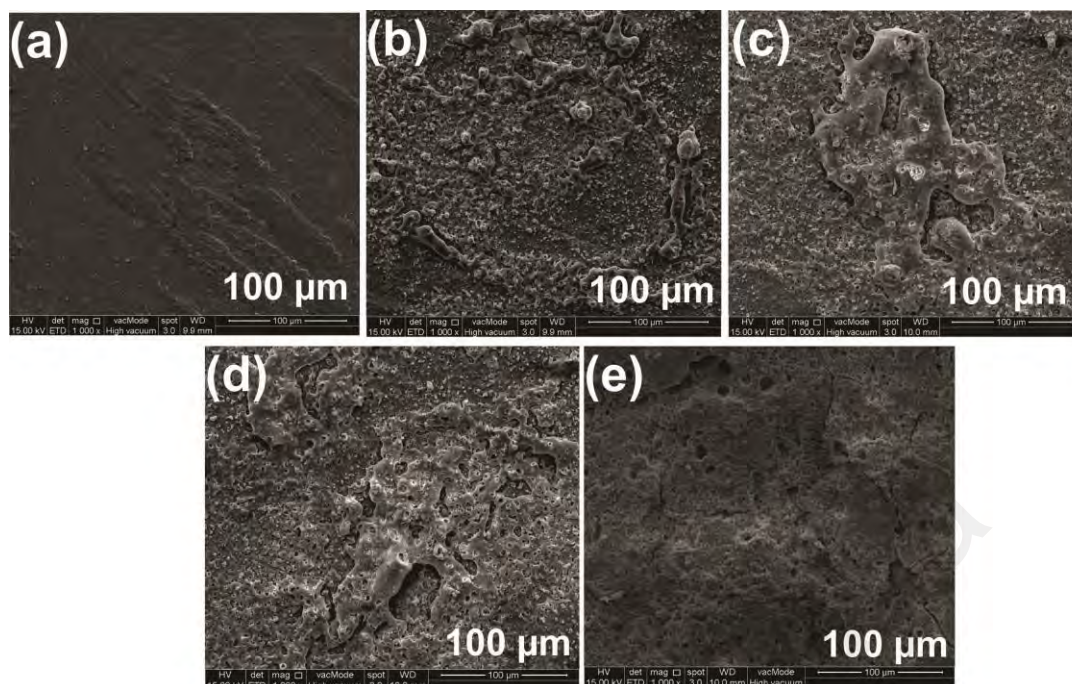


Figure 5.2: Surface SEM morphologies of PEO coatings formed at different voltages (a) 225 V, (b) 250 V, (c) 275 V, (d) 300 V, and (e) 325 V

During PEO process, the local temperature in the discharge channel can be as high as several thousand degree Celsius (Yerokhin et al., 2004), and quenching effect provided by the cold electrolyte ($\leq 35\text{ }^{\circ}\text{C}$) is appreciable. Generally, the temperature within the discharge channels at higher voltages/current density are greater than those at lower voltages/current density (Hussein et al., 2010), which results in mild crack length in the coating formed at high voltage (Figure 5.2e).

5.2.4 Surface chemistry and phase composition

Typical EDS analysis of the PEO-BHA coatings obtained at different applied voltages reveals that, the coatings are mainly composed of the elements Mg, Ca, P, Al, O, Ti and Na, irrespective of the applied voltages. Therefore, the PEO-BHA coating processed with highest voltage is shown in Figure 5.3 with the relative atomic concentrations been summarized in Table 5.2.

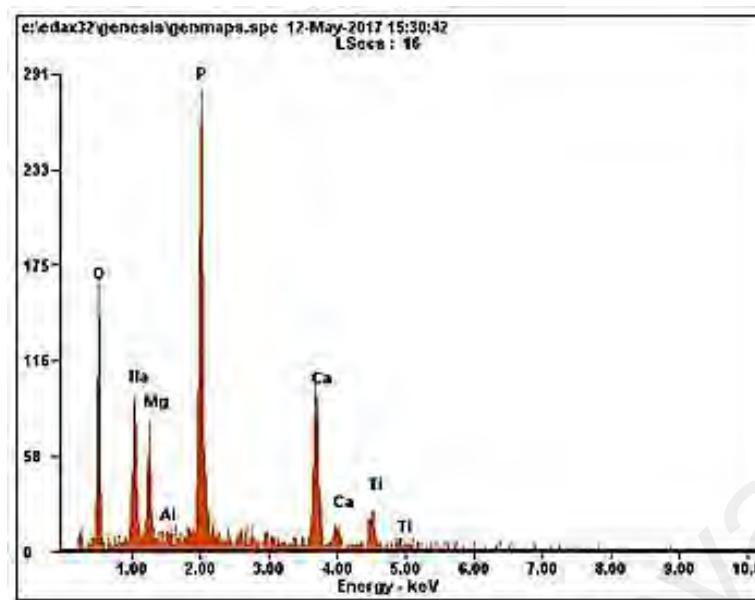


Figure 5.3: Representative EDS of PEO-BHA coating produced at 325 V

Table 5.2: Elemental chemical composition of the PEO-BHA coatings produced at varying voltages (at. %)

Voltage (V)	Ca	P	Mg	O	Ti	Al	Na	Ca/P
225	14.41	21.48	03.99	40.50	16.64	00.89	02.09	0.67
250	13.99	16.77	04.98	48.28	08.65	03.11	04.22	0.83
275	18.05	20.50	04.91	43.83	06.77	03.06	02.88	0.88
300	15.32	17.00	05.58	47.92	07.89	00.63	05.66	0.90
325	16.05	17.60	05.52	46.64	05.57	00.37	08.25	0.91

The Mg element in the coating originates from the electrolyte which shows that the bovine bone particles take part in the coating. Magnesium is a mineral supplement and vitally important for healthy muscles and bones (Farzadi et al., 2014; Shadanbaz & Dias, 2012). Considering that Mg can facilitate bone growth and enhance the mechanical properties of the coating, the identification of Mg in the coating is encouraging. Compared with the results of the commercial HA PEO coating presented in Chapter 4, it is obvious that the presence of Mg in the coating is due to the application of natural bovine bone particles. Based on the atomic concentration results

from the Table 5.2, it is found that Ca/P ratio was increased with the increasing of the applied voltages.

The spatial distribution of the elements present in the coating is shown in the elemental mapping images in Figure 5.4. From the figure 5.4, it can be seen that the Mg, Ca and P, are conspicuously present over the surface of the PEO coating.

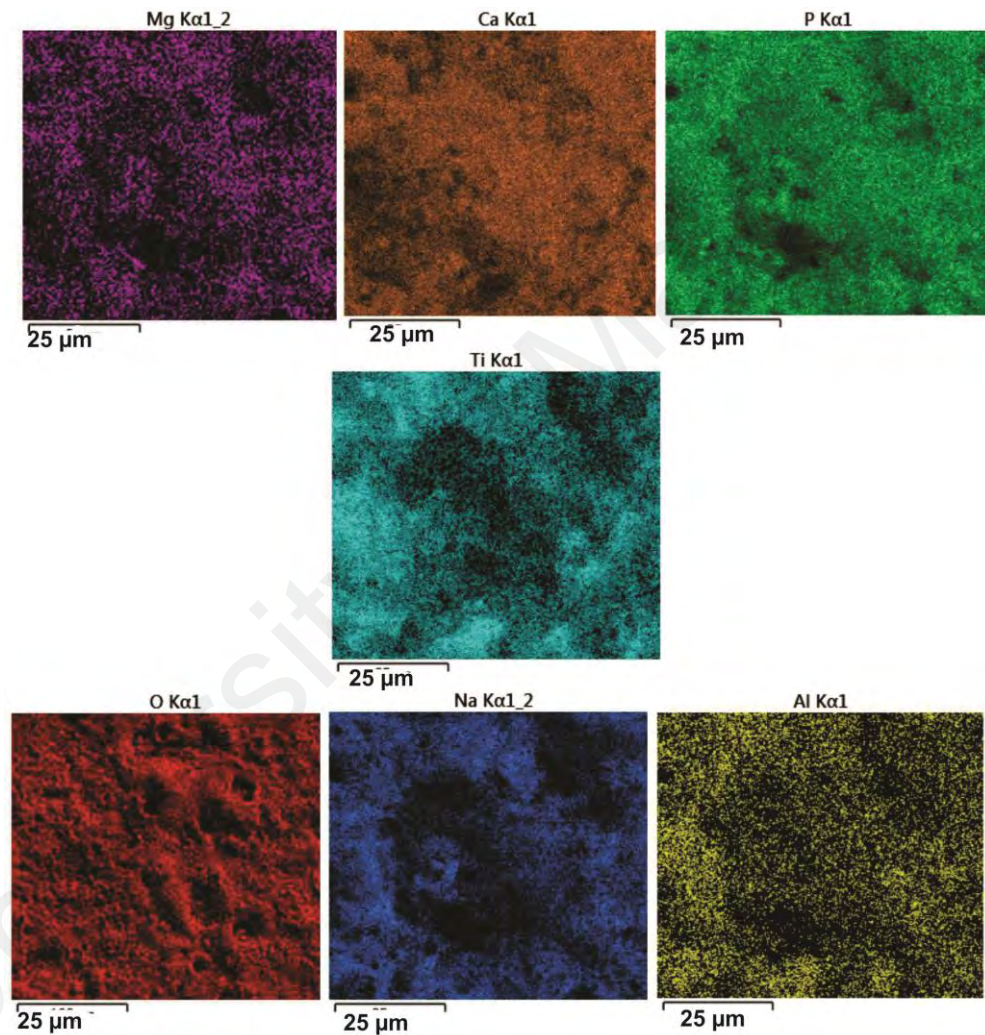


Figure 5.4: Elemental mappings of PEO-BHA coatings produced at 325 V

To facilitate better understanding of how the elements detected by EDS analysis are combined in the coatings, XRD patterns of the PEO-BHA coatings formed at different applied voltages are shown in Figure 5.5. It can be seen that the phases are mainly

composed of hexagonal HA, anatase and MgO. The Ti phase is from the Ti6Al4V substrate.

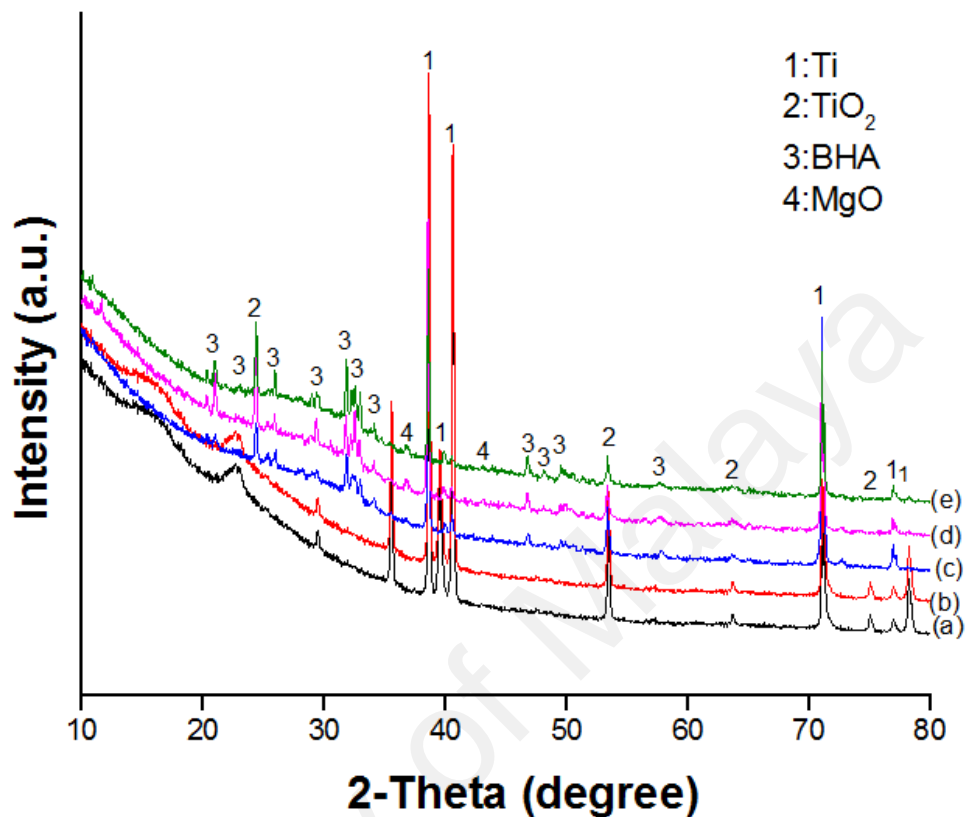


Figure 5.5: XRD patterns of the PEO coatings produced at varying voltages: (a) 225 V, (b) 250 V, (c) 275 V, (d) 300 V, and (e) 325 V

The peaks of the BHA are more intense than those of the anatase, suggesting a greater presence of BHA in the coating. The relatively weak and broad peaks 2θ ranging from 31.7° to 34.4° on the PEO-BHA pattern indicates the presence of a single hexagonal crystalline BHA in the coating. The Bragg peaks at 37° and 43.1° observed for the cubic MgO are due to the thermochemical reaction of Mg element from bovine bone particles and hydroxyl ion (OH^-). At a low voltage ($\leq 275 V$), MgO diffraction peak is weak. Above this voltage, MgO peaks were identified by XRD in each applied voltages, suggesting that cubic MgO phase can be obtained through regulation of voltage electrolyte.

Due to the consistent surface chemical composition of the coatings (Table 5.2), only the surface that produced the highest amount of BHA phase was further evaluated by XPS technique. The XPS spectrum is depicted in Figure 5.6 confirming the existence of the Ca, P, Mg, Ti, O, Na, and C elements. It should be noted that the concentration of carbon in the surface is generally happening in the XPS survey because of the washing of the sample with acetone and chemisorption of CO₂ molecules from the environment.

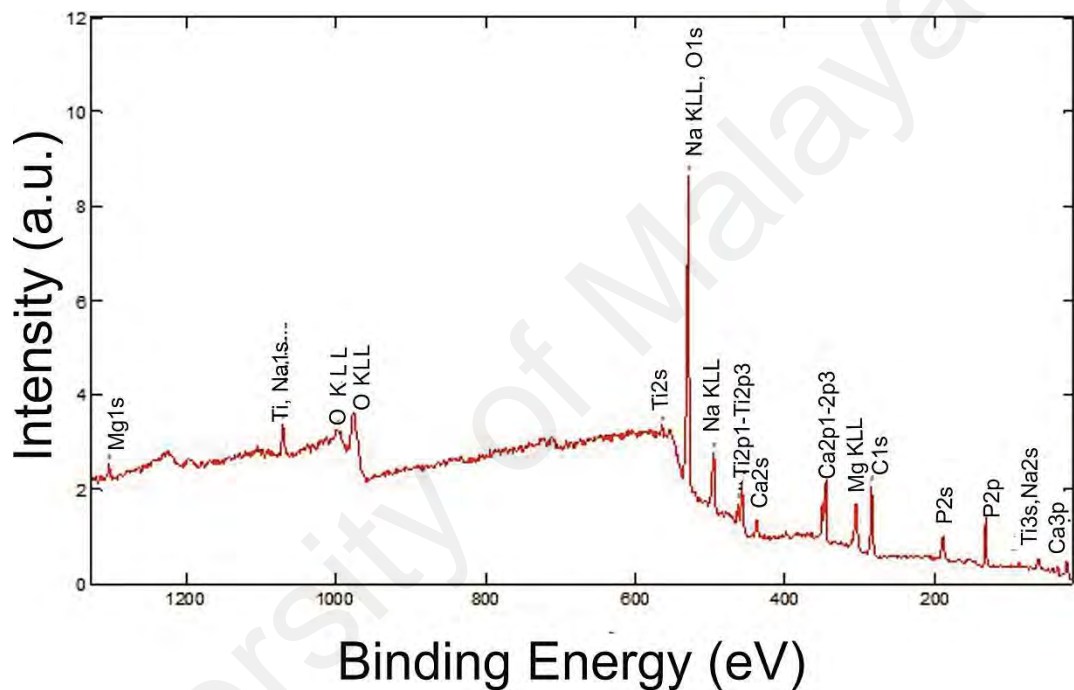


Figure 5.6: XPS survey spectrum of PEO-BHA coating produced at 325 V

The core binding energy of the elemental compositions of the coating is depicted in Figure 5.7. It can be seen that the high resolution of O (1s) could be deconvoluted to 4 distinct peaks. The peak A located at the binding energy 529.8 eV, is assigned to oxygen in the TiO₂ lattice. The peak B at the binding energy of 530.9 eV, reveals the existence of oxygen in the hydroxyl group in the HA_p molecules. The peaks C and D, found at the binding energies of 530.5 and 532.1 eV, correspond to the oxygen in the oxide lattice of MgO and existence of O⁻.

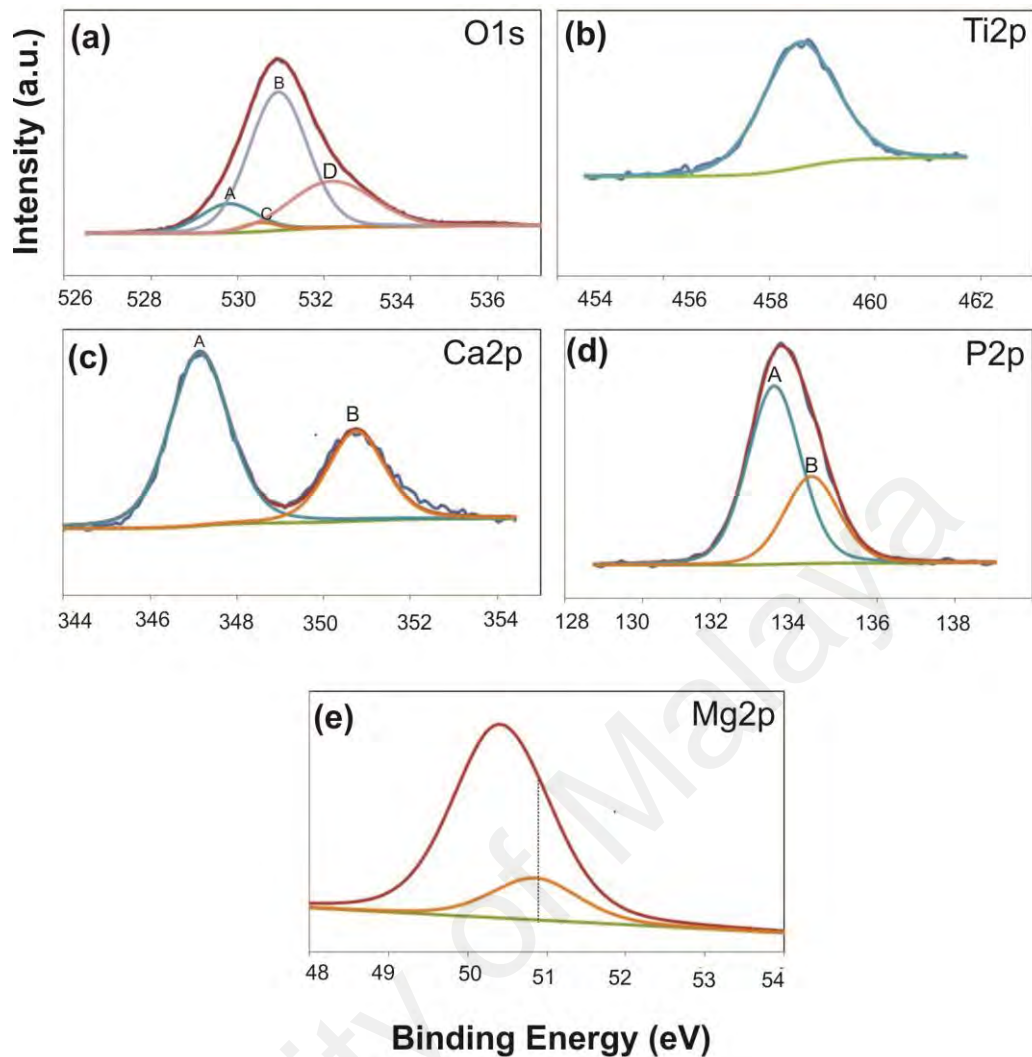


Figure 5.7: XPS binding energies of the PEO coating produced at 325 V: (a) O (1s), (b) Ti (2p_{3/2}), (c) Ca (2p), (d) P (2p), and (e) Mg (2p)

Figure 5.7b shows the Ti (2 p_{3/2}) core level binding energy at 458.6 eV. From the shape of the Ti peak, it can be deduced that titanium exists in the form of ions (Ti⁴⁺). During PEO process, the application of the high voltage would lead to the formation of the oxides with higher states (Golestani-Fard et al., 2011). The high resolution spectrums of Ca (2p) core level binding energies are depicted in Figure 5.7c. The peak for Ca splits into A and B. The doublets of Ca (2p) component could be attributed to the spin-orbit splitting due to the oxidation state of Ca ions in the inorganic calcium-oxygen compounds. The peaks A and B, with core binding energies of 347.1 and 350.8 eV, are attributed to Ca (2p_{3/2}) and Ca (2p_{1/2}), respectively. The results are consistent with the

Ca in the HA_p structure. As shown in Figure 5.7d, the high resolution spectrum for P (2p) could be divided into two peaks A and B, 133.4 and 134.3 eV, which correspond to the 2p_{3/2} and 2p_{1/2} core levels, respectively. These peaks confirm the existence of phosphorus in the HA_p structure. The negligible difference in the core binding energies of Ca (2p) and P (2p) revealed the formation of HA_p on the PEO surface layer. The high resolution of Mg2p only displayed one peak at binding energy level 50.8 eV, suggesting that the Mg-related phase existed in the coating and found to be in the form of MgO. Thus, the XPS results indicated that the PEO-coatings produced in a solution containing natural bovine bone HA particles consisted of TiO₂, MgO and HA compound layers.

5.2.5 Coating thickness of PEO-BHA films

The cross-sectional SEM micrographs of the PEO-BHA coatings presented in Figure 5.8 give more insight into the morphological features across the coating thickness as well as its metallurgical bonding to the substrate material. The values of the thick layer obtained are reported in Table 5.3. No distinct separation was observed between the substrate and the coating layers, indicating a good metallurgical bonding between the coating and the substrate. Even though some mild defects were noticed in the layers, the major part of the coating was relatively dense. The PEO-BHA coatings are porous and rough, which is consistent with corresponding surface morphologies in Figure 5.2. The PEO coating layers are porous due to the effervescence of gases and micro discharges during PEO process.

The cross-sectional coating thickness of the coatings enhances with increasing voltage as seen in Figure 5.8a-e. At 225 V, a relatively compact and uniform layer with $6.8 \pm 0.6 \mu\text{m}$ thickness is obtained. With increasing in applied voltage, a much thicker layer was obtained due to the surge in the PEO energy. The thickness obtained at 300 and 325 V, showed an undulating coating layer, suggesting that coating formation are localized inward rather than uniform oxide growth across the entire surface.

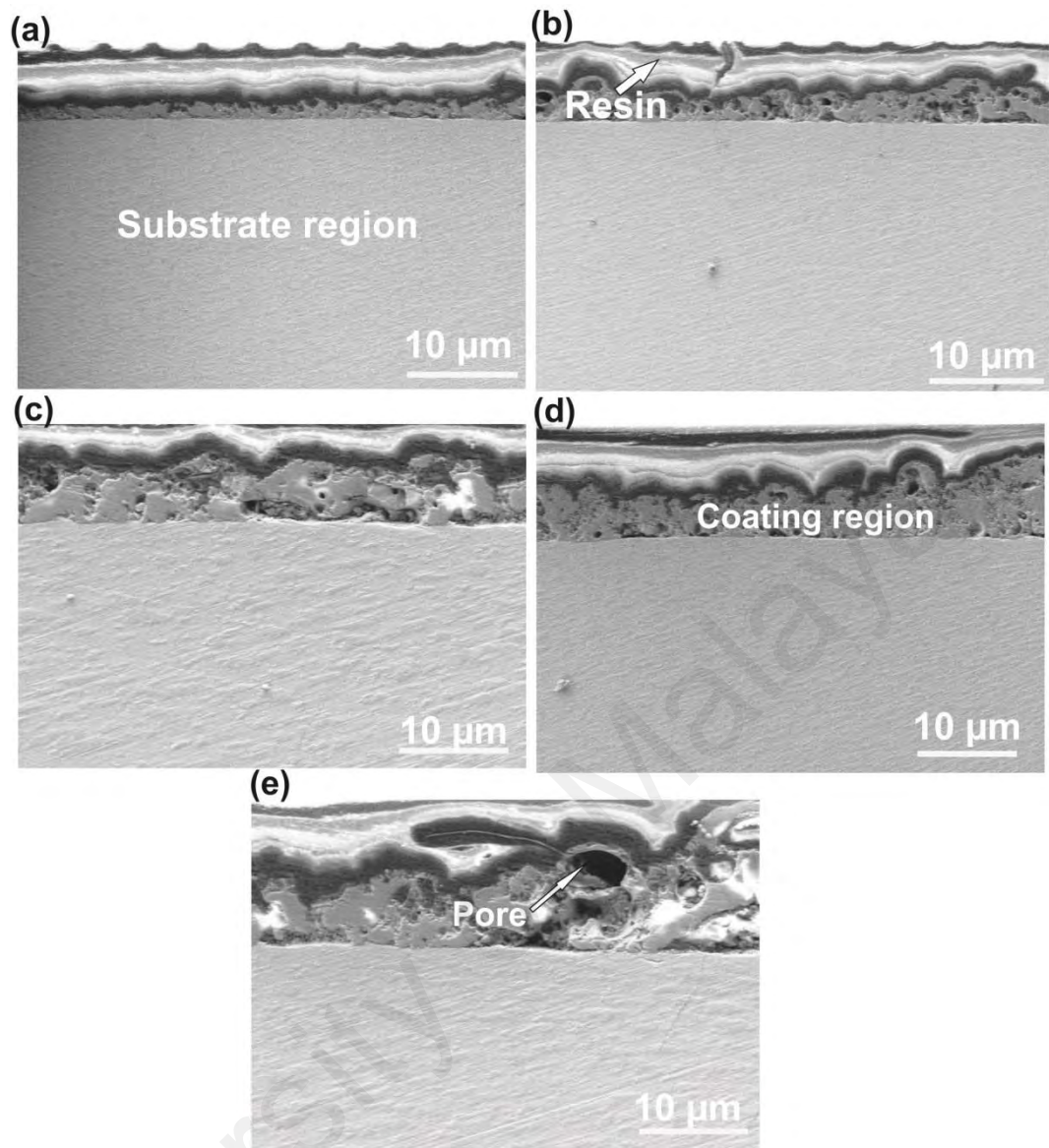


Figure 5.8: Cross-sectional SEM morphologies of PEO-BHA coatings produced at different voltages: (a) 225 V, (b) 250 V, (c) 275 V, (d) 300 V, and (e) 325 V

A larger pore could be observed in the cross-section of PEO-BHA coating processed at 325 V due to extensive exothermic energy during the PEO process.

Table 5.3: Average thickness of PEO-BHA coatings produced at varying voltages

Coating voltage (V)	Average thickness (μm)
225	6.8 ± 0.6
250	9.4 ± 1.2
275	15.9 ± 1.4
300	20.3 ± 2.1
325	26.9 ± 3.4

The coatings that have a compact layer display greater mechanical properties than the one with a loose interface layer (Durdu & Usta, 2014; Polat et al., 2010). Thus, the compact and thicker film layers can have greater coating quality in terms of mechanical and wear properties.

5.2.6 Mechanical properties of PEO film

5.2.6.1 Surface roughness of PEO-BHA film

The surface roughness of the PEO-BHA coatings is shown in Figure 5.9. It can be seen that the surface of PEO coatings formed at the lowest voltage is much smoother compared to the one processed at higher voltages. From figure 5.9, it is obvious that the PEO coating, which was about $6.8 \mu m$ thick, has a much smoother surface ($R_a = 0.82 \pm 0.04 \mu m$) compared to the coatings produced at higher voltages. The coating roughness is strongly related to the applied voltage. The coating roughness increases with increasing voltage, which is in agreement with the earlier study conducted by Sowa et al. (2015) and Li et al. (2004).

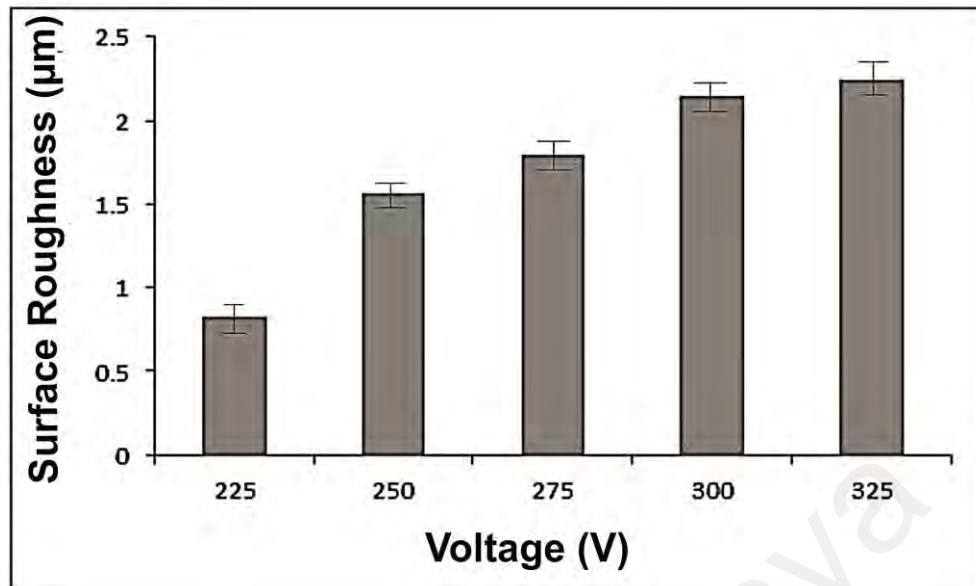


Figure 5.9: Dependence of coating roughness on the applied voltages

The PEO-BHA coatings processed with higher voltage produce a rougher coating surface because the increase in voltage produces higher intense discharges. The highest roughness (2.14 ± 0.06) is observed in the coating formed at 325 V. The greater surface roughness is due to the chemical reaction of Ti6Al4V and electrolyte borne ingredients, and the subsequent formation of the complex layer on the substrate surface.

5.2.6.2 Adhesion strength of the PEO-BHA coating

The adhesion strength of the PEO-BHA coatings formed on Ti6Al4V alloy at different applied voltages was measured by the micro scratch tester. Figure 5.10 shows the adhesion strength of the PEO-BHA coatings. The adhesion strength of the coatings appears to be significantly influenced by the applied voltages. The overall adhesion strength increased with the increasing of the voltages. The adhesion values obtained was in the range of 813 ± 10.2 to 2010 ± 16.5 mN. The increase in adhesion strength is due to the formation of a dense coating structure. The coating thickness increased with the applied voltages due to a larger amount of ions incorporation into micro-discharge channels during the PEO process (Figure 5.8).

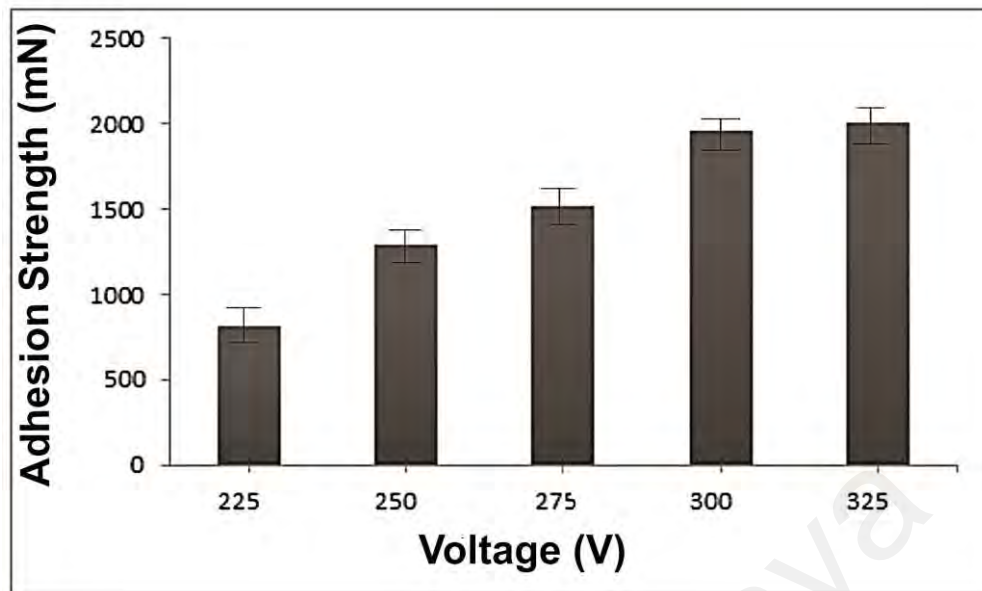


Figure 5.10: Adhesion strength of PEO-BHA coatings formed at different applied voltages

This is one of the prominent factors to increase the adhesion strength of the PEO coatings. For coating produced at the lowest voltage (225 V), the maximum adhesion value is 813 mN, and it increased to 2010 mN when the PEO-voltage increased to 325 V. The lowest adhesion strength in the case of the PEO treated with 225 V is due to the incomplete incorporation/melting of the BHA powders as a result of insufficient energy. The adhesion value of the coating obtained at 325 V is slightly higher than the coating obtained at 300 V. This indicates that there is a good metallurgical bonding of the coating produced at 325 V, although the coating formed at 325 V is more porous and contained mild cracks than the one produced at 300 V (Figure 5.2). This could be explained by the higher compact layer and the existence of periclase-MgO (Figure 5.5) in the coating structure because the MgO increased the bonding strength between the substrate and the hydroxyapatite coating structure (Pan et al., 2013; Pan et al., 2012). It can be concluded that the adhesion of the coatings depends on the morphology and the phase composition of the coatings.

5.2.6.3 Wear resistance of the PEO-BHA coatings

Figure 5.11 shows the coefficient of friction (COF) against the cumulative time for the untreated Ti6Al4V and the PEO coatings. The values of COF obtained are summarized in Table 5.4. It can be seen that the PEO coatings processed at varying voltage show a lower COF compared to the untreated Ti6Al4V alloy. The coatings produced at different applied voltages display common feature in the frictional behaviour as the applied voltage increases (Figure 5.11b).

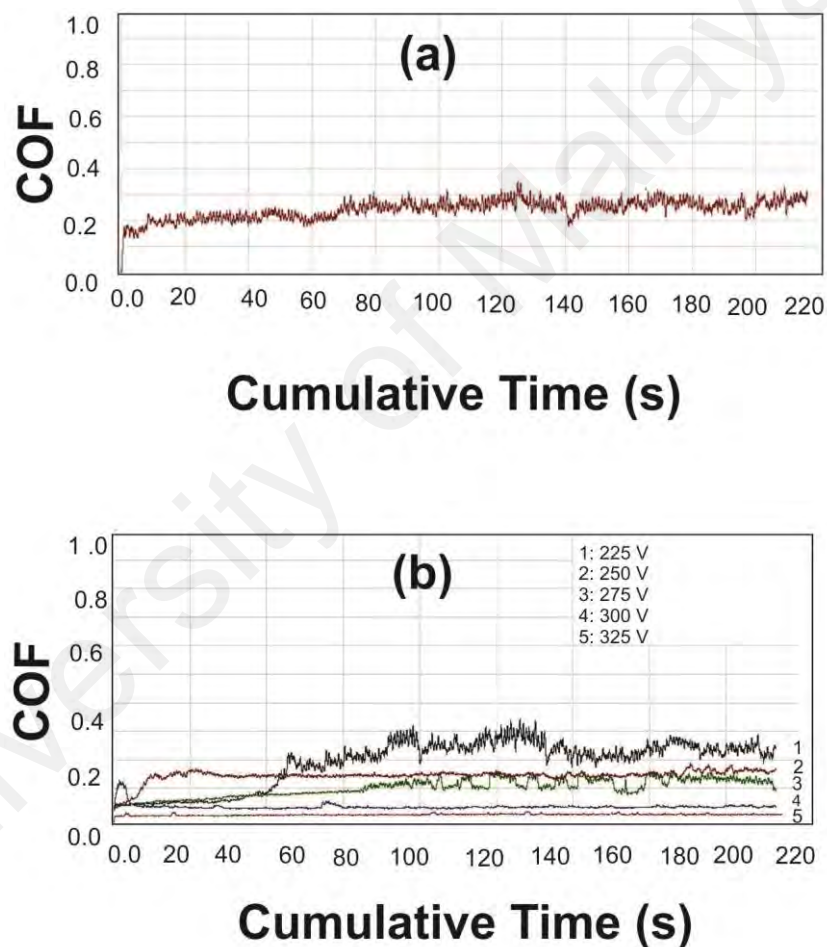


Figure 5.11: COF of the untreated (a) Ti6Al4V and (b) coatings at varying voltages

This is due to the continuous wear of surface asperities. Wear normally occurs due to brittle micro-fracture in the surface grains and tribo-chemical reaction (Stachowiak,

2006). The COF of PEO-BHA coatings were between 0.129 and 0.223, while the COF of Ti6Al4V was 0.256. Generally, the COF decreases with the coating voltage as indicated in Table 5.4. This could be attributed to incremental growth of thin layer during the PEO process and the existence of higher amount of phase structure. However, when the voltage is increased from 300 to 325 V, no much significance difference is seen in the COF obtained (Table 5.4). The COF of the coatings produced at 325 V is almost the same with the one produced at 300 V because the coating produced at 325 V is characterized with micro-cracks and pores as seen in Figure 5.2e. As mentioned earlier, the PEO coating processed at 325 V is very rough and has fewer numbers of cracks due to the high intensity of micro-arc discharges during the PEO process.

Table 5.4: COF test results obtained under dry conditions for untreated Ti6Al4V and PEO coatings at different applied voltages

Voltage (V)	COF
Substrate	0.256
225	0.223
250	0.206
275	0.199
300	0.134
325	0.129

Previous studies investigated that micro-pores were formed due to molten oxide and gas evolution from the micro-arc discharge channels (Duan et al., 2006; Guo et al., 2005; Kazek-Kęsik et al., 2014). The micro-pores, micro cracks or dimples, which normally accompanied the PEO process, can affect the performance of sliding surfaces (Erdemir, 2005). It can be concluded that the dominant parameters for the COF of the coatings are morphology, phase structure and thickness of the coatings. Generally, the surface features of the system can be changed during wear due to the removal or displacement of the material. These characteristics will often change during the lifespan

of the material system. The interpretations of the different wear mechanisms are multifaceted as explained in Chapter 2 because it involves various combinations of chemical and mechanical processes (Stachowiak, 2006). In the present work, SEM imaging was employed to assess the worn surfaces of the untreated titanium alloy and the PEO coatings. Figure 5.12 shows the wear track SEM images of the untreated Ti6Al4V alloy and the PEO coatings produced at varying applied voltages.

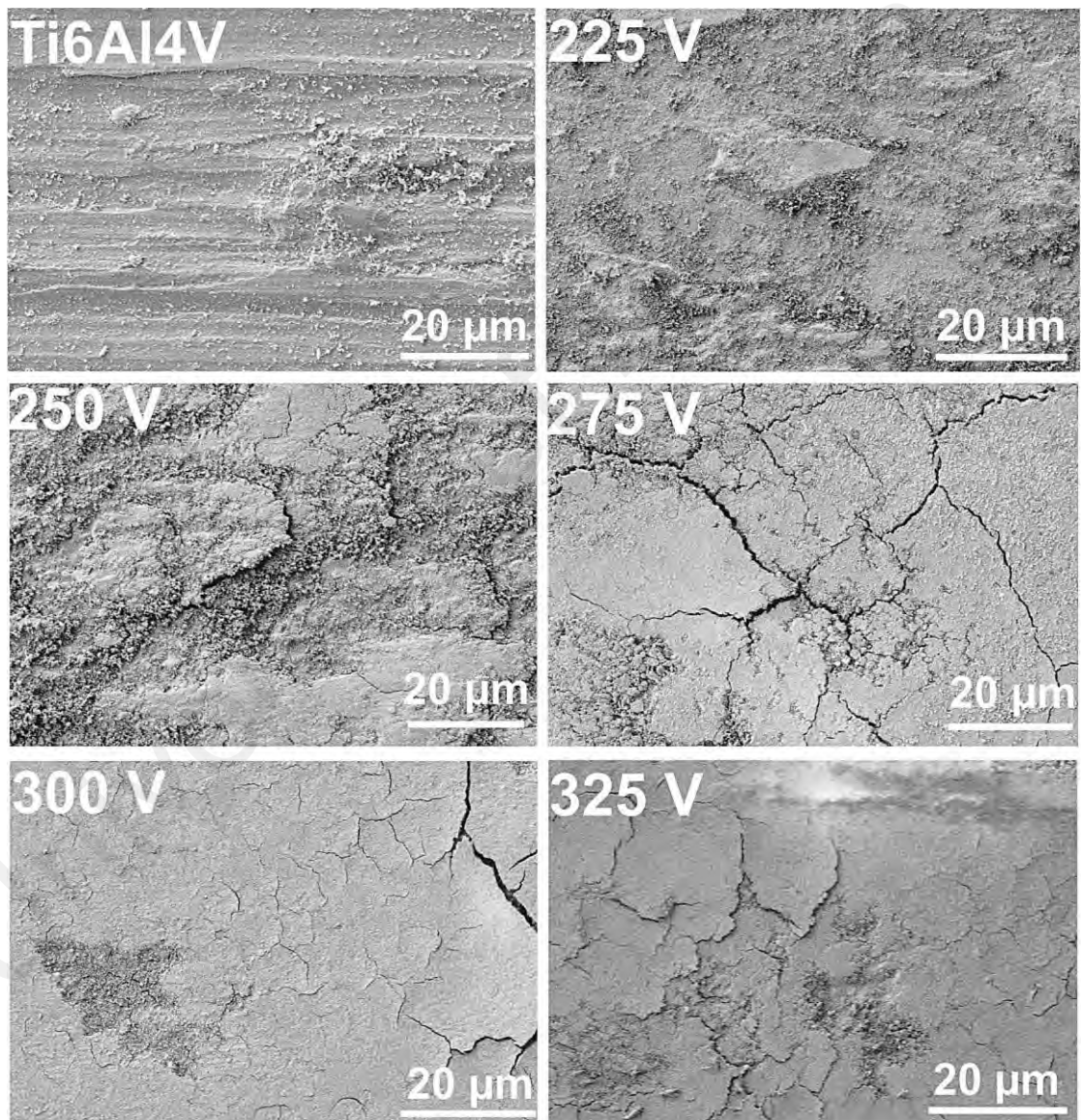


Figure 5.12: Wear tracks of untreated Ti6Al4V alloy and the PEO-BHA coatings

By observing the width and depths of the wear surfaces, it can be seen that the wear track of the untreated Ti6Al4V is wider and deeper than the PEO-BHA coatings as seen in Figure 5.12. The appearance of reefs and galling caused by the severe plastic deformation is the main characteristic feature of the worn surface of the untreated alloy. This is because the counterpart steel ball is harder than the untreated alloy. This result is consistent with previous studies, where the wear occurred by deformation and through which the material was detached as a result of the higher hardness of the counterpart material against the untreated substrate material (Ezazi et al., 2014; Sakiru & Shahjahan, 2015; Yetim, 2010). With regards to the untreated Ti6Al4V alloy, there are many plastic deformations on the worn track. Therefore, the wear mechanism of untreated alloy is dominantly adhesive wear. The SEM worn images of the surface covered with BHA layers were also gathered. The PEO-BHA coated film exhibited a compact structure. The presence of composite layers (TiO₂-MgO-BHA) as the main component of coating gives a valid reason for the lesser wear surface as compared to the bare alloy (Figure 5.10 b-e). Several fine crumb or particles and patches are seen on the PEO-BHA coated surfaces. The fine crumb and patches were removed from the surface during the wear test. It is believed that these fine crumbs and patches were removed from the outer surface of PEO during the wear test and acted as a lubricant between the dense layer and counterpart steel ball, leading to less wear of the coatings. In the coating produced at low voltages, the wear was much more pronounced than the coating produced at high voltage, because the PEO coating at high voltage is denser than the one produced at low voltage (Figure 5.2). The crumb particles occur on the surface after the wear test because the coating produced at high voltage is very porous and rough. The average surface roughness of PEO coatings R_a is approximately, 0.16, 0.75, 1.51, 1.53, 1.92, and 2.14 μm for the untreated Ti6Al4V, 225, 250, 275, 300, and 325 V, respectively. Additionally, after the wear test, the dense coating structure appears

beneath the outer layer because the outward layer of the PEO coating with high adhesion strength is very porous and rough. Therefore, it can be concluded that the wear mechanism of the PEO-BHA coatings is an abrasive type due to the presence of patches and crumb particles during the wear test.

5.3 Summary

The morphological features of PEO coatings processed in a solution containing bovine bone hydroxyapatite particles have been investigated. In summary, the following can be drawn from this investigation:

- The surface of the coatings obtained at varying applied voltages was filled with compound particles during the PEO process. The structure and the compound particles were mainly composed Mg, P, Ca, O, Ti, Al and Na while cubic MgO was detected in the coatings. Elemental mapping analyses revealed that the elemental constituent are sparsely distributed throughout the coating.
- All the coatings produced with different applied voltages exhibited relatively compact and uniform structures.
- XRD and XPS analyses indicated that the PEO coatings were composed of cubic MgO, anatase and hexagonal crystalline HA, varying in relative proportion throughout the coating.
- The coating thickness, surface roughness and adhesion strength increased with increasing of the applied voltages.
- The PEO-BHA coatings significantly improved the wear performance of titanium alloy. The COF of the coatings reduced with increasing voltage, although the COF of the coating formed at 325 V is almost the same with the

one produced at 300 V. This could be due to the fact that the coating formed at 325 V is much porous and looser than the one produced at 300 V.

The PEO treatment processed in a solution containing bovine derived HA particles provide an additional MgO phase on the titanium-based material. The corrosion and bioactivity of the titanium implant may be enhanced with this additional phase. This, however, would be verified in subsequent Chapter 6.

University of Malaya

CHAPTER 6: INVESTIGATION OF PEO COATING PERFORMANCE IN A SOLUTION CONTAINING CHA AND BHA PARTICLES

6.1 Introduction

The significance of electrolyte composition in the PEO process and its effect on the final coating properties has been pointed out in Chapter 2. It is widely acknowledged that electrolyte composition significantly affects the PEO process and coating properties. However, the comparison between the electrolyte composition of the conventional HA and bovine derived HA on the PEO coatings has not been investigated. Therefore, in the present study, two different electrolyte solutions were prepared, in which the PEO coating is produced under the same processing condition in order to give an insight into their performance. The final coating morphology was characterized using the experimental procedures described in Chapter 3. Specifically, the Chapter focuses on the microstructure-property relationship. The in vitro corrosion and bioactive properties were also investigated.

6.2 Influence of electrolyte CHA and BHA composition on PEO coatings

6.2.1 Coating fabrication

For the coating formulation, two different electrolytes were utilized. Firstly, PEO electrolyte composed of 0.12 M NAP solution and 1.5 g/L commercial HA, termed as the CHA was prepared. The second aqueous electrolyte was prepared by replacing CHA with bovine derived HA particles, this was termed as BHA. Details of the electrolyte concentration, voltage/current density and deposition time are presented in Table 6.1.

Table 6.1: PEO parameters for CHA and BHA deposition

PEO parameters	Quantity
BHA concentration (g/L)	1.5
CHA concentration (g/L)	1.5
NAP concentration (M)	0.12
Current density (mAcm^{-2})	250
Deposition time (mins.)	5
Voltage (V)	300

6.2.2 PEO voltage-time process characterization

Figure 6.1 shows the rate of voltage for CHA and BHA coating in 0.12 M NAP electrolyte solution during the PEO process. For the two coatings, the trend of the voltage-time plot was the same. Similar to the results recorded in Chapter 4 and 5 when the voltage-time response experienced a steady increase at the start of DC process at a current density of 500 mAcm^{-2} . During the first 52 s, the voltage increases proportionally with the treatment time. In this stage of PEO process, a thin barrier layer is developed on the sample surface due to dissolution-ionization of Ti6Al4V substrate. The formation of thin barrier layer shows that the potential difference of the oxide film layer increases linearly as the oxide thickness grows.

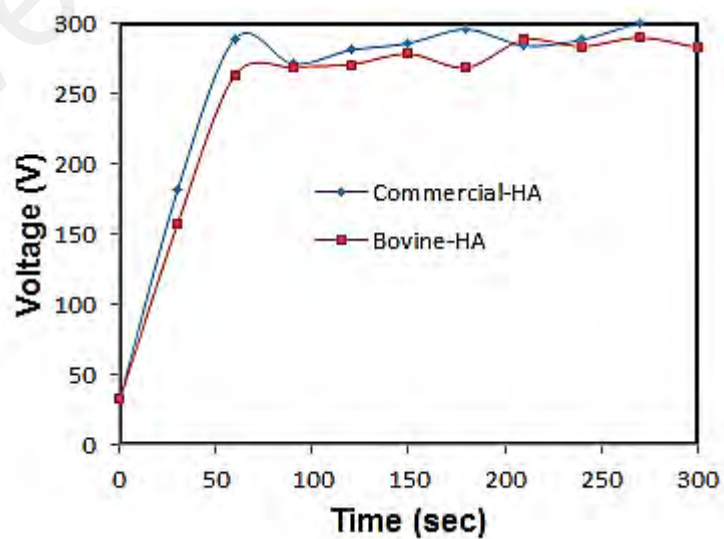


Figure 6.1: Voltage-time response of the PEO coatings: (a) CHA and (b) BHA

There is no visible micro-sparks, only effervescence/bubbling of oxygen gas can be noticed on the sample surface. As the voltage exceeds the critical voltage (breakdown voltage, 263 V), plentiful of micro-sparks were observed on the sample surface which marks the termination of a uniform film thickening. The rate of voltage increase drops, bright sparks become more intense and distributed randomly over the entire surface. After initial breakdown voltage, fluctuation of cell voltage ensues which depicts the stages of oxide breakdown and rebirth of new oxide film. The process of breakdown can be attributed to high electric field generated within the coating film layer (Duarte et al., 2014; Ikonopisov et al., 1979).

Comparing the voltage-time curves, it is found that the final voltage reached for BHA coating (~283 V) is less compared to CHA coating (~300 V). The difference in the maximum voltage attained may be attributed to electrolyte composition and the avalanche of electron injections at the electrolyte/anodic interface. While the breakdown voltage is basically governed by the electric field/compressive forces generated within the coating film, the subsequent behaviour of the cell voltage is influenced by the combined effect of the resistive force of the electrolyte solution/surface interface and electrolyte composition/concentration.

6.2.3 Coating morphologies of PEO-CHA-BHA coated layers

The morphological appearance of the PEO coatings produced with different electrolytes is presented in Figure 6.2. The film surface shows a distinct variation in morphological features. It can be seen from Figure 6.2a, that CHA-PEO coated surface reveals a tiny micro-pore. The spherical tiny pores were seen to be well distributed over the entire film surface. Comparing the morphology of the PEO coatings, the BHA-PEO coating (Figure 6.2b) was relatively rougher and exhibited a flake and droplet-like morphology with tiny and irregular circular pores of different diameters (1 – 5 μm) in

size. The surface of the BHA-PEO coating appears to be uneven compared to CHA-PEO film. No crack was detected on the two different surfaces. The presence of the pores on the PEO coating surface has been ascribed to micro-arc discharges event during the PEO treatment. The higher discharge intensity normally produces larger pore diameter. Since the electrolyte concentration and the electrical parameters remain the same in the present study, it is likely that the electrolyte ingredient particles of BHA promotes anodic breakdown, which eventually led to generation of larger pore diameter within the PEO coating. According to Sah et al. (2012), intense anodic breakdown would result in several pore diameters during the PEO formation.

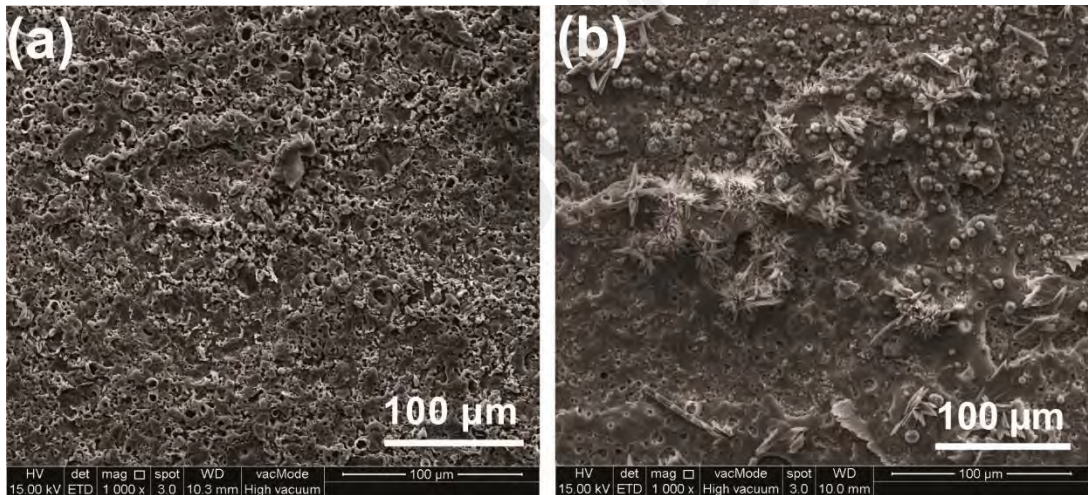


Figure 6.2: SEM images of PEO coatings fabricated with different electrolytes:

(a) CHA and (b) BHA

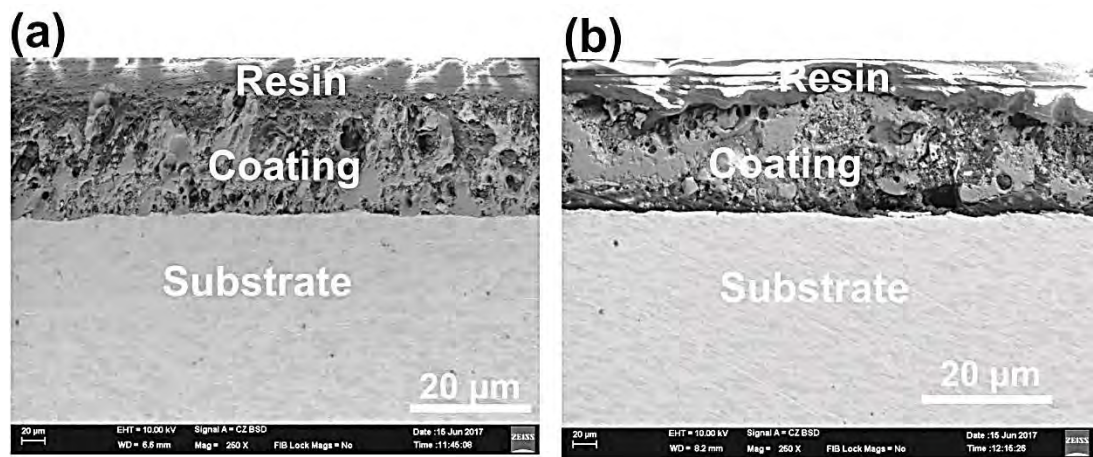


Figure 6.3: Cross-sectional morphologies of the PEO coatings produced at different electrolyte (a) CHA and (b) BHA

Cross-sectional morphologies of the coatings produced in the present study are shown in Figure 6.3. Cross-sectional examinations revealed that the thickness of the film layers was about $26 \pm 1.3 \mu\text{m}$ for both CHA and BHA-PEO coatings. The coating thickness layer reveals voids and micro-flaws which are typical features of the PEO coating process. There is no separation between the deposited film and the underlying Ti6Al4V substrate, indicating that the coating is firmly adhered to the substrate.

6.2.4 Elemental and phase composition of the coatings

The elemental compositions of the two coatings can be obtained from the EDS spectra shown in Figure 6.4. The peaks show the relative proportion of elements on the coating surfaces. It is obvious that Ca, P, O, and Ti are the major elements in the coatings. Taking account of the accuracy of the EDS technique, there was no significant difference in the intensity of chemical elements in the coatings. The presence of Mg in the coating (Figure 6.4b) was consistent with the previous results published by Ma et al. (2017) and was in good agreement with the result presented in Chapter 5.

The results of EDS analysis of the hydroxyapatite coatings are presented in Table 6.2. Since the presence of Ca and P will facilitate the proper connection between an implant material and cell tissues, this was given the prime attention to in the CHA and BHA coatings. The EDS analysis results reveal that the PEO coating had a Ca/P ratio of ~ 0.70 .

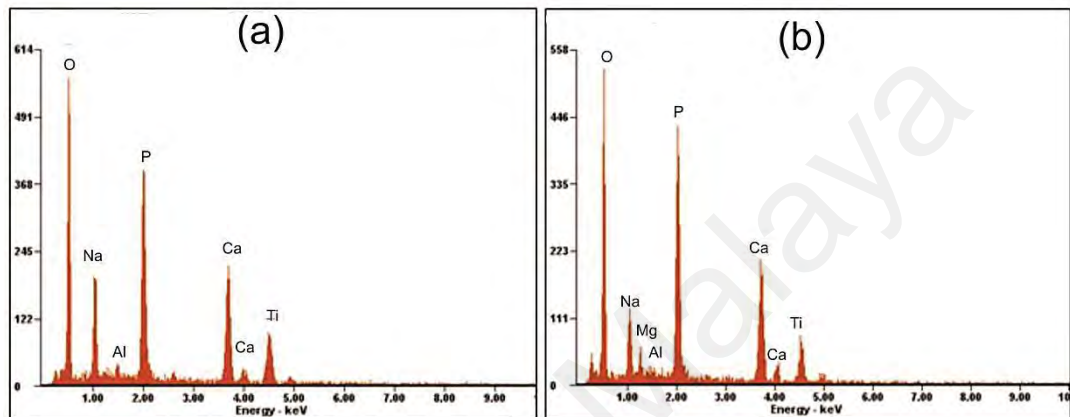


Figure 6.4: EDS spectra of PEO coatings produced under different hydroxyapatites: (a) CHA and (b) BHA

Table 6.2: Elemental chemical composition of the PEO coatings with two different hydroxyapatite (at.%)

Samples	Mg	Ca	P	O	Ti	Al	Na
CHA	-	07.33	11.00	65.30	04.60	00.58	11.20
BHA	03.82	08.31	12.76	67.17	03.84	00.35	03.75

XRD patterns of the PEO-coated titanium with CHA and BHA layers are shown in Figure 6.5. The XRD patterns of the coatings show that they contain a higher degree of hexagonal HA phase structure ($2\theta = 31.7^\circ$). The spectra revealed an additional phase, perovskite tetragonal CaTiO_3 (space group: $I4 m c m$; $t\text{-CaTiO}_3$; $2\theta = 22.9^\circ, 29.3^\circ$) in the PEO-coating modified with commercial-HA which is absent in the BHA coating. The formation of $t\text{-CaTiO}_3$ is likely to be caused by partial melting of commercial-HA.

The lower current density (250 mAcm^{-2}) promotes only the ejection of Ca from $\text{Ca}_{10}(\text{PO}_4)_6(\text{OH})_2$ during the PEO process. Unlike the decomposition of HA phase to TCP that was noticed at a current density of 500 mAcm^{-2} (Chapter 4), the lower current density only resulted in partial melting of HA. Similar phase structure was also identified in the coating produced by Cimenoglu et al. (2011), while investigating the biological performance of the two competitive alloys.

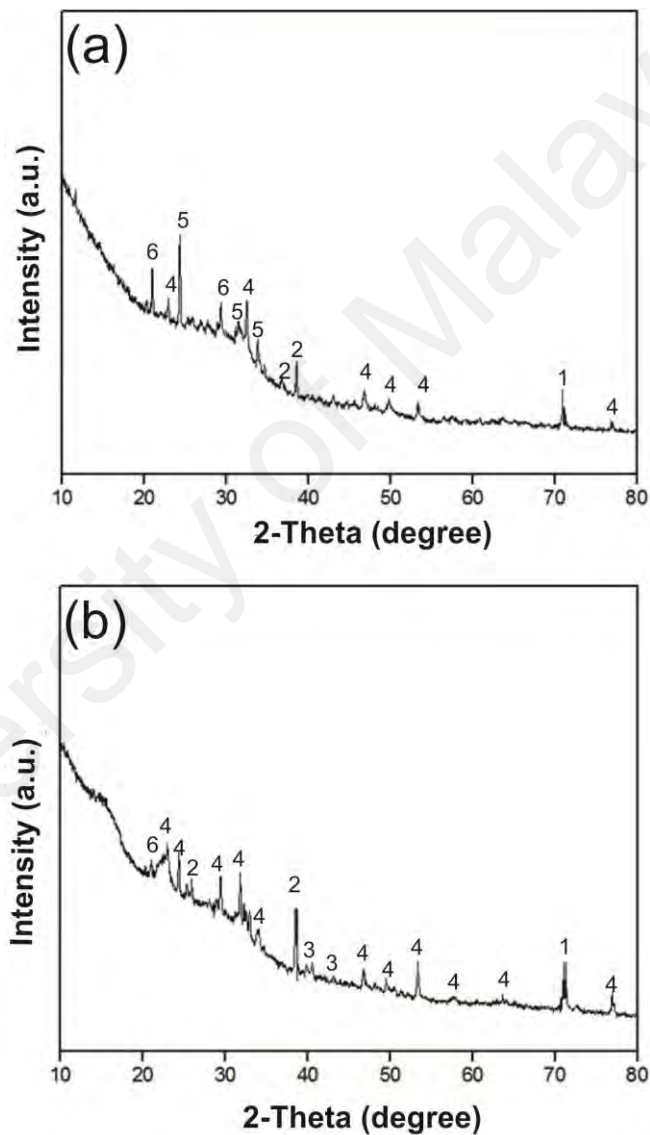


Figure 6.5: XRD patterns of PEO coatings: (a) CHA and (b) BHA (1: Titanium-Ti6Al4V, 2: Anatase-TiO₂, 3: Magnesium oxide-MgO, 4: Hydroxyapatite-HA, 5: Calcium titanate-CaTiO₃, and 6: Sodium titanium phosphate-NaTi₂(PO₄)₃)

The reaction of Ca^{2+} from HA melting, Ti^{4+} and OH^- is believed to have led to the formation of perovskite phase structure. Comparing the phase content of the BHA coatings, it was observed that the characteristic of the bovine-HA was retained under the same processing condition. In addition to space group $\text{P6}_3/\text{m}$ HA hexagonal system, the XRD pattern also showed tiny diffraction peak that corresponds to MgO (space group: Fm-3m ; c-cubic; $2\theta = 41^\circ, 43.1^\circ$). The thermochemical interactions between the bovine-HA containing mg element and the hydroxyl ion (OH^-) from the water molecule could be the cause of the MgO formation. Sodium titanium phosphate, $\text{NaTi}_2(\text{PO}_4)_3$ (space group: R-3c ; Rhombohedral; $2\theta = 20.2^\circ$ and 25.6°) was also detected on the oxidized titanium alloy processed with CHA and BHA powders. In addition to the peaks of anatase (space group: I41/amd ; tetragonal; $2\theta = 38.4^\circ, 25.3^\circ, 36.8^\circ$) hydroxyapatite and sodium titanium phosphate, the appearance of the peaks corresponding to the metal substrate is most likely due to the penetration of X-rays beyond the coating layer. The reduction in the intensity of anatase and titanium peaks (Figure 6.5a) could be due to their participation in the formation of perovskite and sodium titanium phosphate structure. Thus, it can be concluded that the coatings produced from CHA and BHA electrolyte suspension had significant differences in chemical and phase composition/structures.

6.2.5 Surface roughness of PEO coatings

The surface profile graphs of the untreated Ti6Al4V and the PEO treated layers is presented in Figure 6.6. As can be seen in Figure 6.6, the peak-to-valley heights of the PEO-treated surfaces are significantly higher than that of untreated substrate. The R_a values of the CHA-PEO and BHA-PEO coated surfaces were measured as $R_a = 1.5 \pm 0.03 \mu\text{m}$; $R_z = 9.9 \pm 0.16 \mu\text{m}$ and $R_a = 1.9 \pm 0.13 \mu\text{m}$; $R_z = 11.8 \pm 0.53 \mu\text{m}$; respectively. This indicates that the modification of the oxide film layer with CHA and

BHA powders was accompanied by a remarkable change in surface roughness as compared to that of the untreated surface ($R_a = 0.2 \pm 0.06 \mu\text{m}$; $R_z = 2.9 \pm 0.5 \mu\text{m}$).

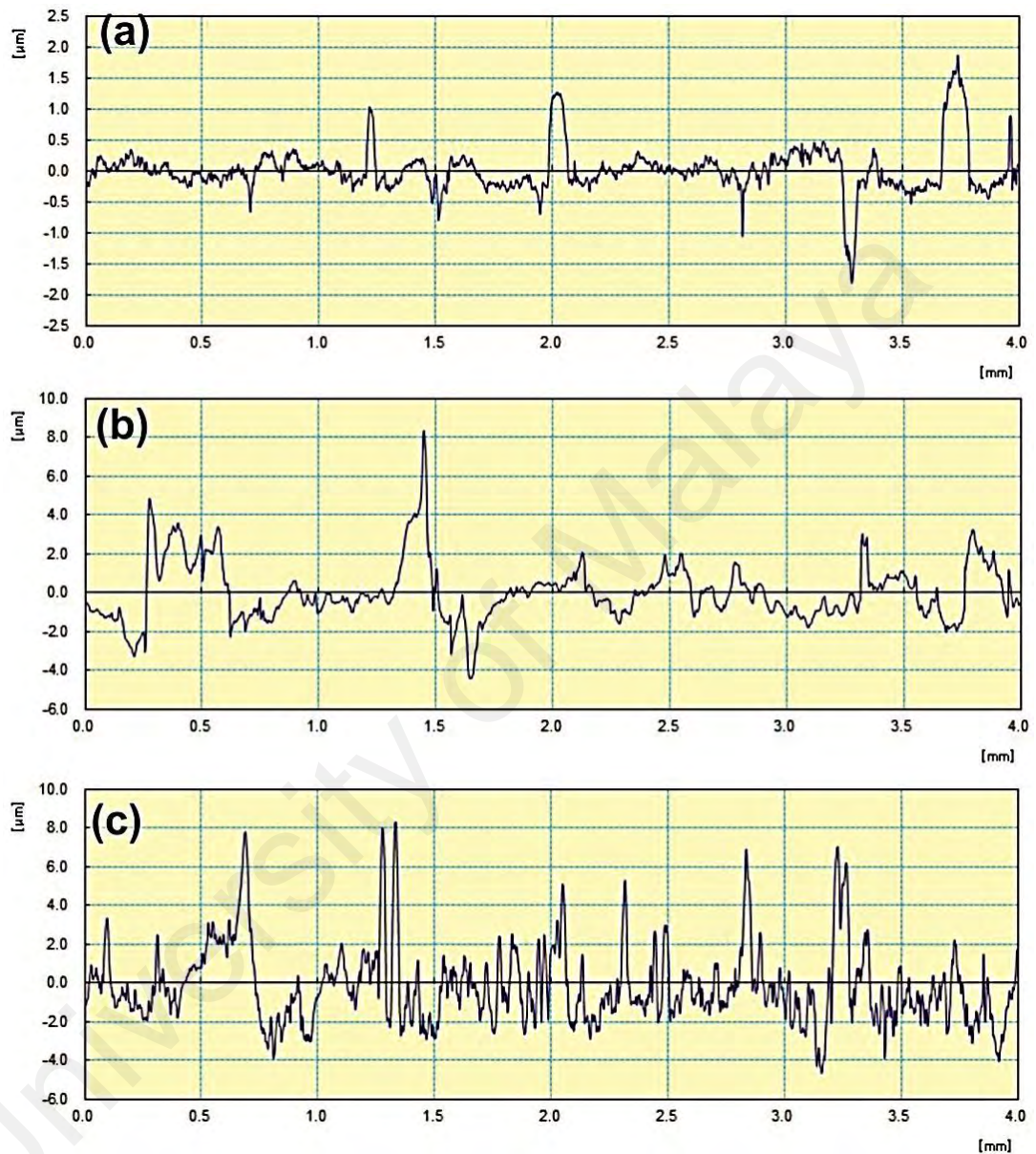


Figure 6.6: Surface profile graphs of: (a) untreated Ti6Al4V, and PEO layers (b) CHA, and (c) BHA

In Figure 6.2, the scanning electron micrographs show the general features of the treated surfaces as relatively smooth (Figure 6.2a) and uneven (Figure 6.2b), with increase in the number and size of pores (Figure 6.2b)), which resulted in different

surface roughness recorded. The R_a of the films was found to correlate well with their corresponding observed SEM micrographs.

6.2.6 Potentiodynamic corrosion evaluation

The cathodic and anodic polarization curves of untreated Ti6Al4V and HA-coated films are shown in Figure 6.7 and the data obtained from the curves using the Tafel extrapolation method are reported in Table 6.3. As can be seen for the untreated substrate, the corrosion potential was about $-0.531 V_{SCE}$, at which the corresponding current density was quite high ($0.61 \mu A cm^{-2}$) and active dissolution and release of significant amounts of ions occurred in the absence of films. In contrast, in the case of PEO-treated layers, the E_{corr} shift towards less negative values and stable passivation was achieved. It can be seen in Figure 6.7 and Table 6.3, the corrosion potential of the CHA film ($-0.474 V_{SCE}$) and BHA film ($-0.394 V_{SCE}$) are shifted towards more positive noble direction than that of untreated Ti6Al4V. This shift indicates that the corrosion reaction of untreated substrate and diffusion of Cl^{-1} in the Ti6Al4V/coating interface is suppressed by the formation of composite layers on Ti6Al4V surface.

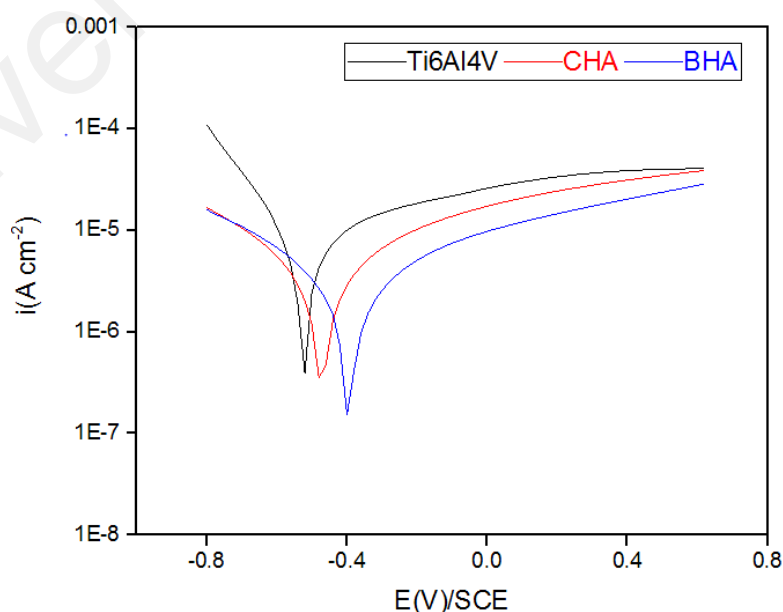


Figure 6.7: Potentiodynamic polarization Tafel plots of untreated Ti6Al4V, CHA and BHA films in Ringer's solution

The PEO-HA films inhibit corrosion and keep the release of corrosion products at a very low level. Furthermore, the anodic current densities of the films were one order of magnitude lower than that of untreated substrate. In fact, the Tafel hyperbolic plots move towards a lower current density for BHA coating, signifying that the Ti6Al4V substrate protective effects improve with the BHA film.

Table 6.3: Electrochemical corrosion parameters of untreated Ti6Al4V and PEO films in Ringer's solution

Sample code	β_a (V/dec)	β_c (V/dec)	E_{corr} (V_{SCE})	I_{corr} ($\mu A/cm^2$)	R_p (Ω)	CR (mm/year)	PE (%)
Ti6Al4V	0.194	0.106	-0.531	0.610	3.650×10^3	0.569	—
CHA	0.225	0.202	-0.474	0.033	1.506×10^4	0.038	94.5
BHA	0.237	0.207	-0.394	0.024	2.195×10^4	0.023	96.0

Based on the obtained data, the corrosion rate (CR) of the CHA-film showed a decrease of $\sim 93\%$ compared with untreated substrate, and that of the BHA-film demonstrated a reduction of $\sim 96\%$. The protection efficiency (PE) of the film was also calculated using Equation 3.4 and compared for the two different HA coatings. It was found that the BHA-film exhibited a slight increment of about 1.5% in the protection efficiency compared to CHA-film. Thus, by considering the E_{corr} , I_{corr} , CR , and R_p of untreated Ti6Al4V and PEO-films, the PEO-films display higher corrosion resistance over a potential range of -500 mV to $+500\text{ mV}$ in Ringer's solution.

6.2.7 In vitro-bioactivity of the PEO coatings

It is known that after the implantation of an implant in the human body, the implant surface comes directly in contact and interacts with the tissues and cells. The formation of bone-like apatite on the surface implant is an essential requirement as it provides vital information in predicting the in vivo bone bioactivity of a material (Durdu et al., 2016).

In order to investigate the apatite-forming ability of the PEO-treated layers, the coatings produced were immersed in SBF solution at 36.5 °C for 14 days. For comparison, the untreated Ti6Al4V was also tested for its bioactivity under similar experimental condition. The surface morphologies of the PEO-films and untreated Ti6Al4V after soaking in SBF are presented in Figure 6.8. It can be noticed that the micro-rough surface of the PEO treated films shown in (Figure 6.2) undergoes an obvious change after immersion in SBF solution for 14 days. The CHA-PEO film layers were covered with numerous fine and flaky-like precipitates, which are distributed over the entire surface (Figure 6.8a). In contrast to this observation, a thick and dense white spherical bone-like apatite particle, which assembled into larger particle-like aggregates, was precipitated on the BHA-coated surface (Figure 6.8b). On the other hand, little tiny spherical-like particles are observed on the surface of untreated Ti6Al4V, indicating its poor ability of apatite mineralization (Figure 6.8c).

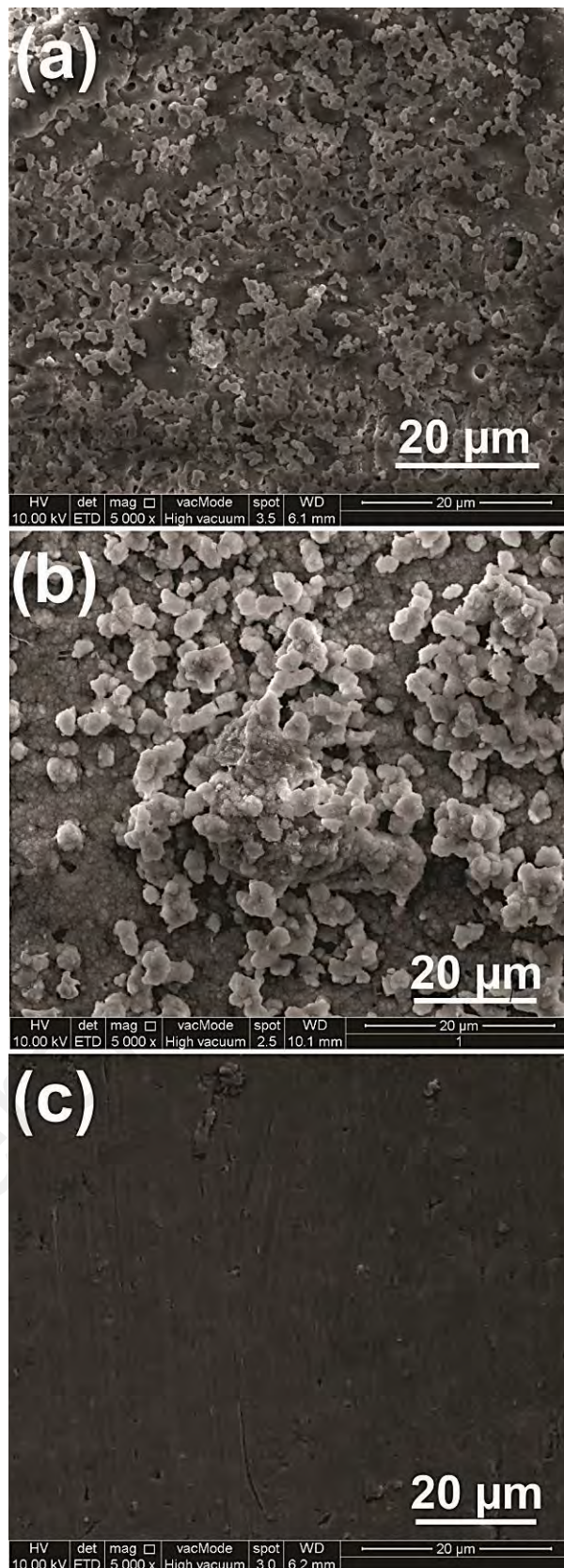


Figure 6.8: The surface SEM micrographs of PEO treated films: (a) CHA, (b) BHA and (c) untreated Ti6Al4V after immersion in 7.3 pH SBF solutions for 14 days

The EDS analyses of the elemental constituents for the obtained apatite layers were conducted and shown in Figure 6.9, while the atomic concentrations of the elements are presented in Table 6.4. Because the atomic concentration of Ca/P ratio is an integral factor in predicting the bioactivity of orthopaedic implant material, these values are calculated for different samples and included in Table 6.4. The EDS spectral analysis reveals that the apatite layers were rich in calcium and phosphorus (Figure 6.9). It can be observed from Figure 6.9 and Table 6.4, that the Ca and P count increases after SBF immersion, compared to the EDS Figure 6.4.

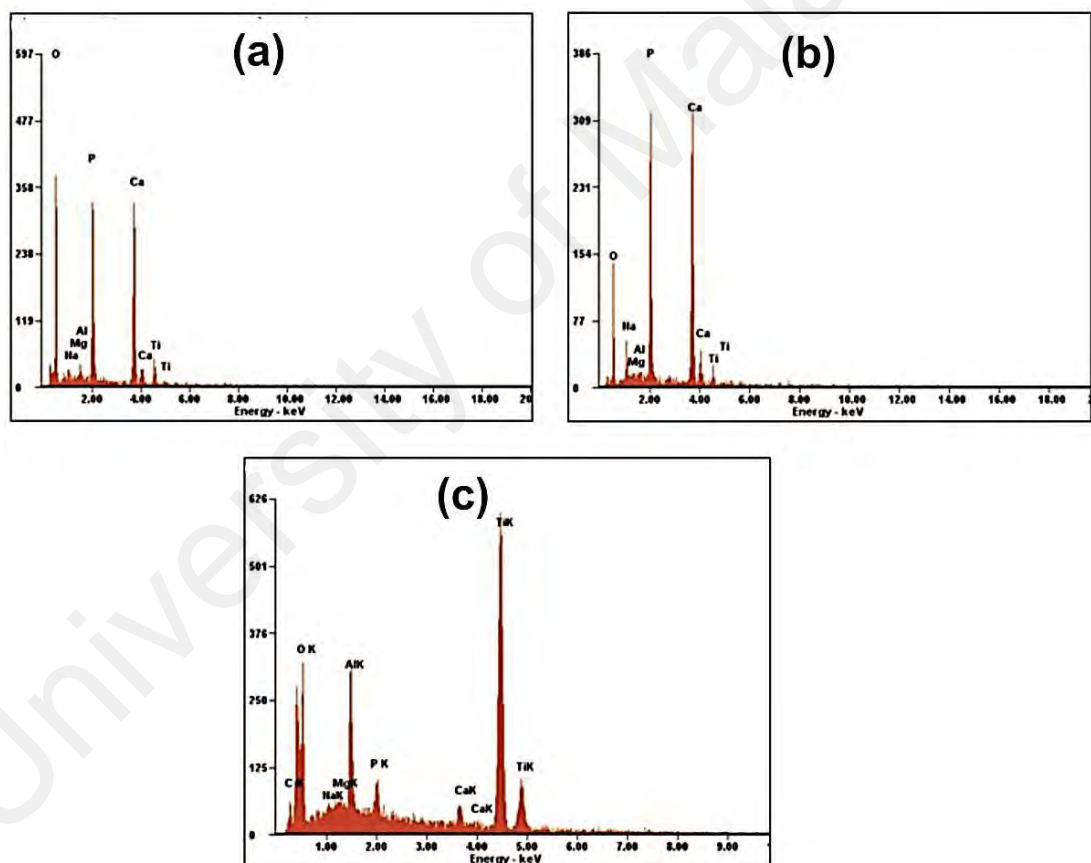


Figure 6.9: EDS spectra of PEO treated films: (a) CHA, (b) BHA, and (c) Ti6Al4V substrate

Table 6.4: Elemental composition of the PEO coatings with different hydroxyapatite particles (at.%)

Sample code	Ca	P	Mg	Ti	O	Al	Na	Ca/P
CHA	16.56	10.52	00.21	02.17	68.91	00.71	00.92	1.57
BHA	24.37	14.32	01.14	01.76	53.82	00.12	04.47	1.70
Ti6Al4V	01.86	01.92	00.40	47.46	40.95	07.25	00.16	0.96

The emergence of strong signals for Ca and P content (with Ca and P ratio of 1.7) which is almost equal to Ca/P ratio of stoichiometry bonelike apatite (1.67) signifies the formation of white dense bonelike apatite particles on the PEO surfaces. On the other hand, elemental composition analysis of untreated Ti6Al4V (Figure 6.9c) shows lower content of Ca and P on its surface. The results obtained corroborate with the SEM micrograph exhibiting the poor bioactivity of the untreated substrate (Figure 6.8c).

In order to confirm the formation of bonelike apatite on the sample surface after immersion in SBF for 14 days, FTIR analyses were performed as shown in Figure 6.10. It can be seen from Figure 6.10, that apatite formation on the sample surfaces induced a remarkable change in the bandwidth, frequency and reflection peaks of the FTIR bands after soaking in SBF solution. The PEO treated films are characterized by broad reflection bands while untreated alloy shows shallow bandwidth. The remarkable changes observed from Figure 6.10 (a, b, c) are attributed to the formation of a layer of bone-like apatite particles covering the surface of the treated films.

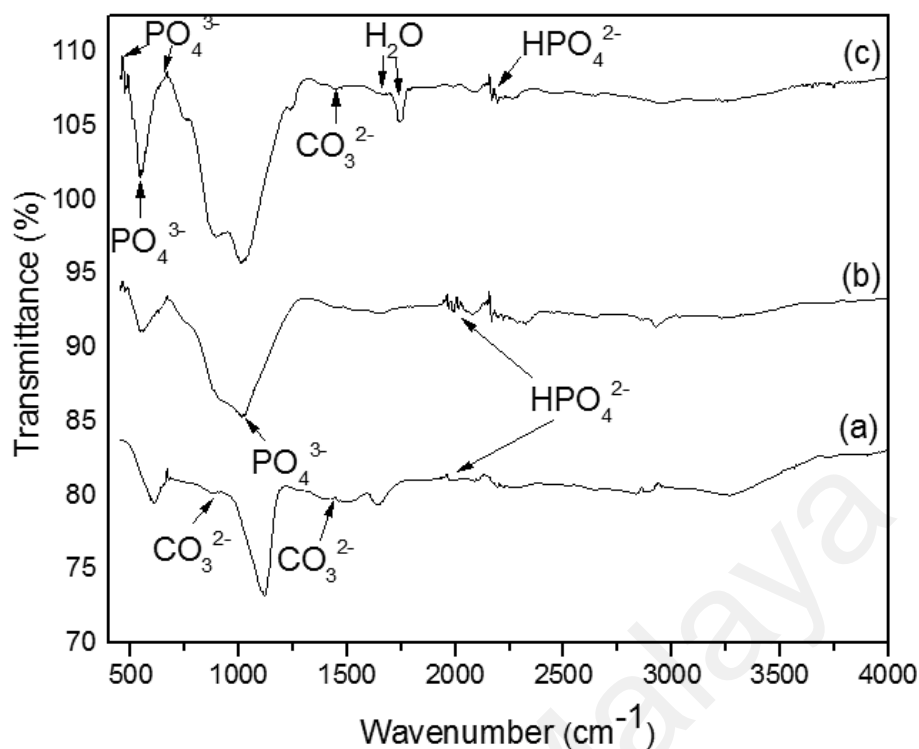


Figure 6.10: ATR-FTIR patterns of (a) untreated Ti6Al4V, (b) BHA film, and (c) CHA film after soaking in SBF solution for 14 days

The FTIR spectrum reveals the presence characteristic peaks of phosphate, hydrogen phosphate bands, carbonate species, and absorbed water on the samples after immersion in SBF (Figure 6.10). The ATR-FTIR spectrum confirms the existence of P-O bending of phosphate ions groups (PO_4^{3-} , ν_4) in the range of $472 - 639 \text{ cm}^{-1}$ (Farzadi et al., 2014; Rad et al., 2014) and P-O stretching type (PO_4^{3-} , ν_3) in the range of $1030 - 1137 \text{ cm}^{-1}$, which are associated with *HAp* structure. The duplets located around 1000 cm^{-1} are originated by phosphates modes (Figure 6.10b,c). The bands, mainly at 1030 cm^{-1} and 1111 cm^{-1} (Bai et al., 2011; Durdu et al., 2016), suggest the formation of a well-crystallized apatite structure. The C-O bending of carbonate absorption band (CO_3^{2-} , ν_3 or ν_4) and C-O stretching type (CO_3^{2-} , ν_1), that can substitute sites of apatite structure appeared at 875 cm^{-1} and in the ranges of $1420 - 1463 \text{ cm}^{-1}$ wave numbers, respectively. O - H bending mode of water observed

between $1641 - 1654 \text{ cm}^{-1}$ is attributed to the presence of water in the samples. The region between $1920 - 2382 \text{ cm}^{-1}$ (Durdu et al., 2013) is populated by absorption bands arising from P-H (HPO_4^{2-}, ν_s) stretching vibration in the formation of apatite structure. The C-H stretching absorption bands that are found between 2903 and 3060 cm^{-1} (Baszkiewicz et al., 2005), correspond to stretching vibration of organic compounds. Based on the FTIR spectroscopy findings, it can be concluded that bonelike apatite particles formed on the samples after soaking in SBF.

University of Malaya

6.3 Discussion

The plasma electrolytic oxidation is a low cost electrochemical surface treatment commonly employed to coat ceramic thin film on the surface of metal and their alloys. During PEO process, when a current density moves through the anodic metal/electrolyte interface at voltage exceeding the critical breakdown potential of the oxide film, an intense micro-plasma discharges are created on the surface. Owing to local temperature, which could vary from 10,000 to 20,000 K because of electron collision during the PEO process (Yerokhin et al., 1999), thermochemical reaction ensues between the metal surface and the electrolyte, thus modifying the metal surface into the oxide film layer. In this respect, the deposition of commercial hydroxyapatite and bovine hydroxyapatite in the trisodium phosphate solution was performed using plasma electrolytic oxidation. The formation of PEO coatings with different hydroxyapatite not only changed the Ti6Al4V surface chemistry but also its topography. Therefore, studying the variation of the two different hydroxyapatites would contribute to a better understanding of the biomedical implant behaviour. The PEO coating formation with different surface features has been reported for titanium implant materials, which are majorly dependent on electrolyte ingredients/composition and electrical parameter regime (voltage, current and time) (Cimenoglu et al., 2011; Shin et al., 2015).

In this study, the PEO coatings developed on Ti6Al4V in the electrolyte containing commercial-HA, bovine-HA and Na_3PO_4 under the applied voltage of 300 V, current density of 250 mAcm^{-2} , and deposition time of 5 min resulted in the formation of thick (about $26 \mu\text{m}$), rough and well adherent film layer (Figure 6.2 and 6.3). Even though the two coatings were formed under the same/identical parameters, the thick layer formed using different HA revealed somewhat different surface morphologies, topography (Figure 6.2) and phase constituents (Figure 6.5). It is a known fact that the deposition of HA onto an implant material promotes cell attachment and enhances the stability of

biomedical material. These findings demonstrated that with the single PEO process, a highly crystalline hexagonal HA can be produced in the coating with a relatively Ca/P ratio ~ 0.70 . A homogeneous distributed tiny micro-pore was produced on Ti6Al4V surface using CHA powder, while the BHA-PEO coating exhibited a flake and drop like morphology with various diameters of pores. The uneven surface and larger pores produced using BHA powder (Figure 6.2b) was due to a high complex series of chemical reaction due to higher ionic participation in the coating formation. Using of BHA electrolyte solution, more ions are likely to participate in the reaction, owing to the elemental cations of bovine bone powder (Mg^{2+} and Na^+), which could have made the electrolyte solution more aggressive during the PEO process compared to CHA solution. Due to the significant amount of ions participation, high temperature and pressure arose instantly with intense micro-sparking and cell voltage climbed to a terminating voltage of ($\sim 283 V$) (Figure 6.1). Subsequently, the pores are formed by the molten of the oxide layer and excessive effervescence of oxygen gas ejected out of micro-arc discharge channel. As a result of the differences in the surface defective nature, higher surface roughness were obtained on the surface of the BHA-PEO film ($1.9 \pm 0.13 \mu m$) as compared to that of the CHA-PEO coating ($1.5 \pm 0.3 \mu m$) (Figure 6.6). Knowing full well that porous structure and rough surface provide good bone fixation by enhancing the bone growth of tissues, the surface roughness of implant having R_a values in the range of 0.3 to 2 μm have been reported to improve bone responses favourably (Sandhyarani et al., 2014; Sul et al., 2005). The R_a values measured on the PEO-treated surfaces are within the range of micro-rough topography. Although, a higher surface roughness may promote good interfacial contact and better osseointegration at the implant-bone interface, micro-rough surfaces are generally preferred to prevent the release of ionic particles concentration into the physiological environment (Narayanan et al., 2008). The XRD patterns of the PEO coated surfaces in

Figure 6.5 showed that the anatase phase was formed on titanium implant after the PEO process. The anatase layer is generally produced at voltages as low as 250 V (Teh et al., 2003). In addition to anatase phase structure, hexagonal hydroxyapatite was formed on both coatings, MgO was also precipitated within the oxide film layer formed with bovine powder.

The potentiodynamic tests showed that the PEO-coated HA films exhibited superior corrosion resistance and lower corrosion current density in Ringer's solution compared to untreated substrate. This can be attributed to the protective barrier film on the Ti6Al4V substrate, which inhibits corrosive Cl^{-1} ion from penetrating into the substrate. The compact barrier layer at the interface of the Ti6Al4V/films acts as a shield between the corrosive media and the substrate. The electrochemical behaviour test performed on the dense coated layers in the present study shows that a 26 μm thick layer (Figure 6.3) of consolidated film effectively prevents ions transfer and metal dissolution. In addition, it can also be observed that the BHA-PEO coating showed better corrosion resistance as compared to CHA-PEO coating. In general, the anticorrosion behaviour of PEO coatings depends on the property of the oxide layers such as the thickness of the layer, dense structure/phase compositions, elemental chemical composition of the coating and structural defects (Gan et al., 2013; Srinivasan et al., 2010). Since the coating thickness obtained for the two coatings are the same, the phase composition, structural imperfections and chemical compositions are considered to be the main contributing factors for the difference in corrosion resistance. The precipitated flake and droplet like film on the BHA-PEO coating surface acts as a mechanical barrier between the substrate and the aggressive solutions and contributes to the protection behaviour of the BHA-PEO coating. Similar observation has also been reported elsewhere (Jamesh et al., 2012). A highly crystalline HA/MgO produced on the anodic oxide film layer shifts the surface potential and suppresses the adsorption of ions at the metal/electrolyte interface.

A similar situation exists in other literatures in which the phosphate-based oxide coatings containing MgO inhibits corrosion under corrosive environmental conditions (Gan et al., 2013). Since a relatively porous film is adjudged to support the infiltration of calcium and phosphorus ions which are essential for interaction between titanium implant and physiological environments. The difference in the chemical composition of BHA, and CHA is another reason for the lower corrosion rate of BHA, compared to CHA. This explains the reason why the BHA is more stable in Ringer's solution than CHA. Thus, the lower value of CR and I_{corr} obtained for BHA-PEO coating showed its ability in preventing the onset of corrosion. The performance of the PEO-treated films in Ringer's solution with respect to the Ti6Al4V substrate during the PEO process are in the following order $Ti6Al4V < CHA - PEO < BHA - PEO$.

Researchers have shown the favourable effect of the TiO_2 film containing calcium and phosphorus in the precipitation of apatite structure (Cimenoglu et al., 2011; Nie et al., 2000), as confirmed by the SBF and FTIR test in the present study (Figure 6.8 and 6.10), respectively. Considering the chemical composition of the hydroxyapatite, which is similar to that of bone, its deposition during SBF test is generally presumed as a primary indicator of a bioactive surface, which leads to good bonding between the implant and the bone (Kokubo & Takadama, 2006). Deposition of apatite on a material surface in SBF fluid is mainly governed by surface chemistry and free radical chemical groups. When the PEO porous surface is immersed in the solution, negatively charge such as the $-OH$ is created due to exchange of the ions and different chemical potential of TiO_2 phase and OH^- ions in the body fluid. Previous studies have confirmed that negatively charged surface have great induction capability and provides favourable sites for heterogeneous nucleation and growth of apatite in SBF (Durdu et al., 2016). The generation of Ti-OH on the micro-rough surface promotes the nucleation sites for the growth of apatite structure. The nucleation is initiated on the chemical group Ti-OH by

sorption of Ca^{2+} , and then adsorb PO_4^{3-} ion from the surrounding body fluid via electrostatic interaction. Due to the interaction and ionic activity of the Ti-OH, Ca^{2+} and PO_4^{3-} species at the surface, apatite structure, which allows cell growth and bond adhesion, precipitates on the PEO surface. Apatite (HA) structure has zero toxicity and can directly bond to the bone and it is considered as one of the most suitable calcium phosphates based ceramic material for hard tissue replacement implants. The apatite structure grows on the rough, porous surfaces of PEO coatings because the microporous-rough of PEO (R_a value close to 2 μm) (Figure 6.2) favours the sinking of Ca and P ions liquids into the pores, which are more favourable for the formation of apatite structure. The enrichment of apatite structure on the BHA coated surface (Figure 6.8b) is due to increase in crater-like region at the surface of BHA (Figure 6.2b). The Ca and P ions would deposit more on the rougher porous surface due to increase in the surface area/energy and number of nucleation sites at the BHA coated surface. It has been demonstrated that surfaces with porous microstructure triggers the induction of the more bone-like apatite in SBF (Deng et al., 2010). In line with the SBF test results, the BHA-PEO coating with rougher porous surface have a larger surface area and are favourable for the formation of chemical groups and adsorption of more Ca^{2+} and PO_4^{3-} ions. Besides, the existence of crystalline hydroxyapatite phases containing MgO layers on the PEO surface exposed to SBF provides further capacity for the induction of apatite layer (Pan et al., 2013). Pan et al. (2013) reported that hydroxyapatite incorporated MgO layers generated by PEO process promote the formation of apatite deposition during SBF test. The presence of magnesium oxide acted as the nucleation site in the induction of hydroxyapatite during SBF test. As in the case of commercial-HA, the contribution of perovskite- CaTiO_3 in the apatite formation has been reported by various researchers (Cimenoglu et al., 2011; Han et al., 2003). It should be noted that CaTiO_3 is not detected on the BHA-PEO coated surface (Figure 6.5b). However, the

formation of CaTiO_3 is a prerequisite for the nucleation and growth of apatite layer in SBF fluid. SBF test results showed that the applied PEO process and the existence of crystalline hydroxyapatite containing MgO phase enhanced the biocompatibility of the Ti6Al4V substrate by promoting the heterogeneous nucleation of apatite layer on the surface. Based on these results, it can be inferred that the use of natural bovine hydroxyapatite promoted the rapid growth of thick white bonelike apatite layer on the surface.

From this investigation, it can be seen that both the corrosion and bioactive test in SBF solution revealed an obvious improvement in the corrosion resistance and apatite formation resulting from morphology, elemental composition and phases of PEO coatings on Ti6Al4V substrate. The CHA-PEO and BHA-PEO coatings exhibited reduced corrosion rate and good apatite formation having a Ca/P ratio of about 1.67. As such, the bioactivity of these coatings in vivo is also expected to be enhanced.

6.4 Summary

Conventional-HA and natural-BHA have been successfully deposited on the surface of the Ti6Al4V alloy by plasma electrolytic oxidation under a current density of 250 mAcm⁻², and the corrosion and bioactivity performance were evaluated using potentiodynamic polarization and simulated body fluid test, respectively. The findings in the present work are as follows:

- The application of PEO process has a significant effect on the biocompatibility of Ti6Al4V, as the result produced a thick crater like and microporous layer.
- The porous PEO coatings consist of hexagonal HA, NaTi₂(PO₄)₃ and anatase in spite of different hydroxyapatite in the electrolyte. However, the oxide film layers were not identical from the aspect of HA particles ingredients and topography. The oxide pore layer containing conventional-HA particles possess perovskite-calcium titanate (CaTiO₃), whereas periclase magnesium oxide (MgO) with a flake and droplet like morphology was produced with natural bovine-HA.
- The oxide layers containing different phase structures exhibited superior corrosion rate compared to untreated Ti6Al4V substrate and the PEO/compositions of the coatings play a vital role in the protection of the Ti6Al4V substrate.
- The in vitro bioactivity results indicate that the coatings displayed excellent bioactivity. The coatings formed in bovine-derived HA electrolyte exhibit better apatite induction ability and higher protection efficiency than that of layer containing conventional-HA particles.

The in vitro and bioactivity test results indicate that PEO coating formed in bovine solution could be a promising candidate material to improve the bioactive performance of metallic implant material.

University of Malaya

CHAPTER 7: CONCLUSION AND RECOMMENDATION

7.1 Conclusions

The research work presented in this thesis characterized the microstructures and properties of PEO coatings on Ti6Al4V implant in order to establish the microstructure-property relationship with different hydroxyapatite particles electrolyte solution. Firstly, the conventional hydroxyapatite (CHA) electrolyte processed in a benign and familiar compound (NAP) was selected. Then, the influence of CHA concentration has been studied by comparing the coatings produced with different CHA concentration. Finally, a mechanism associated with the evolution of phase structure on the PEO coatings as well as mechanical integrity and failure modes of the coatings was also investigated to facilitate better understanding of the CHA particle incorporation and its effect on the oxide film layer. To develop a more biocompatible implant with good bioactive properties and biological response. A promising electrolyte composed of natural bovine hydroxyapatite (BHA) particles was also selected for the modification of titanium implant material. The PEO process parameters have been selected based on the optimized HA parameter. To this end, three basic experimental procedures have been conducted: PEO-CHA process characterization and evaluation of resulting coatings. The morphological-property relationship of Ti6Al4V substrate with PEO-BHA coatings produced using different voltages regime. The comparative study on the in vitro corrosion and bioactive performance of CHA and BHA coatings developed under the same processing conditions has also been studied to demonstrate their applicability in the biomedical area. The findings of this project are summarized under various sections in the following part of this chapter:

- a) Growing of PEO coating in CHA-NAP electrolyte solution:
 - i. CHA concentration in the range of 0-2 g/L strongly influences the anodic oxide film and the coating characteristics. Increasing in CHA concentration

during the PEO process would possibly affect the oxide layer stability, especially at 2 g/L HA concentration. The coatings produced at varying concentration showed that the pore size and the dense layer structure are concentration dependent. The 2 g/L CHA depicted higher thickness and lesser porosity compared with those produced at lower HA concentration.

- ii. The PEO-CHA coatings consist of hexagonal hydroxyapatite, tricalcium phosphates, and anatase. The tricalcium phosphates are more than hydroxyapatite phase structure in the PEO coatings and this is mainly due to increase in temperature during the PEO process. A simple growth mechanism is proposed to account for the observed phase structure.
- iii. The mechanical properties of the PEO-CHA coatings are influenced more by the amount of HA concentration in the anodic film. In the scratch test of the coatings, the coating formed at 2 g/L HA revealed greater detachment compared to the one produced at 1.5 g/L HA, and this is due to the enrichment of the TiO₂ film with larger amount of CaP. A maximum scratch adhesion strength of 2099 mN was achieved using 1.5 g/L HA solution, while coatings without HA addition demonstrated a critical load of 1247 mN. The failure of the PEO-TiO₂ coating was characterized by large periodic hemispherical chipping, while the PEO-CHA film failure was dominated by intermittent delamination. It was concluded therefore, that the 2 g/L HA is not an option for the modification of the anodic film.

b) Growing of PEO coating in BHA-NAP electrolyte solution:

- i. The PEO voltage in the range of 225-325 V and current density of 500 mAcm⁻² can be considered as low PEO energy input conditions for the

formation of thick layers because under these conditions PEO coatings exhibited relatively compact and uniform structures.

- ii. For the first time, MgO phase was formed on the Ti6Al4V implant in addition to the hexagonal HA and anatase phase due to the preparation of PEO coatings in natural bovine hydroxyapatite electrolyte solution.
- iii. The COF of the PEO coatings is low because of the co-existence of the composite layers (TiO₂-MgO-BHA) on the titanium surface. Even though the formation of the dense layer improved the wear performance of the Ti6Al4V, the emergence of micro-porous, tiny micro-crack and loose layer at the highest voltage later affects the performance of the sliding surface. Therefore, the voltage for the deposition of BHA should not exceed 300 V to avoid micro-crack in the coating.

c) Growing of PEO coating in CHA and BHA electrolyte solution:

- i. The PEO coatings have been successfully prepared on the surface of Ti6Al4V by PEO process in CHA and BHA-containing electrolyte solution under a lower current density of 250 mAcm⁻². The coating consists of a dense layer structure. In spite of the same processing conditions, the dense layer displayed a different surface morphologies and phase structure. The PEO treated with BHA are found to contain MgO phase and larger pore diameter, whereas CaTiO₃ are present on the surface of PEO treated with CHA.
- ii. The PEO-CHA and PEO-BHA coatings can provide corrosion protection and effectively reduce the corrosion rate. The coating formed in BHA showed higher protection efficiency and better induction capability for apatite layer formation compared to PEO-CHA due to the differences in their morphologies, phase structure and surface topography.

7.2 Contributions to knowledge

The present study offers an opportunity to widen the scope of the fundamental understanding of the influences of conventional hydroxyapatite and natural bovine hydroxyapatite on the morphologies and properties of PEO coatings particularly how the Ti6Al4V implant can be improved by incorporation of hydroxyapatite particles. The specific contributions of this research work to the frontiers of knowledge are:

- a. The study shows that it is feasible to deposit HA in a solitary sodium phosphate solution without employing other materials to charge HA particles negatively.
- b. For the first time, the study established the failure modes of the PEO coating.
- c. The natural bovine hydroxyapatite coating is developed for the first time to evaluate its biocompatibility and bioactive performance on the Ti6Al4V alloy implant. This provides a very scientific and objective evaluation of the performance natural bovine bone material.
- d. The range of hydroxyapatite concentration identified as a low concentration condition in the present investigation appears relevant to other research work as it will give insight on its influence on the PEO-oxide film.
- e. The characteristic behaviour of TiO₂-HA film has been established with its performance in terms of mechanical characteristics, scratch hardness and entrance mechanism of the HA in the anodic film.
- f. The use of micro-imaging software to measure the percentage porosity is adaptable to other PEO coatings whose porosity level is being sought for improvement.

7.3 Recommendation for future work

During the course of this work, a number of issues which deserve further investigation were encountered. The issues are hereby presented for further studies:

1. The nano-mechanical, tensile, fatigue performance as well as residual stress of the coatings produced in this thesis can be studied.
2. There is a need to compare the dry and SBF wear performance of CHA and BHA coatings to understand the difference in their wear behaviour.
3. Incorporation of silicon in BHA coatings for bone mineralization may equally be investigated.
4. Future work with TiO₂-MgO-BHA coatings should consider parametric study to understand the influence of process parameters on the dense layer formation.
5. In terms of bioactive properties, the present work evaluates the in vitro performance of the coated samples using potentiodynamic electrochemical methods and SBF test. However, the toxicity of the PEO treated layers remains to be assessed, which could be conducted via simple in vitro cell culture or through practical in vivo implant operation.

REFERENCES

- Abbasi, S., Bayati, M., Golestani-Fard, F., Rezaei, H., Zargar, H., Samanipour, F., & Shoaee-Rad, V. (2011). Micro arc oxidized HAp–TiO₂ nanostructured hybrid layers-part I: Effect of voltage and growth time. *Applied Surface Science*, 257(14), 5944-5949.
- Ágata de Sena, L., Calixto de Andrade, M., Malta Rossi, A., & de Almeida Soares, G. (2002). Hydroxyapatite deposition by electrophoresis on titanium sheets with different surface finishing. *Journal of Biomedical Materials Research Part A*, 60(1), 1-7.
- Aktuğ, S. L., Durdu, S., Yalçın, E., Çavuşoğlu, K., & Usta, M. (2017). Bioactivity and biocompatibility of hydroxyapatite-based bioceramic coatings on zirconium by plasma electrolytic oxidation. *Materials Science and Engineering: C*, 71, 1020-1027.
- Albella, J., Montero, I., & Martinez-Duart, J. (1987). A theory of avalanche breakdown during anodic oxidation. *Electrochimica Acta*, 32(2), 255-258.
- Aliasghari, S., Němcová, A., Čížek, J., Gholinia, A., Skeldon, P., & Thompson, G. (2016). Effects of reagent purity on plasma electrolytic oxidation of titanium in an aluminate–phosphate electrolyte. *Transactions of the IMF*, 94(1), 32-42.
- Aliasghari, S., Skeldon, P., & Thompson, G. (2014). Plasma electrolytic oxidation of titanium in a phosphate/silicate electrolyte and tribological performance of the coatings. *Applied Surface Science*, 316, 463-476.
- Alsaran, A., Purcek, G., Hacisalihoglu, I., Vangolu, Y., Bayrak, Ö., Karaman, I., & Celik, A. (2011). Hydroxyapatite production on ultrafine-grained pure titanium by micro-arc oxidation and hydrothermal treatment. *Surface and Coatings Technology*, 205, S537-S542.
- Andreeva, V. (1964). Behavior and nature of thin oxide films on some metals in gaseous media and in electrolyte solutions. *Corrosion*, 20(2), 35t-46t.
- Antônio, C. A., Cruz, N. C., Rangel, E. C., Rangel, R. d. C. C., Araujo, T. d. E. S., Durrant, S. F., . . . Duek, E. A. R. (2014). Hydroxyapatite coating deposited on grade 4 titanium by plasma electrolytic oxidation. *Materials Research*, 17(6), 1427-1433.
- Apachitei, I., Leoni, A., Riemslog, A., Fratila-Apachitei, L., & Duszczuk, J. (2011). Enhanced fatigue performance of porous coated Ti6Al4V biomedical alloy. *Applied Surface Science*, 257(15), 6941-6944.
- Apachitei, I., Lonyuk, B., Fratila-Apachitei, L., Zhou, J., & Duszczuk, J. (2009). Fatigue response of porous coated titanium biomedical alloys. *Scripta Materialia*, 61(2), 113-116.

- Arrabal, R., Matykina, E., Hashimoto, T., Skeldon, P., & Thompson, G. (2009). Characterization of AC PEO coatings on magnesium alloys. *Surface and Coatings Technology*, 203(16), 2207-2220.
- ASTM. (2009). G171 standard test method for scratch hardness of materials using a diamond stylus. *ASTM Stand*, 3.
- Bai, Y., Park, I. S., Lee, S. J., Bae, T. S., Duncan, W., Swain, M., & Lee, M. H. (2011). One-step approach for hydroxyapatite-incorporated TiO₂ coating on titanium via a combined technique of micro-arc oxidation and electrophoretic deposition. *Applied Surface Science*, 257(15), 7010-7018.
- Baszkiewicz, J., Krupa, D., Mizera, J., Sobczak, J., & Biliński, A. (2005). Corrosion resistance of the surface layers formed on titanium by plasma electrolytic oxidation and hydrothermal treatment. *Vacuum*, 78(2), 143-147.
- Blackwood, D., & Seah, K. (2009). Electrochemical cathodic deposition of hydroxyapatite: improvements in adhesion and crystallinity. *Materials Science and Engineering: C*, 29(4), 1233-1238.
- Blau, P. J. (1997). Fifty years of research on the wear of metals. *Tribology International*, 30(5), 321-331.
- Blawert, C., Dietzel, W., Ghali, E., & Song, G. (2006). Anodizing treatments for magnesium alloys and their effect on corrosion resistance in various environments. *Advanced Engineering Materials*, 8(6), 511-533.
- Boinet, M., Verdier, S., Maximovitch, S., & Dalard, F. (2005). Plasma electrolytic oxidation of AM60 magnesium alloy: Monitoring by acoustic emission technique. Electrochemical properties of coatings. *Surface and Coatings Technology*, 199(2), 141-149.
- Budinski, K. G. (1991). Tribological properties of titanium alloys. *Wear*, 151(2), 203-217.
- Bunshah, R. (2001). Handbook of hard films: Noyes publications, New York.
- Cakmak, E., Tekin, K. C., Malayoglu, U., & Shrestha, S. (2010). The effect of substrate composition on the electrochemical and mechanical properties of PEO coatings on Mg alloys. *Surface and Coatings Technology*, 204(8), 1305-1313.
- Cengiz, S., Uzunoglu, A., Stanciu, L., Tarakci, M., & Gencer, Y. (2016). Direct fabrication of crystalline hydroxyapatite coating on zirconium by single-step plasma electrolytic oxidation process. *Surface and Coatings Technology*, 301, 74-79.
- Chaturvedi, T. (2009). An overview of the corrosion aspect of dental implants (titanium and its alloys). *Indian Journal of Dental Research*, 20(1), 91.
- Chen, F., Lam, W., Lin, C., Qiu, G., Wu, Z., Luk, K., & Lu, W. (2007). Biocompatibility of electrophoretic deposition of nanostructured hydroxyapatite coating on roughen titanium surface: in vitro evaluation using

mesenchymal stem cells. *Journal of Biomedical Materials Research Part B: Applied Biomaterials*, 82(1), 183-191.

- Cimenoglu, H., Gunyuz, M., Kose, G. T., Baydogan, M., Uğurlu, F., & Sener, C. (2011). Micro-arc oxidation of Ti6Al4V and Ti6Al7Nb alloys for biomedical applications. *Materials Characterization*, 62(3), 304-311.
- Davis, J. R. (2001). *Surface engineering for corrosion and wear resistance*. United States of America: ASM International.
- Deng, F., Zhang, W., Zhang, P., Liu, C., & Ling, J. (2010). Improvement in the morphology of micro-arc oxidised titanium surfaces: a new process to increase osteoblast response. *Materials Science and Engineering: C*, 30(1), 141-147.
- Dinçer, M., Teker, D., Sağ, C. P., & Öztürk, K. (2013). Enhanced bonding of biomimetic apatite coatings on surface-modified titanium substrates by hydrothermal pretreatment. *Surface and Coatings Technology*, 226, 27-33.
- Donald, M., Brunette, P. T., & Marcus Textor, P. T. (2001). Titanium in medicine: material science, surface science, engineering, biological responses and medical applications.
- Duan, H., Du, K., Yan, C., & Wang, F. (2006). Electrochemical corrosion behavior of composite coatings of sealed MAO film on magnesium alloy AZ91D. *Electrochimica Acta*, 51(14), 2898-2908.
- Duan, H., Li, Y., Xia, Y., & Chen, S. (2012). Transient voltage-current characteristics: new insights into plasma electrolytic oxidation process of aluminium alloy. *International Journal of Electrochemistry Science*, 7, 7619-7630.
- Duarte, L. T., Bolfarini, C., Biaggio, S. R., Rocha-Filho, R. C., & Nascente, P. A. (2014). Growth of aluminum-free porous oxide layers on titanium and its alloys Ti-6Al-4V and Ti-6Al-7Nb by micro-arc oxidation. *Materials Science and Engineering: C*, 41, 343-348.
- Dumelié, N., Benhayoune, H., Rouse-Bertrand, C., Bouthors, S., Perchet, A., Wortham, L., . . . Balossier, G. (2005). Characterization of electrodeposited calcium phosphate coatings by complementary scanning electron microscopy and scanning-transmission electron microscopy associated to X-ray microanalysis. *Thin Solid Films*, 492(1), 131-139.
- Durdu, S., Deniz, Ö. F., Kutbay, I., & Usta, M. (2013). Characterization and formation of hydroxyapatite on Ti6Al4V coated by plasma electrolytic oxidation. *Journal of Alloys and Compounds*, 551, 422-429.
- Durdu, S., & Usta, M. (2014). The tribological properties of bioceramic coatings produced on Ti6Al4V alloy by plasma electrolytic oxidation. *Ceramics International*, 40(2), 3627-3635.
- Durdu, S., Usta, M., & Berkem, A. S. (2016). Bioactive coatings on Ti6Al4V alloy formed by plasma electrolytic oxidation. *Surface and Coatings Technology*, 301, 85-93.

- Erdemir, A. (2005). Review of engineered tribological interfaces for improved boundary lubrication. *Tribology International*, 38(3), 249-256.
- Ezazi, M., Quazi, M., Zalnezhad, E., & Sarhan, A. A. (2014). Enhancing the tribo-mechanical properties of aerospace AL7075-T6 by magnetron-sputtered Ti/TiN, Cr/CrN & TiCr/TiCrN thin film ceramic coatings. *Ceramics International*, 40(10), 15603-15615.
- Faghihi-Sani, M.-A., Arbabi, A., & Mehdinezhad-Roshan, A. (2013). Crystallization of hydroxyapatite during hydrothermal treatment on amorphous calcium phosphate layer coated by PEO technique. *Ceramics International*, 39(2), 1793-1798.
- Farnoush, H., Sadeghi, A., Bastami, A. A., Moztarzadeh, F., & Mohandesi, J. A. (2013). An innovative fabrication of nano-HA coatings on Ti-CaP nanocomposite layer using a combination of friction stir processing and electrophoretic deposition. *Ceramics International*, 39(2), 1477-1483.
- Farzadi, A., Bakhshi, F., Solati-Hashjin, M., Asadi-Eydivand, M., & abu Osman, N. A. (2014). Magnesium incorporated hydroxyapatite: Synthesis and structural properties characterization. *Ceramics International*, 40(4), 6021-6029.
- Freese, H. L., Volas, M. G., & Wood, J. R. (2001). Metallurgy and technological properties of titanium and titanium alloys *Titanium in Medicine* (pp. 25-51): Springer.
- Gan, J., Tan, L., Yang, K., Hu, Z., Zhang, Q., Fan, X., . . . Li, W. (2013). Bioactive Ca-P coating with self-sealing structure on pure magnesium. *Journal of Materials Science: Materials in Medicine*, 24(4), 889-901.
- Gao, Y. (2014). *Investigation of plasma electrolytic oxidation of commercially pure magnesium for biomedical applications*. University of Sheffield.
- Golestani-Fard, F., Bayati, M., Zargar, H., Abbasi, S., & Rezaei, H. (2011). MAO-preparation of nanocrystalline hydroxyapatite-titania composite films: Formation stages and effect of the growth time. *Materials Research Bulletin*, 46(12), 2422-2426.
- Gordienko, P., & Gnedenkov, S. (1997). Microarc oxidation of titanium and its alloys, Dalnauka, Vladivostok, 1997: Russian.
- Gray, J., & Luan, B. (2002). Protective coatings on magnesium and its alloys—a critical review. *Journal of Alloys and Compounds*, 336(1-2), 88-113.
- Guo, H., An, M., Xu, S., & Huo, H. (2005). Formation of oxygen bubbles and its influence on current efficiency in micro-arc oxidation process of AZ91D magnesium alloy. *Thin Solid Films*, 485(1), 53-58.
- Han, Y., Hong, S.-H., & Xu, K. (2003). Structure and in vitro bioactivity of titania-based films by micro-arc oxidation. *Surface and Coatings Technology*, 168(2), 249-258.

- Han, Y., Sun, J., & Huang, X. (2008). Formation mechanism of HA-based coatings by micro-arc oxidation. *Electrochemistry Communications*, 10(4), 510-513.
- Harun, W., Asri, R., Alias, J., Zulkifli, F., Kadirgama, K., Ghani, S., & Shariffuddin, J. (2017). A comprehensive review of hydroxyapatite-based coatings adhesion on metallic biomaterials. *Ceramics International*.
- Hayakawa, T., Yoshinari, M., Takahashi, K., & Nemoto, K. (2004). Deposition of thin calcium phosphate film onto titanium using RF magnetron sputtering technique. *Journal of Oral Tissue Engineering*, 1(1), 41-49.
- Hermawan, H., Ramdan, D., & Djuansjah, J. R. (2011). Metals for biomedical applications. *Biomedical Engineering-from Theory to Applications*: InTech.
- Holmberg, K., & Mathews, A. (1994). Coatings tribology: a concept, critical aspects and future directions. *Thin Solid Films*, 253(1-2), 173-178.
- Huang, Y., Wang, Y., Ning, C., Nan, K., & Han, Y. (2007). Hydroxyapatite coatings produced on commercially pure titanium by micro-arc oxidation. *Biomedical Materials*, 2(3), 196.
- Hussein, R., Nie, X., & Northwood, D. (2013). An investigation of ceramic coating growth mechanisms in plasma electrolytic oxidation (PEO) processing. *Electrochimica Acta*, 112, 111-119.
- Hussein, R., Nie, X., Northwood, D., Yerokhin, A., & Matthews, A. (2010). Spectroscopic study of electrolytic plasma and discharging behaviour during the plasma electrolytic oxidation (PEO) process. *Journal of Physics D: Applied Physics*, 43(10), 105203.
- Hutchings, I. (1992). Tribology: friction and wear of engineering materials. *Materials and Design*, 13(3), 187.
- Hwang, I., Hwang, D., Ko, Y., & Shin, D. (2012). Correlation between current frequency and electrochemical properties of Mg alloy coated by micro arc oxidation. *Surface and Coatings Technology*, 206(15), 3360-3365.
- Ikonopisov, S., Girginov, A., & Machkova, M. (1979). Electrical breaking down of barrier anodic films during their formation. *Electrochimica Acta*, 24(4), 451-456.
- Ishizawa, H., Fujino, M., & Ogino, M. (1995). Mechanical and histological investigation of hydrothermally treated and untreated anodic titanium oxide films containing Ca and P. *Journal of Biomedical Materials Research Part A*, 29(11), 1459-1468.
- Ishizawa, H., & Ogino, M. (1995). Characterization of thin hydroxyapatite layers formed on anodic titanium oxide films containing Ca and P by hydrothermal treatment. *Journal of Biomedical Materials Research Part A*, 29(9), 1071-1079.

- Jackson, M., Kopac, J., Balazic, M., Bombac, D., Brojan, M., & Kosel, F. (2016). Titanium and titanium alloy applications in medicine *Surgical Tools and Medical Devices* (pp. 475-517): Springer.
- Jafari, H., Hessam, H., Shahri, S. M. G., Assadian, M., Shairazifard, S. H. P., & Idris, M. H. (2016). Characterizing sintered nano-hydroxyapatite sol-gel coating deposited on a biomedical Ti-Zr-Nb alloy. *Journal of Materials Engineering and Performance*, 25(3), 901-909.
- Jamesh, M., Kumar, S., & Narayanan, T. S. (2012). Electrodeposition of hydroxyapatite coating on magnesium for biomedical applications. *Journal of Coatings Technology and Research*, 9(4), 495-502.
- Jiang, J., Zhou, Q., Yu, J., Ma, A., Song, D., Lu, F., . . . Chen, J. (2013). Comparative analysis for corrosion resistance of micro-arc oxidation coatings on coarse-grained and ultra-fine grained AZ91D Mg alloy. *Surface and Coatings Technology*, 216, 259-266.
- Jun, D., Liang, J., Hu, L.-t., Hao, J.-c., & Xue, Q.-j. (2007). Effects of sodium tungstate on characteristics of microarc oxidation coatings formed on magnesium alloy in silicate-KOH electrolyte. *Transactions of Nonferrous Metals Society of China*, 17(2), 244-249.
- Kamachimudali, U., Sridhar, T., & Raj, B. (2003). Corrosion of bio implants. *Sadhana*, 28(3), 601-637.
- Kaya, C. (2008). Electrophoretic deposition of carbon nanotube-reinforced hydroxyapatite bioactive layers on Ti-6Al-4V alloys for biomedical applications. *Ceramics International*, 34(8), 1843-1847.
- Kazek-Kęsik, A., Krok-Borkowicz, M., Pamuła, E., & Simka, W. (2014). Electrochemical and biological characterization of coatings formed on Ti-15Mo alloy by plasma electrolytic oxidation. *Materials Science and Engineering: C*, 43, 172-181.
- Khan, R., Yerokhin, A., Li, X., Dong, H., & Matthews, A. (2010). Surface characterisation of DC plasma electrolytic oxidation treated 6082 aluminium alloy: Effect of current density and electrolyte concentration. *Surface and Coatings Technology*, 205(6), 1679-1688.
- Kim, D.-Y., Kim, M., Kim, H.-E., Koh, Y.-H., Kim, H.-W., & Jang, J.-H. (2009). Formation of hydroxyapatite within porous TiO₂ layer by micro-arc oxidation coupled with electrophoretic deposition. *Acta Biomaterialia*, 5(6), 2196-2205.
- Kokubo, T., Kushitani, H., Sakka, S., Kitsugi, T., & Yamamuro, T. (1990). Solutions able to reproduce in vivo surface-structure changes in bioactive glass-ceramic A-W3. *Journal of Biomedical Materials Research Part A*, 24(6), 721-734.
- Kokubo, T., & Takadama, H. (2006). How useful is SBF in predicting in vivo bone bioactivity? *Biomaterials*, 27(15), 2907-2915.

- Kollath, V. O., Chen, Q., Mullens, S., Luyten, J., Traina, K., Boccaccini, A. R., & Cloots, R. (2016). Electrophoretic deposition of hydroxyapatite and hydroxyapatite–alginate on rapid prototyped 3D Ti6Al4V scaffolds. *Journal of Materials science*, 51(5), 2338-2346.
- Komotori, J., Hisamori, N., & Ohmori, Y. (2007). The corrosion/wear mechanisms of Ti–6Al–4V alloy for different scratching rates. *Wear*, 263(1), 412-418.
- Kossenko, A., Lugovskoy, S., Astashina, N., Lugovskoy, A., & Zinigrad, M. (2013). Effect of time on the formation of hydroxyapatite in PEO process with hydrothermal treatment of the Ti-6Al-4V alloy. *Glass Physics and Chemistry*, 39(6), 639-642.
- Krishna, L. R., Poshal, G., & Sundararajan, G. (2010). Influence of electrolyte chemistry on morphology and corrosion resistance of micro arc oxidation coatings deposited on magnesium. *Metallurgical and Materials Transactions A*, 41(13), 3499-3508.
- Kumar, S., & Narayanan, T. S. (2008). Corrosion behaviour of Ti–15Mo alloy for dental implant applications. *Journal of Dentistry*, 36(7), 500-507.
- Kumar, S., Narayanan, T. S., Raman, S. G. S., & Seshadri, S. (2010). Evaluation of fretting corrosion behaviour of CP-Ti for orthopaedic implant applications. *Tribology International*, 43(7), 1245-1252.
- Kwok, C., Wong, P., Cheng, F., & Man, H. (2009). Characterization and corrosion behavior of hydroxyapatite coatings on Ti6Al4V fabricated by electrophoretic deposition. *Applied Surface Science*, 255(13), 6736-6744.
- Li, L.-H., Kong, Y.-M., Kim, H.-W., Kim, Y.-W., Kim, H.-E., Heo, S.-J., & Koak, J.-Y. (2004). Improved biological performance of Ti implants due to surface modification by micro-arc oxidation. *Biomaterials*, 25(14), 2867-2875.
- Liang, J., Hu, L., & Hao, J. (2007). Characterization of microarc oxidation coatings formed on AM60B magnesium alloy in silicate and phosphate electrolytes. *Applied Surface Science*, 253(10), 4490-4496.
- Liu, X., Chu, P. K., & Ding, C. (2004). Surface modification of titanium, titanium alloys, and related materials for biomedical applications. *Materials Science and Engineering: R: Reports*, 47(3), 49-121.
- Long, M., & Rack, H. J. (1998). Titanium alloys in total joint replacement—a materials science perspective. *Biomaterials*, 19(18), 1621-1639.
- López, E. O., Rossi, A. L., Archanjo, B. S., Ospina, R. O., Mello, A., & Rossi, A. M. (2015). Crystalline nano-coatings of fluorine-substituted hydroxyapatite produced by magnetron sputtering with high plasma confinement. *Surface and Coatings Technology*, 264, 163-174.
- Lütjering, G., & Williams, J. C. (2007). Special properties and applications of titanium. *Titanium*, 383-415.

- Lyman, C. E., Goldstein, J. I., Romig Jr, A. D., Echlin, P., Joy, D. C., Newbury, D. E., . . . Lifshin, E. (1990). Bulk specimens for SEM and X-ray microanalysis *scanning electron microscopy, X-Ray Microanalysis, and Analytical Electron Microscopy* (pp. 159-171): Springer.
- Ma, H., Gu, Y., Liu, S., Che, J., & Yang, D. (2017). Local corrosion behavior and model of micro-arc oxidation HA coating on AZ31 magnesium alloy. *Surface and Coatings Technology, 331*, 179-188.
- Martin, J., Melhem, A., Shchedrina, I., Duchanoy, T., Nomine, A., Henrion, G., . . . Belmonte, T. (2013). Effects of electrical parameters on plasma electrolytic oxidation of aluminium. *Surface and Coatings Technology, 221*, 70-76.
- Matykina, E., Arrabal, R., Mingo, B., Mohedano, M., Pardo, A., & Merino, M. (2016). In vitro corrosion performance of PEO coated Ti and Ti6Al4V used for dental and orthopaedic implants. *Surface and Coatings Technology, 307*, 1255-1264.
- Mello, A., Hong, Z., Rossi, A., Luan, L., Farina, M., Querido, W., . . . Webster, T. (2007). Osteoblast proliferation on hydroxyapatite thin coatings produced by right angle magnetron sputtering. *Biomedical Materials, 2*(2), 67.
- Mohseni, E., Zalnezhad, E., & Bushroa, A. (2014). Comparative investigation on the adhesion of hydroxyapatite coating on Ti-6Al-4V implant: A review paper. *International Journal of Adhesion and Adhesives, 48*, 238-257.
- Montazeri, M., Dehghanian, C., Shokouhfar, M., & Baradaran, A. (2011). Investigation of the voltage and time effects on the formation of hydroxyapatite-containing titania prepared by plasma electrolytic oxidation on Ti-6Al-4V alloy and its corrosion behavior. *Applied Surface Science, 257*(16), 7268-7275.
- Moon, S., & Jeong, Y. (2009). Generation mechanism of microdischarges during plasma electrolytic oxidation of Al in aqueous solutions. *Corrosion Science, 51*(7), 1506-1512.
- Morais, L. S., Serra, G. G., Muller, C. A., Andrade, L. R., Palermo, E. F., Elias, C. N., & Meyers, M. (2007). Titanium alloy mini-implants for orthodontic anchorage: immediate loading and metal ion release. *Acta Biomaterialia, 3*(3), 331-339.
- Narayanan, R., Seshadri, S., Kwon, T., & Kim, K. (2008). Calcium phosphate-based coatings on titanium and its alloys. *Journal of Biomedical Materials Research Part B: Applied Biomaterials, 85*(1), 279-299.
- Natarajan, K., Riemer, S., & Iwasaki, I. (1984). Influence of pyrrhotite on the corrosive wear of grinding balls in magnetite ore grinding. *International Journal of Mineral Processing, 13*(1), 73-81.
- Nelea, V., Morosanu, C., Iliescu, M., & Mihailescu, I. (2003). Microstructure and mechanical properties of hydroxyapatite thin films grown by RF magnetron sputtering. *Surface and Coatings Technology, 173*(2), 315-322.

- Niakan, A., Ramesh, S., Ganesan, P., Tan, C., Purbolaksono, J., Chandran, H., & Teng, W. (2015). Sintering behaviour of natural porous hydroxyapatite derived from bovine bone. *Ceramics International*, *41*(2), 3024-3029.
- Nie, X., Leyland, A., & Matthews, A. (2000). Deposition of layered bioceramic hydroxyapatite/TiO₂ coatings on titanium alloys using a hybrid technique of micro-arc oxidation and electrophoresis. *Surface and Coatings Technology*, *125*(1), 407-414.
- Nledengvist, P., & Hogmark, S. (1997). Experiences from scratch testing of tribological PVD coatings. *Tribology International*, *30*(7), 507-516.
- Ntsoane, T. P., Topic, M., Härting, M., Heimann, R. B., & Theron, C. (2016). Spatial and depth-resolved studies of air plasma-sprayed hydroxyapatite coatings by means of diffraction techniques: Part I. *Surface and Coatings Technology*, *294*, 153-163.
- Olding, T., Sayer, M., & Barrow, D. (2001). Ceramic sol-gel composite coatings for electrical insulation. *Thin Solid Films*, *398*, 581-586.
- Ooi, C., Hamdi, M., & Ramesh, S. (2007). Properties of hydroxyapatite produced by annealing of bovine bone. *Ceramics International*, *33*(7), 1171-1177.
- Pan, Y., Chen, C., Wang, D., & Lin, Z. (2013). Preparation and bioactivity of micro-arc oxidized calcium phosphate coatings. *Materials Chemistry and Physics*, *141*(2), 842-849.
- Pan, Y., Chen, C., Wang, D., & Yu, X. (2012). Microstructure and biological properties of micro-arc oxidation coatings on ZK60 magnesium alloy. *Journal of Biomedical Materials Research Part B: Applied Biomaterials*, *100*(6), 1574-1586.
- Perren, S. M., Pohler, O. E., & Schneider, E. (2001). Titanium as implant material for osteosynthesis applications. *Titanium in Medicine* (pp. 771-825): Springer.
- Pillai, R. S., Frasnelli, M., & Sglavo, V. M. (2018). HA/ β -TCP plasma sprayed coatings on Ti substrate for biomedical applications. *Ceramics International*, *44*(2), 1328-1333.
- Polat, A., Makaraci, M., & Usta, M. (2010). Influence of sodium silicate concentration on structural and tribological properties of microarc oxidation coatings on 2017A aluminum alloy substrate. *Journal of Alloys and Compounds*, *504*(2), 519-526.
- Qiao, L., Lou, J., Zhang, S., Qu, B., Chang, W., & Zhang, R. (2016). The entrance mechanism of calcium and phosphorus elements into micro arc oxidation coatings developed on Ti6Al4V alloy. *Surface and Coatings Technology*, *285*, 187-196.
- Rad, A. T., Solati-Hashjin, M., Osman, N. A. A., & Faghihi, S. (2014). Improved biophysical performance of hydroxyapatite coatings obtained by electrophoretic deposition at dynamic voltage. *Ceramics International*, *40*(8), 12681-12691.

- Rafieerad, A., Bushroa, A., Nasiri-Tabrizi, B., Vadivelu, J., Baradaran, S., Mesbah, M., & Zavareh, M. A. (2016). Mechanical properties, corrosion behavior and in-vitro bioactivity of nanostructured Pd/PdO coating on Ti-6Al-7Nb implant. *Materials and Design*, **103**, 10-24.
- Rožić, L., Petrović, S., Radić, N., Stojadinović, S., Vasilić, R., Stefanov, P., & Grbić, B. (2013). Fractal approach to surface roughness of TiO₂/WO₃ coatings formed by plasma electrolytic oxidation process. *Thin Solid Films*, **539**, 112-116.
- Sah, S. P., Tsuji, E., Aoki, Y., & Habazaki, H. (2012). Cathodic pulse breakdown of anodic films on aluminium in alkaline silicate electrolyte—Understanding the role of cathodic half-cycle in AC plasma electrolytic oxidation. *Corrosion Science*, **55**, 90-96.
- Sakiru, A., & Shahjahan, M. (2015). Thin surface layers of iron-based alloys deposited by TIG hardfacing. *Tribology Online*, **10**(6), 434-440.
- Sandhyarani, M., Rameshbabu, N., & Venkateswarlu, K. (2014). Fabrication, characterization and in-vitro evaluation of nanostructured zirconia/hydroxyapatite composite film on zirconium. *Surface and Coatings Technology*, **238**, 58-67.
- Schutz, R., & Grauman, J. (1986). Corrosion behavior of titanium and other alloys in laboratory FGD scrubber environments. *Materials Performance;(United States)*, **25**(4).
- Shadanbaz, S., & Dias, G. J. (2012). Calcium phosphate coatings on magnesium alloys for biomedical applications: a review. *Acta Biomaterialia*, **8**(1), 20-30.
- Shin, K. R., Kim, Y. S., Kim, G. W., Yang, H. W., Ko, Y. G., & Shin, D. H. (2015). Effects of concentration of Ag nanoparticles on surface structure and in vitro biological responses of oxide layer on pure titanium via plasma electrolytic oxidation. *Applied Surface Science*, **347**, 574-582.
- Shokouhfar, M., Dehghanian, C., Montazeri, M., & Baradaran, A. (2012). Preparation of ceramic coating on Ti substrate by plasma electrolytic oxidation in different electrolytes and evaluation of its corrosion resistance: Part II. *Applied Surface Science*, **258**(7), 2416-2423.
- Shukor, B. A., Hamdi, M., Toque, J., & Ide-Ektessabi, A. (2010). *Wear characteristics and adhesion behavior of calcium phosphate thin-films*. Paper presented at the Key Engineering Materials.
- Simka, W., Krzakała, A., Korotin, D. M., Zhidkov, I. S., Kurmaev, E. Z., Cholakh, S. O., . . . Suchanek, K. (2013). Modification of a Ti-Mo alloy surface via plasma electrolytic oxidation in a solution containing calcium and phosphorus. *Electrochimica Acta*, **96**, 180-190.
- Smith, A. M., Paxton, J. Z., Hung, Y.-P., Hadley, M. J., Bowen, J., Williams, R. L., & Grover, L. M. (2015). Nanoscale crystallinity modulates cell proliferation on plasma sprayed surfaces. *Materials Science and Engineering: C*, **48**, 5-10.

- Snizhko, L., Yerokhin, A., Gurevina, N., Patalakha, V., & Matthews, A. (2007). Excessive oxygen evolution during plasma electrolytic oxidation of aluminium. *Thin Solid Films*, 516(2), 460-464.
- Song, W. H., Ryu, H. S., & Hong, S. H. (2005). Apatite induction on Ca-Containing titania formed by micro-arc oxidation. *Journal of the American Ceramic Society*, 88(9), 2642-2644.
- Sowa, M., Piotrowska, M., Widziołek, M., Dercz, G., Tylko, G., Gorewoda, T., . . . Simka, W. (2015). Bioactivity of coatings formed on Ti–13Nb–13Zr alloy using plasma electrolytic oxidation. *Materials Science and Engineering: C*, 49, 159-173.
- Sowa, M., & Simka, W. (2018). Electrochemical behavior of plasma electrolytically oxidized niobium in simulated physiological environment. *Surface and Coatings Technology*, 344, 121-131.
- Srinivasan, P. B., Liang, J., Blawert, C., Störmer, M., & Dietzel, W. (2010). Characterization of calcium containing plasma electrolytic oxidation coatings on AM50 magnesium alloy. *Applied Surface Science*, 256(12), 4017-4022.
- Stachowiak, G. W. (2006). *Wear: materials, mechanisms and practice*: John Wiley & Sons.
- Sul, Y.-T., Johansson, C., Byon, E., & Albrektsson, T. (2005). The bone response of oxidized bioactive and non-bioactive titanium implants. *Biomaterials*, 26(33), 6720-6730.
- Sundararajan, G., & Krishna, L. R. (2003). Mechanisms underlying the formation of thick alumina coatings through the MAO coating technology. *Surface and Coatings Technology*, 167(2), 269-277.
- Surmenev, R. A. (2012). A review of plasma-assisted methods for calcium phosphate-based coatings fabrication. *Surface and Coatings Technology*, 206(8), 2035-2056.
- Surmenev, R. A., Surmeneva, M. A., & Ivanova, A. A. (2014). Significance of calcium phosphate coatings for the enhancement of new bone osteogenesis—A review. *Acta Biomaterialia*, 10(2), 557-579.
- Takadom, J. (2013). *Materials and surface engineering in tribology*: John Wiley & Sons.
- Takahashi, K., Van Den Beucken, J., Wolke, J., Hayakawa, T., Nishiyama, N., & Jansen, J. (2008). Characterization and in vitro evaluation of biphasic calcium pyrophosphate–tricalciumphosphate radio frequency magnetron sputter coatings. *Journal of Biomedical Materials Research Part A*, 84(3), 682-690.
- Teh, T., Berkani, A., Mato, S., Skeldon, P., Thompson, G., Habazaki, H., & Shimizu, K. (2003). Initial stages of plasma electrolytic oxidation of titanium. *Corrosion Science*, 45(12), 2757-2768.

- Teng, H.-P., Yang, C.-J., Lin, J.-F., Huang, Y.-H., & Lu, F.-H. (2016). A simple method to functionalize the surface of plasma electrolytic oxidation produced TiO₂ coatings for growing hydroxyapatite. *Electrochimica Acta*, 193, 216-224.
- Variola, F., Brunski, J. B., Orsini, G., de Oliveira, P. T., Wazen, R., & Nanci, A. (2011). Nanoscale surface modifications of medically relevant metals: state-of-the art and perspectives. *Nanoscale*, 3(2), 335-353.
- Walsh, F., Low, C., Wood, R., Stevens, K., Archer, J., Poeton, A., & Ryder, A. (2009). Plasma electrolytic oxidation (PEO) for production of anodised coatings on lightweight metal (Al, Mg, Ti) alloys. *Transactions of the IMF*, 87(3), 122-135.
- Wang, Y., Lei, T., Jiang, B., & Guo, L. (2004). Growth, microstructure and mechanical properties of microarc oxidation coatings on titanium alloy in phosphate-containing solution. *Applied Surface Science*, 233(1), 258-267.
- Welsch, G., Boyer, R., & Collings, E. (1993). *Materials properties handbook: titanium alloys*: ASM international.
- Xiao, X. F., & Liu, R. F. (2006). Effect of suspension stability on electrophoretic deposition of hydroxyapatite coatings. *Materials Letters*, 60(21), 2627-2632.
- Yang, T.-C., Shu, H.-Y., Chen, H.-T., Chung, C.-J., & He, J.-L. (2014). Interface between grown osteoblast and micro-arc oxidized bioactive layers. *Surface and Coatings Technology*, 259, 185-192.
- Yang, Y., Kim, K.-H., & Ong, J. L. (2005). A review on calcium phosphate coatings produced using a sputtering process—an alternative to plasma spraying. *Biomaterials*, 26(3), 327-337.
- Yerokhin, A., Nie, X., Leyland, A., & Matthews, A. (2000). Characterisation of oxide films produced by plasma electrolytic oxidation of a Ti-6Al-4V alloy. *Surface and Coatings Technology*, 130(2), 195-206.
- Yerokhin, A., Nie, X., Leyland, A., Matthews, A., & Dowey, S. (1999). Plasma electrolysis for surface engineering. *Surface and Coatings Technology*, 122(2), 73-93.
- Yerokhin, A., Snizhko, L., Gurevina, N., Leyland, A., Pilkington, A., & Matthews, A. (2003). Discharge characterization in plasma electrolytic oxidation of aluminium. *Journal of Physics D: Applied Physics*, 36(17), 2110.
- Yerokhin, A., Snizhko, L., Gurevina, N., Leyland, A., Pilkington, A., & Matthews, A. (2004). Spatial characteristics of discharge phenomena in plasma electrolytic oxidation of aluminium alloy. *Surface and Coatings Technology*, 177, 779-783.
- Yetim, A. (2010). Investigation of wear behavior of titanium oxide films, produced by anodic oxidation, on commercially pure titanium in vacuum conditions. *Surface and Coatings Technology*, 205(6), 1757-1763.
- Zhitomirsky, I., & Gal-Or, L. (1997). Electrophoretic deposition of hydroxyapatite. *Journal of Materials Science: Materials in Medicine*, 8(4), 213-219.

LIST OF PUBLICATIONS AND PAPERS PRESENTED

1. The properties of hydroxyapatite ceramic coatings produced by plasma electrolytic oxidation. *Ceramics International*. Vol. 44, pp. 1802-1811, (2018).
2. Preparation, scratch adhesion and anti-corrosion performance of TiO₂-MgO-BHA coating on Ti6Al4V implant by plasma electrolytic oxidation technique. *Journal of Adhesion Science and Technology*, Vol. 32, pp. 1-12, (2018)
3. Recent development of calcium phosphates-based coatings on titanium alloy implants. *Surface Engineering and Applied Electrochemistry*, Vol. 53, Issue 3. pp. 419-433, (2017)
4. Characteristic features of plasma electrolytic treated layers in Na₃PO₄ solution. *Procedia Engineering*, Vol. 184, pp. 732-736, (2017).
5. Hydroxyapatite layer formation on titanium and its alloys using micro-arc oxidation. *Journal of Engineering and Applied Sciences*, pp. 10101-1010, (2015).

SEMINARS AND WORKSHOPS

1. Materials Characterization Workshop (MACH2017). Center of Advanced Materials, University Malaya. Auditorium Resource Centre, Technology Park Malaysia Bukit Jalil Kuala Lumpur, 10 th October, 2017.
2. Green Approaches Via Nanostructured Mesoporous Materials For Catalysis, Biomedical and Energy Storage Applications. *Nanocat*, Auditorium Resource Centre, Technology Park Malaysia, Bukit Jalil, Kuala Lumpur, 12-13 th October, 2017.
3. Seminar on Improvements to Coatings Quality Assurance. Institute of Materials, Malaysia (IMM). Kelab Golf & Rekreasi Petronas, Kerteh, Terengganu, Malaysia, 27 th April, 2016.

4. Symposium on Nano Surfaces Analysis & Characterization. Bruker, Monash University Malaysia. Sunway, Kuala Lumpur, 24 August, 2016.
5. Carbon Nanomaterials and Environmental Workshop. National Nanotechnology Centre, Ministry of Science, Technology & Innovation in Conjunction with Nanotechnology and Catalyst Research Centre. Technology Park Malaysia, Bukit Jalil, Kuala Lumpur, 10 th October, 2016.

University of Malaya